DETERMINATION OF TWO-PHASE MASS FLOW RATE IN REFRIGERANT R-134a PIPE FLOW

DETERMINATION OF TWO-PHASE MASS FLOW RATE IN REFRIGERANT R-134a PIPE FLOW

By

JIANWEI WANG, B.ENG. (SHANGHAI JIAOTONG UNIVERSITY)

A Thesis

Submitted to the School of Graduate Studies

in Partial Fulfilment of the Requirements

for The Degree

Master of Engineering

in Mechanical Engineering

McMaster University

MASTER OF ENGINEERING (1993)
(Mechanical Engineering)

McMASTER UNIVERSITY
Hamilton, Ontario, Canada

TITLE: Determination of Two-Phase Mass Flow Rate in a Refrigerant R-134a Pipe Flow

AUTHOR: Jianwei Wang, B.Eng. (Shanghai Jiaotong University, P.R.China)

SUPERVISORS: Dr. M. Shoukri
Dr. J.S. Chang

NUMBER OF PAGES: xvii, 133

ACKNOWLEDGEMENTS

The author wishes to express his great appreciation to Dr. J.S. Chang and Dr. M. Shoukri for their supervision throughout the course and project of this study.

A sincere thank comes to Dr. A. Abdul-Razzak for his supervision throughout the construction of the test loop and the experiments as well as many useful discussions.

Thanks are also extended to Mr. P. Looy and Mr. R. Lodewyks for their assistance on the construction of the test loop. Helpful discussions with author's colleagues, Dr. W. He, Dr. F. Peng, Mr. G. Harvel, Prof. S. Wang are acknowledged.

This project is supported by ASHRAE-American Society of Heating, Refrigeration, Air-conditioning Engineering. Thanks also are given to McMaster/CIDA for the scholarship.

The author is grateful to his wife, Ying who gives constant love and support.

ABSTRACT

An examination of various methods for mass flow rate measurements was undertaken to evaluate their applicability for measuring refrigerant R-134a two-phase mass flow in refrigeration and air-conditioning equipment. An experimental apparatus was constructed to generate the required two-phase flow conditions. A turbine and a venturi flowmeter were used together with either a capacitance transducer or a gamma densitometer to determine the two-phase mass flow rate.

The time-averaged void fraction was measured using a capacitance transducer and a gamma densitometer. Their measurements were in good agreement. Hence, for mass flow rate measurements, the capacitance transducer was used as the void fraction meter because of its ease of operation.

A number of models were used to combine the output of either the turbine flowmeter or the venturi flowmeter, with the void fraction measurement to estimate the mass flow rate. It was found that, within the range of experimental data tested in the present work, the venturi flowmeter, in conjunction with Chisholm's model, provided the best agreement with the experimental results.

TABLE OF CONTENTS

NOMENCLATURE

A: cross section area of pipe

A_d: cross section area of the throat of venturi flowmeter

A_d: detector area

C: empirical constant of venturi flowmeter

Cp: capacitance in pf

Cp*: dimensionless capacitance

C_p: specific heat

C_t: ratio of drag coefficients of turbine blade

d: diameter of the throat of venturi flowmeter

D: diameter of tube

E_o: transfer characteristic of frequency-to-voltage converter

f: frequency

G: mass flux

h: enthalpy of liquid

h_{fg}: latent heat

H: liquid level

Δh: enthalpy rise

I: intensity of gamma beam

I_0: incident intensity of gamma beam

K: dimensional constant of venturi flowmeter

L: distance between two ring electrodes

M: mass flow rate

M_{Aya}: mass flow rate by dispersed flow model

M_{Chi}: mass flow rate by Chisholm's model

M_{Hom}: mass flow rate by homogeneous flow model

M_{hov}: mass flow rate by homogeneous density

M_{Rou}: mass flow rate by Rouhani's separated flow model

M_{msv}: mass flow rate by mixture density equation in the separated flow model

M_{mev}: mass flow rate by equal pressure drop model

M_{vol}: mass flow rate by separated flow model

M_{Vol}: mass flow rate by volumetric flow model

M_{V-T}: mass flow rate by combined model for turbine and venturi meters

N: detector counting rate

P: pressure

ΔP: pressure drop

ΔP_f: pressure drop when liquid passes flowmeter along

ΔP_g: pressure drop when vapour passes flowmeter along

Q: volumetric flow rate

Q: input power

Q_T: volumetric flow rate by turbine flowmeter

R: uncertainty

s: slip ratio

S: surface tension

S: sensitivity of gamma-rays

t: propagation time of sound wave

T: temperate

T_s: saturated temperature

u_g: vapour velocity

u_f: liquid velocity

Ut: fluid velocity of turbine flowmeter

V: volume covered by capacitance transducer

V_c: velocity of sound

V_{cL}: sound speed of Lucite

V_{cR}: sound speed of R-134a

V_g: volume of vapour covered by instrument

x: distance

x_0 (x): thermodynamic quality

Y: parameter in Aya-model

α: volumetric void fraction

β: diameter ratio

ρ: fluid density

δ: thickness of tube

λ: flow coefficient of the turbine Meter

ϵ: statistical error of gamma-densitometer

ε: dielectric constants

ε: error

σ: standard deviation

η: detector coefficient

μ: absorption coefficient

θ: counting interval

ν: viscosity

X: Lockhart-Martinelli parameter

SUBSCRIPTS

f: liquid

fg: liquid-vapour

g: vapour

in: inlet condition

l: condition of full liquid

m: mixture of vapour and liquid

v: condition of full vapour

s: saturated condition

ss: stainless steel

TP: two-phase

0: incident value

2ϕ: two-phase

LIST OF TABLES

LIST OF FIGURES

CHAPTER 1

INTRODUCTION

1.1 INTRODUCTION

In single phase flow, mass flow rate can be readily determined using commercially available instruments and density determined from state parameters, i.e. temperature and pressure. In two-phase flow, density is a function of void fraction as well as the states of individual phases. The individual phases generally have different velocities. The two-phase flow problem is further complicated by generally non-uniform phase velocity and void fraction profiles which change dramatically with flow regime. The determination of the total mass flow rate of a two-phase mixture thus presents a special problem in measurements.

The determination of two-phase mass flow rate has become increasingly important in many technical applications, such as process control in chemical production, transport of oil-gas mixtures in pipe lines and nuclear reactor safety analysis. Recently, this problem has been extended to applications in the heating, refrigerating, and air-conditioning industry because two-phase vapour-liquid flows are often encountered in refrigeration and heat pump equipment.

A few studies can be found in the literature dealing with the determination of two-phase refrigerant mass flow rate. However, these previous studies do not provide quantitative comparison between different mass flow measurement techniques and no recommendations are made for refrigeration and air-conditioning applications[1].

Standards for rating refrigeration and air-conditioning equipment capacities often rely on the air or water side energy flow measurements, as the refrigerant mass flow cannot be measured accurately under some rating conditions due to two-phase flow present in the system at the refrigerant mass flowmeter. Field applications require mass flow sensors capable of measuring the refrigerant mass flow through liquid overfeed evaporators and condensers where the exit flow is often, or continuously, in a two-phase flow condition. There is a need in the laboratory, in rating procedures, and in field monitoring, to have a mass flow meter capable of handling instantaneous two-phase refrigerant flow[1].

In most laboratory applications, determination of phase velocity and void fraction, or mixture density, generally depend on separate instruments. Combination of the measurements of these different instruments is used in the determination of two-phase mass flow rate. Therefore, for two-phase mass flow measurements in heating, refrigerating, and air-conditioning equipment, the instantaneous output of more than one instrument can be combined to obtain mass flows and other variables of interest.

1.2 PROBLEM STATEMENT

The nature of two-phase flow is the presence of moving internal interfaces which make theoretical predictions of flow parameters immensely more difficult than in single phase flow. Thus, experimental measurements play a key role in providing basic information for parameters of interest. In vapour-liquid two-phase flow, mixture density ρ and mass flux G may be defined as follows respectively:

$$\rho=\alpha\rho_g+(1-\alpha)\rho_f \tag{1.1}$$

$$G=\alpha\rho_g u_g+(1-\alpha)\rho_f u_f \tag{1.2}$$

where α is the void fraction, ρ_g and ρ_f are the densities of vapour and liquid, u_g and u_f are the velocities of vapour and liquid respectively. Because of the different flow patterns in two-phase flow, such as stratified flow, plug flow, dispersed bubble flow, slug flow and annular flow, the void fraction, density and velocity are often expressed in time and cross-sectional averaged values in pipe flow. The densities ρ_g and ρ_f are also related to the pressure and temperature of the vapour and liquid phases through the respective equations of state. Therefore, if α, u_g and u_f , phase temperature and pressure can be measured, the mixture density and mass flux can be determined using the above equations.

However, direct measurement of individual phase velocity is almost impossible using traditional instruments. Accordingly, in determining two-phase mass flow rate, measurement of void fraction, or mixture density, as well as a measure of velocity, complemented with a model for relative velocity, are needed. Appropriate analytical models with some acceptable assumptions are used in the determination of the relative

velocity between the phases. The homogeneous equilibrium model, which assumes that vapour and liquid phases are in thermal and mechanical equilibrium, i.e. having the same temperature and velocity in a given cross section of the pipe, may be used to determine mixture density and mass flux. Separated flow model can also be used to determine mass flux. In the separated flow, the phases are assumed to flow separately with different velocities.

In order to make the determination of refrigerant two-phase mass flow possible, an experimental apparatus was constructed. Refrigerant R-134a was chosen to be the working medium because its thermodynamic properties are similar to refrigerant R-12. R-12 was the most commonly used refrigerant in home refrigerator and air-conditioning equipment before and will be totally phased out in the coming few years.

In this project, two instruments, a turbine flowmeter and a venturi flowmeter, were tested for measuring the average velocity of the refrigerant during two-phase flow. A capacitance transducer and a gamma-densitometer were used to provide the average value of void fraction. Ultrasonic pulse-echo technique was used to calibrate capacitance transducer and gamma-densitometer as well as characterize flow patterns during the two-phase flow.

Some analytical models were used to explain the behaviours of the turbine flowmeter and the venturi flowmeter. Combined with the knowledge of void fraction and thermodynamic state, the two-phase mass flow rate of refrigerant R-134a can be determined. Comparisons between these models and different techniques used have been made in this thesis.

CHAPTER 2

REVIEW OF THE LITERATURE

2.1 INTRODUCTION

The development of measurement techniques and instrumentation for two-phase flow has been the subject of extensive research in the last two decades. Reviews for two-phase flow instrumentation can be found in the literature provided by Banerjee and Lahey[2], Snoek[3], Delhaye[4], Hewitt [5] as well as recently by Shoukri et al.[6] who focused on the measurement of two-phase mass flow rate.

Two-phase mass flow rate measurement is of basic importance in many industrial applications. The complexity of measuring two-phase mass flow rate can be appreciated

if one recalls the single phase case. In single phase flow, the mass flow rate is usually obtained by measuring the mean fluid velocity, either directly or through measuring the dynamic head. The mass flux is then obtained by multiplying the fluid velocity by the density, which is determined from the thermodynamic state. In two-phase flow, the two phases can acquire different velocities and a reliable measurement of the mixture density is also required. Accordingly, in two-phase flow, at least two independent measurements are needed. These are typically a representation of the flow velocity as well as the mixture density. Since the mixture density is dependent on the void fraction, void fraction can be one of the two required measurements.

Previous work on two-phase mass flow rate measurement was focused on steam-water flow in relatively large pipes. However, applications related to refrigeration and air-conditioning equipment are relatively new. Hashizume[7] used quick-closing valves to measure void fraction for R-11, R-12 and R-22. This method is a simple and accurate one, but its response is very slow and it is disruptive to the operation of the system. Mei[8] used a liquid-vapour separator to separate the two phases and measured each phase by a conventional single phase mass flowmeter. The device was installed in a 3.5 ton R-22 split-system heat pump where the quality of the refrigerant at the condenser exit ranged from 6.4% to 14.7%. The device required an additional pressure drop of 2 to 5 psi (13.8 to 34.5 kPa) and its use was limited to laboratory testing. Hawken et al.[9] used a Coriolis mass flowmeter in two-phase R-22 refrigerant flow and recommended that this type of meter can only be applied for single phase flow. Lin[10] used a sharp-edged orifice flowmeter in two-phase R-11 refrigerant flow and obtained an accuracy of 12% for the void fraction measurement ranging from 2% to 100%. However, an orifice plate normally introduces a higher pressure drop to the flow system and it could also be detrimental to system performance.

This chapter deals mainly with available void fraction measuring techniques and suggests methods for two-phase mass flow rate measurements. Particular reference is

made to the suitability of the various techniques for refrigeration and air conditioning equipment. The measurement techniques, which are reviewed in this chapter, are summarized in Tables 1 and 2 for the void fraction and the mass flow rate measurement respectively.

2.2 TECHNIQUES FOR VOID FRACTION MEASUREMENT

2.2.1 Capacitance Transducer Methods

Irons and Chang et al.[11] developed non-intrusive strip and ring type capacitance transducers for gas-powder flow. The measurement of void fraction using a ring type capacitance transducer was found to be less dependent on two-phase flow regimes as compared with strip types. Normally, sensitivity of the output signal can be controlled by selecting the electrode length. For ring type electrode transducers, Chang et al.[12] used a multi-ring configuration to enhance the sensitivity of the transducer for some two-phase flows with low ratios of the dielectric constants. Dynamic response of the ring type capacitance transducer for various two-phase flow patterns illustrates that the capacitance sensor is sensitive enough to characterize all the flow regimes observed in both horizontal and vertical flow systems. Chang et al.[12] also used a ring type capacitance transducer for dynamic void fraction measurement in gas-liquid two-phase flow and no significant two-phase flow regime dependence on the void fraction measurements was observed.

Auracher and Daubert[13] used an intrusive capacitance transducer consisting of two parallel plate electrodes inside a pipe to measure void fraction in R-114 refrigerant horizontal two-phase flow. They observed that the capacitance method was sensitive to non-axisymmetric flow. This can be utilized to reduce its sensitivity to flow regime and is of particular advantage for fluids with high ratios of the dielectric constants.

Xie et al.[14,15] developed an eight-electrode capacitance system for measurement of phase distribution. Those capacitance sensors were mounted externally around the flow pipe. They used a two-dimensional finite element model to investigate the instrument sensitivity and used a linear back-projection image reconstruction algorithm for tomographic flow imaging and flow measurement. In addition, a measurement of the mass or volume flow rate of each component in the two-component flow also was provided by using cross correlation analysis of images at two axially spaced locations on the pipe. However, the tomographic flow imaging required longer time to reconstruct the image, and therefore, may not be suitable for industrial applications which require dynamic measurements.

2.2.2 Ultrasonic Pulse-Echo and Attenuation Techniques

The state of the art of ultrasonic flow measurement techniques is given by Lynnworth[16]. However, no reference is made to two-phase flow applications. There are three ultrasonic methods which are used for two-phase flow diagnostics, namely the pulse echo and attenuation, the transmission and the Doppler shift methods. The Doppler shift method is suitable when applied in low void fraction liquid flow velocity measurements in a two-phase flow system[17]. The transmission method was used to measure void fraction in the bubbly flow[18]. This method is very accurate for the measurement of void fraction below 0.2 with the accuracy of $\pm$ 1%. Lahey et al.[2] and Morala et al.[19] used the pulse-echo method to observe the location and size of a single bubble. Xu[20] used a pair of ultrasonic transducers, transmitter and receiver which were positioned opposite to each other on both sides of the flow pipe, to investigate the pulse echo method suitable for determination of gas concentration and gas velocity in a vertical two-phase flow.

Chang et al.[21,22] and Chang and Morala[23] used the pulse-echo technique for measurement of liquid film thickness and characterization of flow regime for two-phase

gas-liquid flow through a pipe. They also used an accumulation of the instantaneous liquid level data to calculate void fraction for different flow regimes. The results for the case of stratified flow were in good agreement with those from the capacitance void transducer. Successful application of the ultrasonic technique makes it capable of measuring the two-phase flow interface in a horizontal pipe, identifying different flow patterns and calculating void fraction in both instantaneous and time averaged ways. It also demonstrates that ultrasonic pulse echo technique offers a feasible instrumentation alternative for two-phase flow applications. The method can be mounted on the outside pipe wall which can be metallic or transparent pipe, depending on the resonant frequency of the ultrasonic transducer.

Plaskowski and Beck[24] used 12 ultrasonic pulse echo transducers and an acoustic back-projection algorithm for flow image reconstruction. Their effort formed a basis for the development of a successful flow imaging system. Flow imaging by the ultrasonic pulse echo technique is similar to medical computed tomographic imaging in which an image of a cross section of the body can be obtained by using externally mounted ultrasonic transducers. However, in medical imaging the sensing system must be moved axially along the body to obtain a multi-slice cross section which is combined into the image of the cross section by computed tomography. In flow imaging, the flow field moves along the pipe so that only a single image plane can be obtained, but the single imaging plane is sufficient to characterise the flow. If two image planes spaced along the pipe axis can be obtained, the flow velocities of the components may be obtained by using cross correlation of the information from the two image planes.

2.2.3 Neutron, Gamma-Ray and X-Ray Attenuation Methods

Fast neutron scattering, gamma-densitometer, X-ray and neutron attenuation techniques are widely used to measure void fraction and mixture density for two-phase flow in laboratory testing, nuclear reactor safety research and other industrial

applications. The principles of these techniques are explained and reviewed by Banerjee and Lahey[2]. The advantages of these techniques are that the intensity of the beam through the two-phase fluids is linearly proportional to void fraction. The disadvantages of these methods are the shielding problems, and that, if the counting mode is used, these methods usually cannot be used for instantaneous measurements because of the required counting time due to nuclear statistics.

Banerjee et al.[25,26] used fast neutron scattering methods to measure void fraction in two-phase flow through a pipe with and without rod bundles. Neutrons can penetrate complicated geometries and thicknesses of metal and are very sensitive to the hydrogenous material such as water which thermalize the incident neutrons. The thermalized neutron flux will vary with the amount of moderating material in the beam path. Their work indicated that the thermalized neutron flux was independent of the flow regime and decreased linearly with void fraction. These two properties are important in the application to complicated geometries.

Experiments using the neutron scattering technique also can be simulated with a Monte Carlo neutron transport calculation to set up an appropriate incident neutron energy spectrum, for a given geometry and flow regime[27]. Yuen et al.[28] tested a neutron scattering technique with portable sources for the measurement of void fraction and evaluated the effect of the incident neutron energy spectrum. An optimum incident neutron energy spectrum may generate the desired characteristics of linearity and flow regime independence. The optimum spectrum depends on experimental geometry, neutron shielding and reflection around the experimental set-up. The optimum spectra may be obtained in practice by Monte Carlo calculations [28].

For visualization of multiphase flow by the real-time neutron radiography, Chang and Harvel[29] used this technique in natural circulation conditions to observe flow regimes. The results obtained by real-time neutron radiography was compared with those by video

and ultrasonic pulse-echo techniques and agreed well with each other. Fuji et al.[30] carried out an experiment using the neutron radiography technique for void fraction measurement and measured the axial void fraction distribution in two-phase flow through a nozzle. They made the image of two dimensional axisymmetric void fraction measurement and distribution in the same experimental geometry. A reasonable void fraction measurement and distribution were obtained. However, the use of fast neutron scattering and attenuation technique normally cannot be applied to fast transient experiments unless an intense neutron source is available[2].

The use of X-ray attenuation technique for void fraction measurement has some advantages because of its high beam intensity, low photon energy and fast time response. The X-ray attenuation method has been widely used to measure void fraction and to identify phase distribution during transient two-phase flow. Recently, Narabayashi et al.[31] used high-speed X-ray scanner for measurement of void distribution in high pressure steam-water two-phase flow. Their results indicate that this method is a very promising one for making accurate measurements concerning void distribution, flow pattern and average vapour phase velocity. It is also possible to measure void fraction and quality at the same time. However, the X-ray attenuation method has some disadvantages regarding the inherent fluctuations of beam intensity and drift in the photon flux. Normally, at least one beam must act as a reference to obtain accurate void fraction measurement. In general, where speed of response is not critical or where space is available for shielding, gamma-ray devices are to be preferred[2].

Gamma-ray attenuation technique is the most widely used technique for void fraction measurement in two-phase flow among the above three methods. It has been well developed in its theory, design procedure and test condition[32]. Gamma-rays of different energies can be chosen depending on the geometry of the test section. Chan and Banerjee[32,33] summarised the different gamma sources available commercially and the properties of some scintillation crystals. For low energy gamma-rays (<200 keV),

NaI(Tl) scintillators are commonly used to detect the transmitted gamma-rays because of their high light output, good energy resolution and high detection efficiency (close to 100%).

There are different arrangements of gamma beam detection for different pipe sizes. That is single- or multi-beam gamma-densitometers. It depends on how much area in the cross section of the pipe is covered by the gamma beam and how accurate is the required measurement. Flow distribution also can be determined by using multi-beam gamma-densitometers. The application of a gamma-densitometer with single source and multi-detectors also can be found in recent work done by Chan and Bzovey[34]. The multi-detector gamma densitometer together with Pitot tubes was used to measure two-phase mass fluxes in a 9.7 cm inner diameter pipe in both vertical and horizontal set-up. The accuracy for the measurement of two-phase mass flux was $\pm 15\%$.

2.2.4 Application to Refrigerant Flow

As reviewed in this section, most of the experimental studies for void fraction measurement were performed for gas-water or steam-water systems. For refrigerant vapour-liquid two-phase flow systems, the intrusive vs. non-intrusive nature of the techniques has to be taken into account because of the small size tubes used in the refrigeration and air-conditioning equipment. Intrusive methods may disturb the flow and introduce high pressure drop into the system. Therefore, non-intrusive techniques are more suitable for the measurement of void fraction in refrigerant two-phase flow.

The capacitance transducer technique cannot be used in metallic tubes. Hence, a transparent and plastic tube must be installed. Unlike gas-water flow systems, the ratio of the dielectric constant of vapour-liquid refrigerant flow system is low. Thus, multi-ring type capacitance configuration should be applied on the non-metallic tube to enhance the sensitivity of the transducer.

Ultrasonic pulse-echo technique is a promising method used in stratified flow because it can measure liquid level accurately. Ultrasonic transducers can be used on both metallic and plastic tubes. This technique has been developed and applied to air-water and oil-liquid two-phase flow systems and satisfactory results have been obtained in the identification of flow patterns and measurement of liquid level and void fraction. In applying this technique to refrigerant vapour-liquid flow system, it should be noted that the sound velocity in a refrigerant liquid is much lower than that of water. The impedance of the sound wave at the liquid-vapour interface in refrigerant flow is also much lower than that in air-water systems.

The sensitivity of a gamma-densitometer decreases with decreasing pipe diameter. However, sensitivity calculations for refrigerants have shown that it may have enough accuracy to apply to the current work.

The real time imaging methods based on capacitance, ultrasound and radioactive principles are not suitable for application in the present project, since they require intensive image reconstruction for application to small tubes.

2.3 TWO-PHASE MASS FLOW RATE MEASUREMENT TECHNIQUES

2.3.1 Turbine Flowmeter

The theory and application of the turbine flowmeter is well understood for single phase flow. Applications of the turbine flow meters to two-phase flow have also been attempted because of the need for determining two-phase mass flow rate. Some models have been developed to interpret the response of a turbine flowmeter in two-phase flow. In order to use these models, independent measurement of mixture density or void fraction is required.

Rouhani[35] developed a separated flow model for turbine flowmeter based on momentum density. Frank et al.[36] used Rouhani's model to interpret the data of the turbine flowmeter and venturi flowmeter for mass flow rate in steady two-phase flow. The test was carried out in a horizontal stainless steel tube of 26 mm inner diameter. The accuracy obtained in the mass flow rate measurements was in the order of $\pm 10\%$ which is quite satisfactory.

Aya[37] proposed a dispersed flow model for the turbine flowmeter by considering the momentum balance of the turbine blade segments. This model was used to deal with turbine flowmeter response in steady two-phase flow. In the application of this model, a measure of void fraction or mixture density is also required.

Kamath and Lahey[2] developed a model dealing with the transient response of a turbine flowmeter in two-phase flow. It was based on the angular momentum balance around the blades. In this model, the effects of rotor inertia, velocity and void profiles, slip ratio, imperfect guidance by the rotor blades, and bearing friction on the output reading of turbine flowmeter were taken into account.

Banerjee et al.[2] used a homogeneous flow model to interpret their test results for steam-water two-phase mass flow rate in horizontal pipes of different diameters. They used one spool piece consisting of a gamma-densitometer, a Pitot tube rake and a full-flow turbine flowmeter. They also interpreted their turbine flowmeter data in terms of a volumetric model, as well as Aya and Rouhani models. The volumetric model has a simple expression of the sum of both volumetric flow rates of liquid and vapour phases.

Banerjee and Lahey in their review [2] concluded that for the turbine flowmeter, the homogeneous model always predicted a somewhat lower mass flux than the actual values. The Aya and Rouhani models tended to raise the predicted values but increased the scatter. The volumetric model did not increase the scatter and appeared to be the most

suitable for the widest range of conditions.

2.3.2 Pressure Drop Devices

Pressure drop devices used to measure flow rate normally include orifice plates, venturis and nozzles. Orifice plates and nozzles introduce higher pressure drop to the flow system than venturis[38].

Chisholm[39] developed a model for gas-liquid or vapour-liquid mixture flow through sharp-edged orifices based on an assumption of negligible density change of the two phases. The pressure drop of two-phase flow through the device can be expressed in terms of the Lockhart-Martinelli correlations[40], which are functions of pressure drops of the individual phases. Frank[37] applied this model to a venturi flowmeter and obtained a momentum density instead of single phase density in the pressure drop equation. In common with the turbine flowmeter, the accuracy obtained in the two-phase mass flow rate determination was about $\pm 10\%$.

Collins and Gacesa[41] carried out an experiment to investigate the measurement of steam quality with venturi flow meters and orifice plates in vertical upflow configuration. Four throat to pipe diameter ratios were studied in 6.35 cm (2 1/2") and 7.62 cm (3") pipe sizes. The steam quality ranged from 5 to 90% at 6758 kPa (980 psia). An empirical correlation for the steam quality was derived in terms of the total mass flow rate, the flow coefficient of the devices, the pressure drop of two-phase flow, the density ratio of steam and water, the expansion coefficient and the geometry. The basis of Collins' correlation is the separated flow model of two-phase flow. The correlation resulted in an rms deviation of 4% for data from the venturi flowmeter.

Fouda and Rhodes[42] modified Collins' model and tested venturi flow meters of 19.05 mm (3/4") and 25.4 mm (1") inner diameters in a vertical air-water upflow

system. In their modified model, pressure drop for each phase was assumed to be the same as that for the two-phase flow. The modified model covered qualities ranging from 0.001% to 27% at 207 kPa (30 psia). For qualities below 0.01%, the agreement with the model was poor. This was believed to be due to the fact that below this value the flow was almost single phase liquid.

Wan[43] used a flow nozzle to measure the mass flow rate of steam-water mixtures in the range of steam quality of 10% to 90%. The experimental data were compared with the results from the homogeneous model, the Zivi slip model and Chisholm model. It was found that the homogeneous model consistently overpredicts the experimental data, while the Zivi slip model and the Chisholm model consistently underpredict the experimental data. The rms deviation of the model calculations from the experimental data was found to be quite large in the order of 30%.

Reimann et al.[44] tested a full flow turbine flowmeter and a venturi nozzle in steady-state steam-water flow to measure mass flow rate and quality. The instruments were installed vertically and the pipe size was 66.6 mm inner diameter. The tests were performed at pressures between 3.0 and 9.0 MPa and quality between 2% and 80%. The experimental results were treated by combining Rouhani's turbine model and Chisholm's venturi model. Reimann suggested that if the momentum density does not change between the measurement locations, the mass flux evaluation should be very accurate because it is independent of the slip ratio of the flow.

2.3.3 Application to Refrigerant Flow

Successful applications of the turbine flowmeter to air-water or steam-water two-phase flow systems indicate its potential possibility for application to refrigerant vapour-liquid flow systems. However, each turbine flowmeter has some limitation on its measuring range. Therefore, more than one turbine flow meter may be used to cover the

wide flow rate ranges. For pressure drop devices, the venturi flowmeter is better than the orifice flowmeter for refrigerant flow because it introduces the lowest pressure drop into the system as compared with the flow nozzle and orifice plate due to its downstream head-loss saving diffuser.

2.4 PROPOSED TECHNIQUES FOR TWO-PHASE REFRIGERANT FLOW

Based on the above review, a number of techniques are tested for measuring the void fraction and the mixture velocity. For measurement of void fraction, the following techniques were tested:

a: multi-ring type capacitance transducer

b: single beam gamma-densitometer

c: ultrasonic pulse-echo technique for calibrations of the capacitance transducer and gamma-densitometer

For the determination of velocity:

a: turbine flowmeter

b: venturi flowmeter

TABLE 2.1 Void Fraction Measurement

Experimental Technique	Measured Variable	Flow Pattern Dependence	Real-time Response	Comments
Capacitance transducer	capacitance pf	yes	yes	For the strip type electrode, better than accuracy of ± 5% for stratified flow; For the ring type electrode, better than accuracy of 6% for stratified flow. [11],[12],[22]
Ultrasonic pulse-echo	time, sec	no	yes	better than accuracy of ± 2.53%, no entrainments of bubbles and droplets were considered. used transducer: 2.25MHz. [11],[19],[21]
Ultrasonic transmission	time, sec	yes	yes	better than accuracy of ± 1% for $0 < \alpha < 0.2$; For higher void fraction, transmitted signal becomes less sensitive. used transducer: 2.25MHz. [18]
Gamma-densitometer	count rate sec^{-1}	yes	no	better than accuracy of ± 15%; best results was obtained when the beam was perpendicular to the interface in stratified flow. [34]
Neutron scattering	count rate sec^{-1}	yes	no	better than accuracy of ± 5%, and reasonable linearity is obtained for a source energy between 10 and 100 keV. pipe materials didn't affect the measurement. [25],[26]
X- rays	count rate sec^{-1}	yes	no	better than accuracy of ± 4%; good sensitivity and fast response, but sielding problem has to be considered. [3]
Imaging Techniques:				
Neutron radiography	intensity	no	yes	a reasonable two-dimensional distribution of void fraction in a nozzle was obtained. calibration of attenuation rate was needed. [30]
X-rays scanner	intensity	no	yes	accurate measurement of void distribution was obtained. possible to measure void fraction and quality at the same time. [31]
X-rays CT	intensity	no	yes	better than accuracy of ± 10% for $0 < \alpha < 0.80$ with a long counting time. [3]
NMR	intensity	no	yes	expensive in application to thermal fluid research. problem: magnetic susceptibility is discontinuous at the interface between different phases, the discontinuity produces image distortion.[46]

TABLE 2.2 Two-Phase Mass Flow Measurement

Experimental Techniques	Measured Varialbes	Void measuring	Work Medium	Comments
Turbine flowmeter	frequencey sec^{-1}	yes	water	better than accuracy of $\pm$ 10% for .03 $<x<$ .75, 0.3 $<\alpha<$0.99 separated flow was assumed, Rouhani model was used. [36]
Venturi flowmeter	pressure drop kPa	yes	water	better than accuracy of $\pm$ 10% for .03 $<x<$.75, 0.3$<\alpha<$0.99. separated flow was assumed, Chisholm model was used. calibration of flow coefficient is necessary. [36]
Sharp-adged orifice	pressure drop kPa	yes	refrigerant	better than accuracy of $\pm$ 12% for 0.02$<\alpha<$1. separated flow was assumed. but higher pressure drop was introduced. [10]
Drag disc device	momentum flux $kg/m.sec^{-2}$	yes	water	better than accuracy of $\pm$ 5% for $10^4<Re<10^7$. separated flow was assumed. calibration of drag coefficient is necessary. [45],[47]
Electromagnetic flowmeter	magnetic flux intensity	no	water	better than accuracy of $\pm$ 2% for 0$<\alpha<$ 0.2. homogeneous flow was assumed. [49]
True mass flowmeter	torque	no	water	better than accuracy of $\pm$ 10% for 0$<\alpha<$ 0.9. but a high pressure drop was introduced. not available in market. [45]
Coriolis mass flowmeter	time interval sec	no	water	accuracy of $\pm$ 2% for 0$<\alpha<$0.075 in a dual meters arrangement, for 0$<\alpha<$ 0.015 in a single meter arrangement. [48] but when void fraction is higher, the accuracy decressed drastically. [9]

Note: all of these techniques are real-time response

CHAPTER 3

EXPERIMENTAL APPARATUS AND PROCEDURE

3.1 INTRODUCTION

This chapter describes the experimental apparatus and the properties of the selected refrigerant. R-12 (CFC-12, chlorofluorocarbon-12 or dichlorodifluoromethane) has been widely used as a working fluid for domestic refrigeraion systems and automobile air-conditioning systems. However, the release of R-12 to the atmosphere will adversely influence the earth's ozone layer depletion as well as increase the greenhouse effect. R-11 (CFCs) has been widely used in laboratory testing because its normal boiling point is 24 C at atmospheric pressure. However, all conventional refrigerants based on chlorofluorocarbons (CFCs) are scheduled for phaseout within few years due to the ozone layer depletion effects[50].

3.2 ALTERNATIVE REFRIGERANT

The solution suggested to cope with these potential problems is to develop suitable alternative refrigerants to replace the existing CFCs for heating, air-conditioning, and refrigerating equipment.

Among the potential substitutes, compound 1,1,1,2 tetrafluoroethane (HFC-134a or R-134a) has emerged as a leading candidate to replace the conventional refrigerant, dichlorodifluoromethane (CFC-12 or R-12), because its thermodynamic properties are relatively close to those of R-12. R-134a has ozone depletion potential (ODP) of 0.0 and global warming potential of less than 0.1 with respect to R-12. Table 3.1 gives the general features of R-12 and R-134a. Actually R-134a has already been chosen for automotive air-conditioning and home refrigerator applications, it continues to be evaluated for other refrigerating, air-conditioning and heat pump applications[50]. Many experimental studies for thermodynamic properties fo CFC alternative refrigerant R-134a can be found in recent ASHRAE transactions[51] to [56].

Table 3.1 General Features of FC-134a and CFC-12 [51]

	FC-134a	CFC-12
Chemical Formula	CF_3CH_2F	CCl_2F_2
Molar Mass	102.032	120.914
Boiling Point (K)	247	243
Critical Properties		
Tc (K)	374.30	385.01
Pc (MPa)	4.064	4.129
Dc (kg/m^3)	508	568
Freezing Point (K)	172	118
Flammability	none	none
Ozone Depletion Potential*	0	1.0
Global Warming Potential*	< 0.1	1.0

* Relative value to CFC-12

An experimental loop was designed and constructed to carry out various two-phase flow and boiling heat transfer studies using R-134a. The test loop is operated at saturation pressure of 607 kPa to 770 kPa, corresponding to saturation temperature of 22 C to 30 C respectively. The properties of R-134a saturated liquid and vapour are listed in Appendix A.

3.3 EXPERIMENTAL APPARATUS

3.3.1 Description of the Test Loop

Figure 3.1 shows a schematic diagram of the experimental facility. It is a closed refrigerant flow loop charged with R-134a as the working fluid. The main components of the loop are: the pump, electrically heated sections, steam heater, test section, pressurizer, condenser, service unit and various measuring devices.

The R-134a refrigerant was circulated through the loop by a gear pump driven by a variable speed electric motor. Heating was provided by means of direct electrical heating of sections of the loop and by a heat exchanger where steam was used to heat up the refrigerant. Direct electric heating was used in two sections of the loop. Each of the electrically heated sections was 1.8 m long thin-walled stainless steel tube having 12.7 mm outer diameter and 0.15 mm wall thickness. They were connected in parallel to the D.C. power supply and were electrically insulated from the rest of the loop by 10 cm long teflon tubes as shown in Figure 3.2. The electric power was supplied by a 100 kVA welder with a regulated current output of 0 to 100 Amp. The heated sections were connected in parallel to a water cooled stainless steel tube, identical to the heated sections, to reduce the power supply to the refrigerant loop. Additional heating was provided by a 1.2 m long single-pass shell-and-tube heat exchanger. The steam heating was only used to generate a completely dry refrigerant vapour which was required

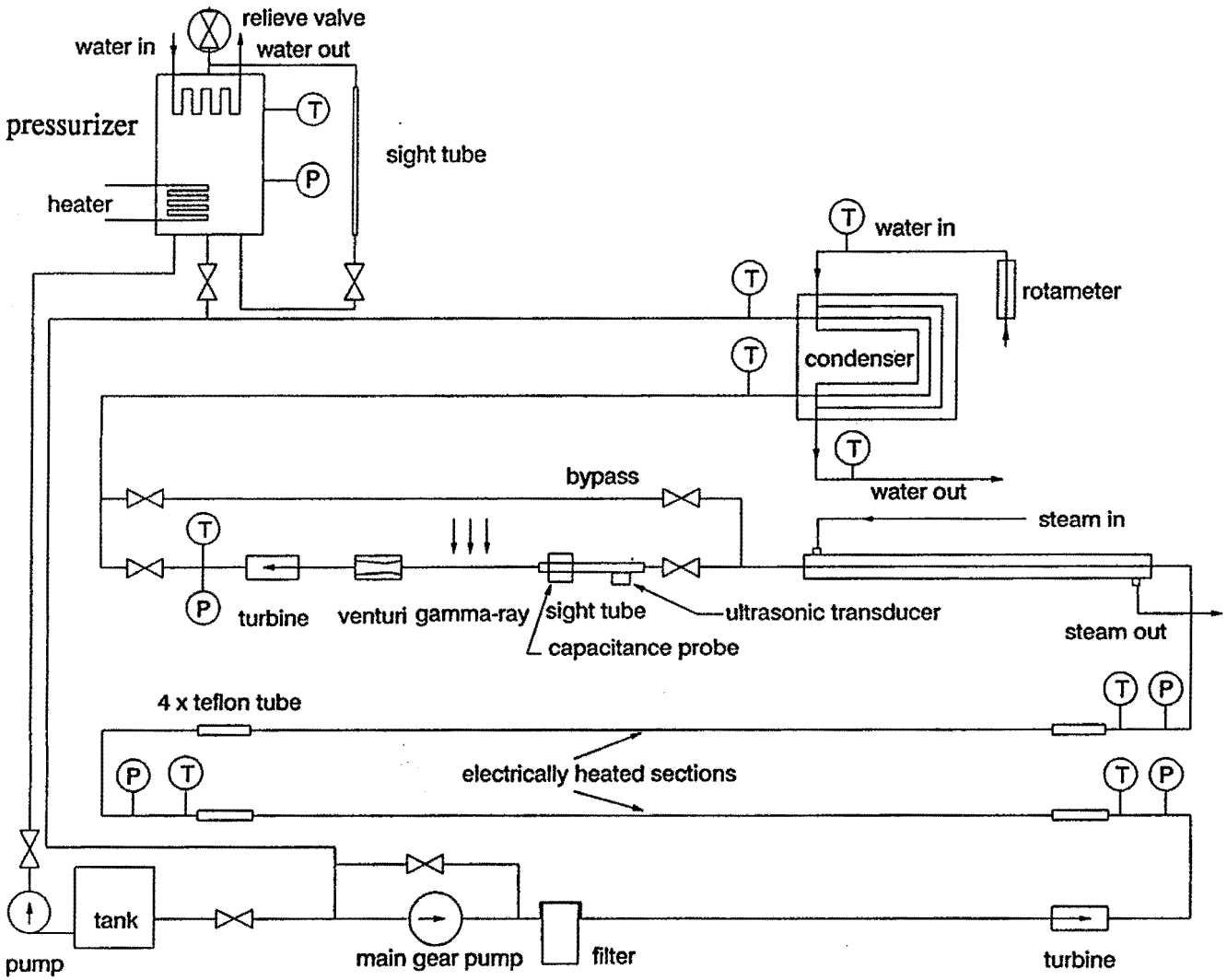

Fig. 3.1 Schematic Flow Diagram of Test Facility

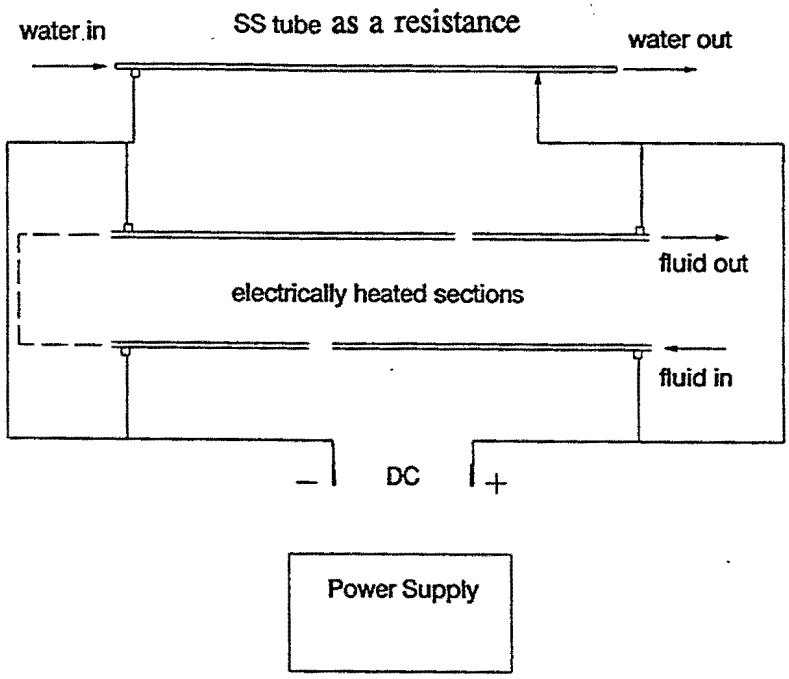

Fig. 3.2 Power Supply on Heated Sections

for calibrating the gamma-densitometer and the capacitance transducer. The condenser was a water cooled heat exchanger of 30 kw capacity.

A pressurizer (15.24 cm in diameter x 30.48 cm height) was used to control the system pressure in the range of 0.276 MPa to 0.9 MPa. The pressure was also controlled by a combination of an immersed electric heater and a water cooling coil. A sight tube was used to indicate the liquid level in the pressurizer. When the system pressure needed to be increased, the heater, which has a power of 1 kw, was switched on to raise the temperature of the refrigerant in the pressurizer. If the system pressure was required to be decreased, the heater was switched off and/or cold water flow was introduced.

A service unit, consisting mainly of a small gear pump and a reservoir, was incorporated in the loop to facilitate charging and emptying the loop of the refrigerant.

Two rotameters covering different flow rate ranges were used to measure the cooling water flow rate of the condenser. Cooling water through the condenser could also be used to adjust the system pressure or temperature of the loop. The calibrations of the two rotameters are given in Appendix B.

The mass flow rate of the single liquid phase refrigerant flow is measured by a turbine flowmeter (OMEGA FTB-101 seial# 43563) located at the inlet of the heated section. A filter was used to protect the turbine flowmeter from impurities. Another turbine flowmeter (serial# 44291) was used to measure the two-phase mass flow rate in the test section. The calibration curves for these turbine flowmeters are shown in Appendix C. These turbine flowmeters have a low mass rotor design that allows for rapid dynamic response. The accuracy offered by the manufacturer is $\pm 1/2\%$ of the reading. The standard calibration provided with these turbine flowmeters consists of a 10 point water calibration over the linear flow range of the meter. This is suitable for fluids with viscosities less than or equal to water (1 cp for water, 0.21 for R-134a at 25 C). A frequency-voltage converter and a power supply of $\pm$ 15 volts were used to convert frequency output from the turbine flow meters to voltage signals.

A venturi flowmeter, which is designed based on the ASME standard, is located in the test section for the measurement of two-phase mass flow rate. Detailed information about the design of the venturi and its calibration is given in Appendix D. Two differential pressure transducers (Validyne type) of 6.89 kPa (1 psi) and 34.47 kPa (5 psi) range were used to measure the pressure drop generated in the venturi flowmeter, where the accuracy of the pressure transducers is 0.1 %.

The refrigerant temperature in both subcooled single phase and saturated two-phase conditions is measured with T-type thermocouples inserted in Swaglok fittings in different key measurement points as shown in Figure 3.1. The accuracy of the thermocouples is better than ± 1 C.

The two-phase flow pressure in the test section is measured using a pressure transducer (Heise-621 model). Several static pressure gauges positioned at strategic points in the system were also used to monitor the pressure around the loop.

3.3.2 Test Section

A schematic diagram of the test section is shown in Figure 3.3. The test section contains a venturi flowmeter, a turbine flowmeter (serial# 44291), and a transparent tube, as well as pressure and temperature measurement points. The venturi flowmeter and turbine flow meters were used to determine phase velocities. The capacitance transducer, ultrasound transducer and gamma-densitometer were used to determine the void fraction. The capacitance transducer and ultrasound transducer were installed on the transparent tube, while the gamma-densitometer was installed vertically at the stainless steel tube between the transparent tube and the venturi flowmeter. The gamma-densitometer consisted of a Co-57 gamma source and a NaI(Tl) scintillator. The gamma beam was collimated using steel plates as shown in Figure 3.4. The sensitivity of the gamma-

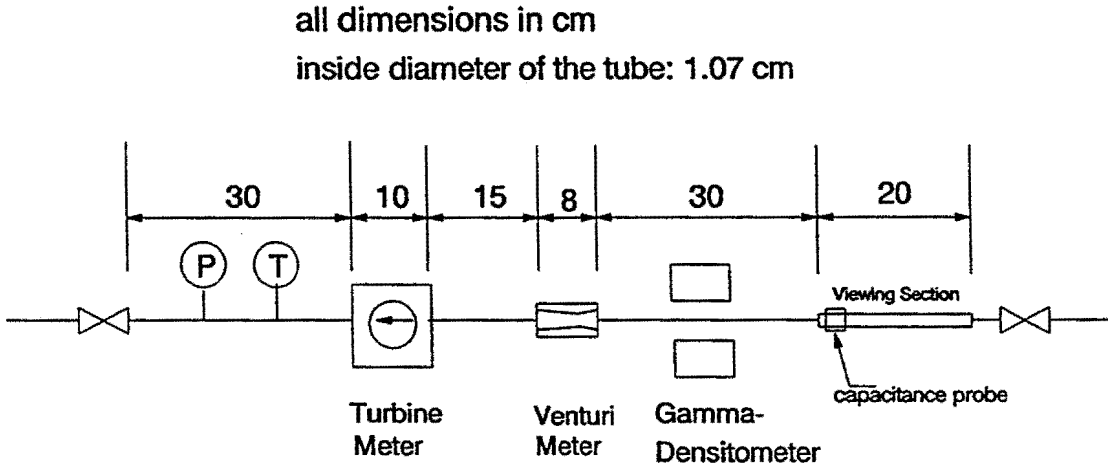

Fig. 3.3 Test Section

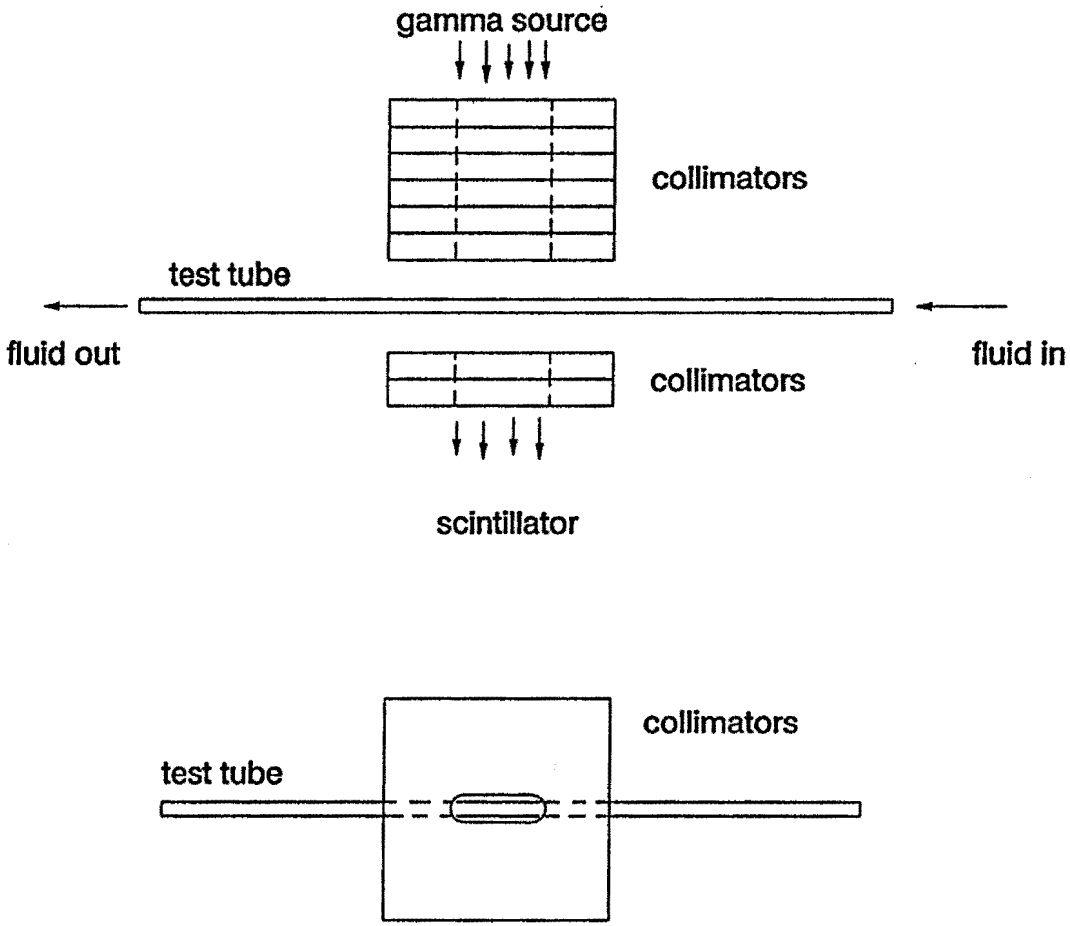

Fig. 3.4 Arrangement of Collimators

densitometer is discussed in Chapter 4. The transparent tube, which had an inside diameter of 9.7 mm and thickness of 1.5 mm, was used as a window to observe the flow patterns during two-phase flow. It also provided a suitable non-conducting section on which the capacitance transducer was installed. A bypass section parallel to the test section was used to facilitate disconnecting the test section without having to recharge the loop completely. The bypass was also used for calibrating the capacitance transducer and gamma-densitometer as will be described later in Appendix E.

3.3.3 Charging of the Loop

The test loop is designed to stand a maximum pressure of 1.034 MPa (150 psig). If the pressure during experimention reaches this critical value, a relief valve located in the top of the pressurizer will open automatically to relieve the excess pressure.

To fill the loop with the refrigerant, the following procedure was followed:

a. Connect the loop to a vacuum pump to partially remove the air and purge the loop with nitrogen.

b. Set the refrigerant supply tank to a position higher than the pressurizer and connect the tank's charging unit to the valve at the top of the pressurizer.

c. Open the tank valve and the pressurizer valve to allow the liquid to flow into the loop until the heater in the pressurizer is covered.

During the late stages of charging the loop, it was possible that the pressure difference between the supply tank and the loop would decrease to near zero. In this case, loop charging was reestablished by lowering the loop pressure. This was achieved by either increasing the cooling water flow in the presurizer and the condenser, or by

heating up the supply tank using warm water. The loop required about 5.5 kg of R-134a refrigerant to be completely charged.

This loop was well insulated by fiberglass so that heat losses were minimized.

3.4 EXPERIMENTAL PROCEDURE

Operating pressures ranging from 0.607 MPa to 0.77 MPa, with the corresponding saturation temperatures ranging from 22 to 30 C, were chosen for the current experimental program.

The steady saturated two-phase flow condition was reached by heating up the subcooled fluid through the electrically heated sections, and then cooling down to subcooled fluid through the condenser before being passed through the main pump.

Before the refrigerant was circulated, cold water was circulated through the condenser and through the stainless steel tube used to control the applied power. Using the speed control of the pump, the refrigerant flow rate was adjusted to the required value. When the temperature of the refrigerant decreased below the saturation temperature, the power was applied to the heated sections to heat up the fluid. Steady state saturated two-phase flow can be maintained by adjusting the flow rate of cold water flowing through the condenser for a given single phase refrigerant flow and power input. The experimental data was acquired using a computer based data acquisition system. The duration of the data acquisition was 100 seconds during which both dynamic history and time-averaged values of each measured parameter were recorded at a frequency of 10 Hz.

The conditions tested during the experiments were in the ranges:

input power: 0.15 to 3.0 kW

system pressure (absolute): 607 to 770 kPa

inlet refrigerant temperature: 10 to 20 C

inlet mass flow rate: 0.02 to 0.12 kg/sec

saturated refrigerant temperature in the test section: 22 to 30 C

volumetric flow rate of two-phase flow in the test section: 1.0 to 15.0 liter/min

void fraction: 0 to 0.9

quality: 0 to 0.5

CHAPTER 4

INSTRUMENTATION OPERATING PRINCIPLES

4.1 INTRODUCTION

Most of the existing instruments used to measure mass flow rate were developed for single phase flow systems. For applications to two-phase flow, it is assumed that these instruments can be applied in two-phase flow through careful calibration of the instrument for the particular flow system. This calibration is expected to include a second independent measurement as explained earlier. It is also useful to note that most previous attempts to develop techniques for two-phase mass flow rate measurements have focused on steam-water and air-water systems.

In many laboratory applications [7,8,36], measurements of the two-phase mass flow rate were obtained in a discontinuous way by sampling the two-phase flow mixture for a known time increment and by weighing the collected mass of each phase. This is a very complicated method for many applications, especially for the refrigeration and air-conditioning industries. Several instruments have been developed for continuous measurements in gas-liquid two-phase flow as summarized by Reimann [45].

It has to be pointed out that most of these instruments measure the mass flow rate indirectly, e.g. by recording its influence on related parameters such as temperature, drag on a plate, pressure drop through a device etc. In addition, when some information on the mixture composition, such as mixture density or void fraction is obtained, the individual mass flow rate or total two-phase mass flow rate can be computed, if the composition and the measured quality are in the calibrated range of the instrument.

In this chapter, description of instruments used for measuring two-phase mass flow rate in the present refrigerant test loop and their basic principles will be given. The venturi flowmeter and turbine flowmeter have been employed for mass flow rate measurements. The capacitance void meter, gamma-densitometer and ultrasonic pulse-echo technique were used for void fraction or mixture density measurements. It is possible to measure a real-time on-line mass flow rate by following the method mentioned above, computing information from individual instruments using a suitable model to obtain the two-phase mass flow rate.

4.2 MASS FLOW MEASUREMENT

The principle of both the venturi flowmeter and the turbine flowmeter is well-understood when applied to single phase flow, but questions regarding their correct functioning arise when applied to two-phase flow.

4.2.1 Venturi Flowmeter

Because small size venturi flowmeters (for pipe size less than 5.08 cm (2")) are not available commercially, a venturi flowmeter with a diameter ratio 0.59 for 1.27 cm (1/2") pipe was designed and made in accordance with the ASME specifications. Figure D.1 in Appendix D gives the venturi flowmeter and its dimensions. Since this device has a diffuser section at its exit, it allows the fluid pressure to recover smoothly and hence it gives excellent pressure recovery when compared with orifice plates or nozzles which cause substantial pressure head loss. Detailed information about the venturi flowmeter is shown in Appendix D.

For single phase fluid flow in a horizontal channel, the mass flow rate M is related to the pressure drop across the venturi flow meter by the following equation:

$$M=K\sqrt{\Delta P\rho} \tag{4.1}$$

where ΔP is the pressure drop across the device (differential pressure between the upstream pressure and the throat pressure), ρ is the density of the fluid, K is the flow coefficient which depends on the geometry of the venturi flowmeter, Reynolds number, and the discharge coefficient. It should be a constant for a specific venturi flowmeter.

For two-phase flow in a horizontal channel, the two-phase mass flow rate and two-phase pressure drop can be expressed in a similar form, if an appropriate two-phase fluid density is used in place of the single phase fluid density and some assumptions are taken into account:

$$M=K_{TP}\sqrt{\Delta P_{TP}\rho_{TP}} \tag{4.2}$$

where K_{TP} is a constant determined by calibration.

Detailed information about different mixture densities used in two-phase flow and different model for calculating the two-phase mass flow rate using a venturi flowmeter are given in Chapter 5.

4.2.2 Turbine Flowmeter

The turbine flowmeter is a volumetric measuring flowmeter. The flowing fluid engages the vaned rotor causing it to rotate at an angular velocity proportional to the fluid volumetric flow rate. The angular velocity of the rotor results in the generation of an electrical signal which is picked up as a meter output by an externally mounted pick-up unit. Summation of the pulsing electrical signals relates directly to the total volumetric flow.

In single phase fluid flow, the rotational frequency of the turbine flowmeter f is proportional to the volumetric flow rate Q_t for a given fluid viscosity:

$$f=\lambda Q_t \tag{4.3}$$

where Q_t is the volumetric flow rate, l/min, λ is the flow coefficient of the turbine meter.

The volumetric flow rate can be expressed in a form of the velocity of the fluid by:

$$Q_t=U_t A \tag{4.4}$$

where U_t is the cross section averaged velocity of the fluid and A is the cross section area.

The λ value is normally provided by the manufacturer along with the turbine flowmeter.

Detailed information about the calibration of the turbine flow meter is given in Appendix C.

The single phase mass flow rate from a turbine flowmeter can be expressed by:

$$M=\rho Q_t \tag{4.5}$$

where M is the mass flow rate and ρ is the density of the fluid.

In two-phase flow, the two-phase mass flow rate from the turbine meter can be expressed by:

$$M=\rho_{TP}Q_{TP}=\rho_{TP}\frac{f}{\lambda_{TP}} \tag{4.6}$$

where Q_{TP} is the two-phase volumetric flow rate, ρ_{TP} is the mixture density and the λ_{TP} is the flow coefficient of the turbine meter in two-phase flow which is independent of the pressure and equal to single phase flow coefficient.

From the principles of turbine and venturi flow meters, one may find that the key to determining two-phase mass flow rate is to find a formulation of the mixture density of two-phase flow. The mixture density, however, is a function of void fraction or

quality. Some models dealing with the mixture density for turbine flowmeters are given in Chapter 5.

4.3 VOID FRACTION MEASUREMENT

Three measurement techniques were used to determine void fraction during the present experiments. Gamma-densitometers and capacitance transducers can be used to determine void fraction. The ultrasonic transducer can be used to measure more local volume averaged void fraction. Both capacitance and ultrasonic techniques can be used to monitor the dynamic behaviour of two-phase flow and give real-time knowledge of void fraction and flow patterns.

4.3.1 Capacitance Transducer

Among several techniques employed for void fraction measurements, the capacitance method is advantageous because it virtually gives an instantaneous response. Its design is relatively simple and it is cheap to construct compared to other methods. The output of the capacitance void meter is an analog voltage signal suitable for process control. The method is based on the difference between the dielectric constants of the two phases. Capacitance is proportional to the dielectric constant of test fluid. The sensitivity of the technique is improved when the difference between the dielectric constants of the two phases is increased.

Consider a simple two ring capacitance transducer as shown in Figure 4.1. The normalized capacitance Cp^* and the void fraction α are defined as:

$$Cp^* = \frac{Cp - Cp_v}{Cp_l - Cp_v} \tag{4.7}$$

$$\alpha = \frac{V_g}{V} \tag{4.8}$$

where Cp^* is the dimensionless capacitance, Cp_v is the capacitance of full vapour, Cp_l is the capacitance of full liquid, Cp is the equivalent capacitance of the two-phase flow mixture, α is the volumetric void fraction, V_g is the volume of the vapour and V is the volume covered by the capacitance transducer.

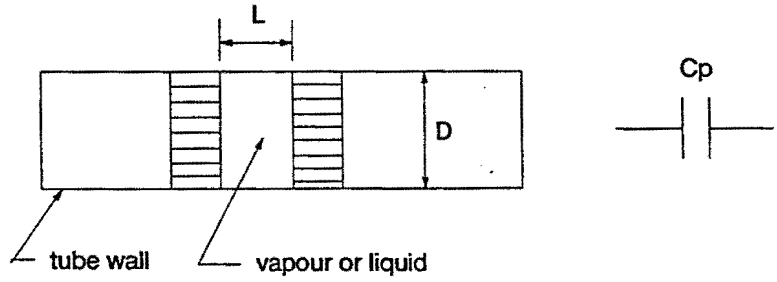

Fig. 4.1 Schematic Diagram of Two Ring Electrodes and Equivalent Capacitance Circuit

In the configuration of the ring capacitance transducer, if an ideal condition is assumed and the radial electric field can be neglected between the two ring electrodes, then the equivalent capacitance between the ring electrodes may be simplified when the axial electric field is constant along the axial direction. In addition, for the expression of dimensionless capacitance given in the above equation, the equivalent capacitance of the tube wall also can be neglected because it always connects the fluids as a parallel capacitance. This equivalent capacitance circuit method only considers that two or more phases can be analyzed in the form of series or parallel connections of the capacitances between parallel plate electrodes as shown in Figure 4.1 and Figure 4.2. Therefore, the capacitances for full vapour Cp_v and for full liquid Cp_l can be written as:

$$Cp_v = \frac{A}{L}\varepsilon_g \tag{4.9}$$

$$Cp_l = \frac{A}{L}\varepsilon_f \tag{4.10}$$

where A is the area of the cross section, L is the distance between two ring electrodes, ε_g and ε_f are the dielectric constants of vapour and liquid respectively.

The equivalent capacitance of an idealized stratified flow pattern between two ring electrodes as shown in Figure 4.2(a) can be theoretically approximated as a parallel connection of the liquid and vapour capacitance[12] by:

$$Cp = Cp_g + Cp_f \tag{4.11}$$

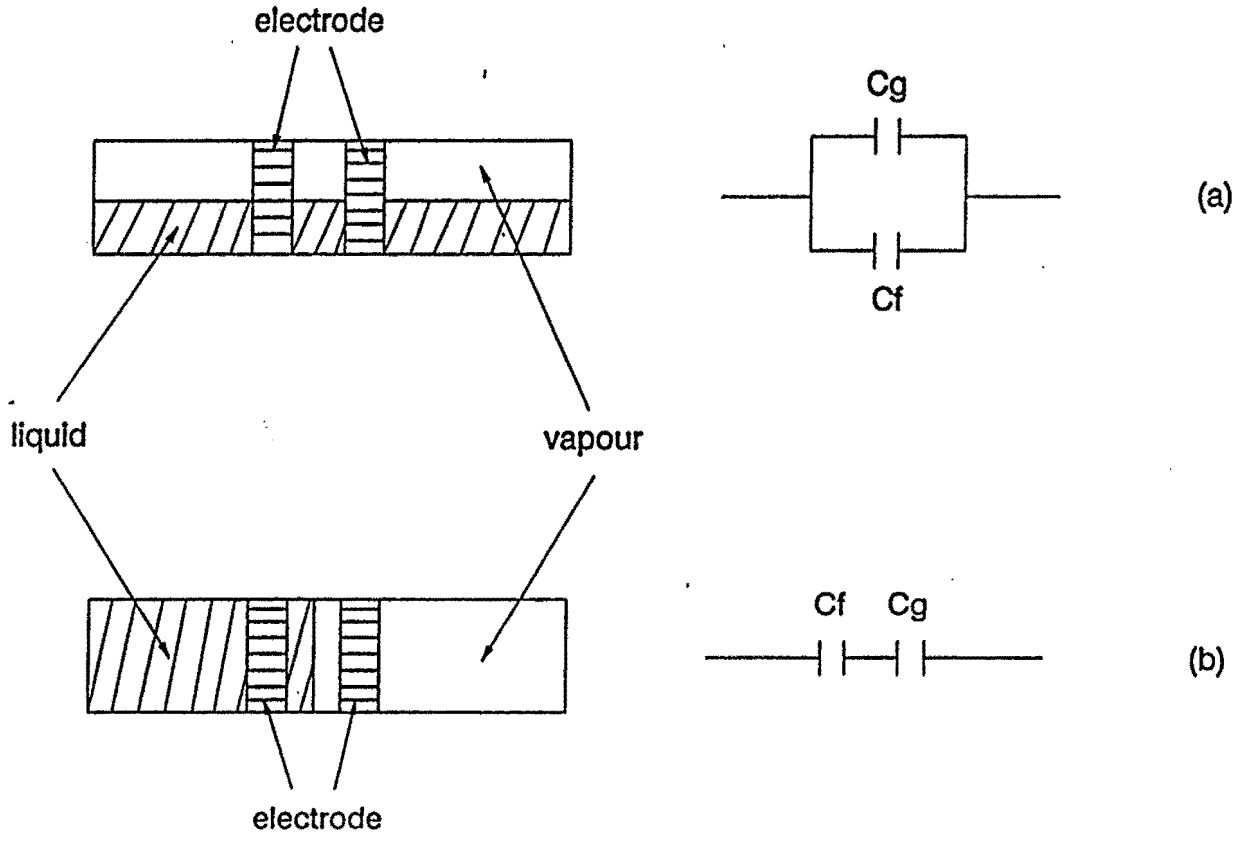

Fig. 4.2 The Flow Regimes and The Correspondent Equivalent Capacitance Circuit for a Ring Electrodes

where Cp_g and Cp_f are determined by the relative dielectric constants ε_g of vapour and ε_f of liquid and void fraction. That is:

$$Cp=\frac{A_g}{L}\varepsilon_g+\frac{A_f}{L}\varepsilon_f \tag{4.12}$$

where A_g and A_f are the net area occupied by the vapour and liquid on the electrode surfaces. So, Cp can be rewritten as:

$$Cp=\frac{A}{L}[\alpha\varepsilon_g+(1-\alpha)\varepsilon_f] \tag{4.13}$$

Substituting Cp into Cp^*, one may obtain a simple formulation of Cp^* and void fraction which does not depend on the dielectric constants of the fluid:

$$Cp^*=1-\alpha \tag{4.14}$$

On the contrary, for an idealized slug flow regime, as shown in Figure 4.2(b), the capacitance is characterized by a series connection[12]:

$$Cp=\frac{Cp_g Cp_f}{Cp_g+Cp_f} \tag{4.15}$$

Substituting into the equation (4.7) for Cp^*, another formulation for the slug flow regime may be expressed by:

$$Cp^* = \frac{1}{1 + \frac{\varepsilon_f}{\varepsilon_g}\frac{\alpha}{(1-\alpha)}} \tag{4.16}$$

From the above equation, one may find that, similar to equation (4.14), Cp^* decreases linearly with void fraction α when the values of $\varepsilon_f/\varepsilon_g$ approaches to unity.

However, for the multi-ring configuration of the capacitance transducer used in this experiment, it is much more complicated and difficult to give a simple analytical formulation to explain the relationship between the capacitance and the void fraction. Therefore, a calibration curve made with the ultrasonic technique is given in Appendix E.

4.3.2 Gamma-Densitometer

The gamma-ray attenuation technique is widely used for void fraction measurement in two-phase flow because it is a non-intrusive method. The schematic diagram of the gamma densitometer is shown in Figure 4.3. The device used in the present work consisted of a sealed gamma source (Co-57), beam collimator, a scintillator and a signal processing system. The overall arrangement of the gamma-densitometer is given in Chapter 3. The principle of the gamma ray attenuation technique is that, for a given tested material, the intensity of a collimated gamma beam decreases exponentially as it goes through the tested material. The attenuation is described by Beer's law [2]:

$$I = I_0 e^{-\mu x} \tag{4.17}$$

where I is the intensity of the gamma beam, I_0 is the incident intensity of the gamma beam, μ is the absorption coefficient of the material, and x is the distance the beam

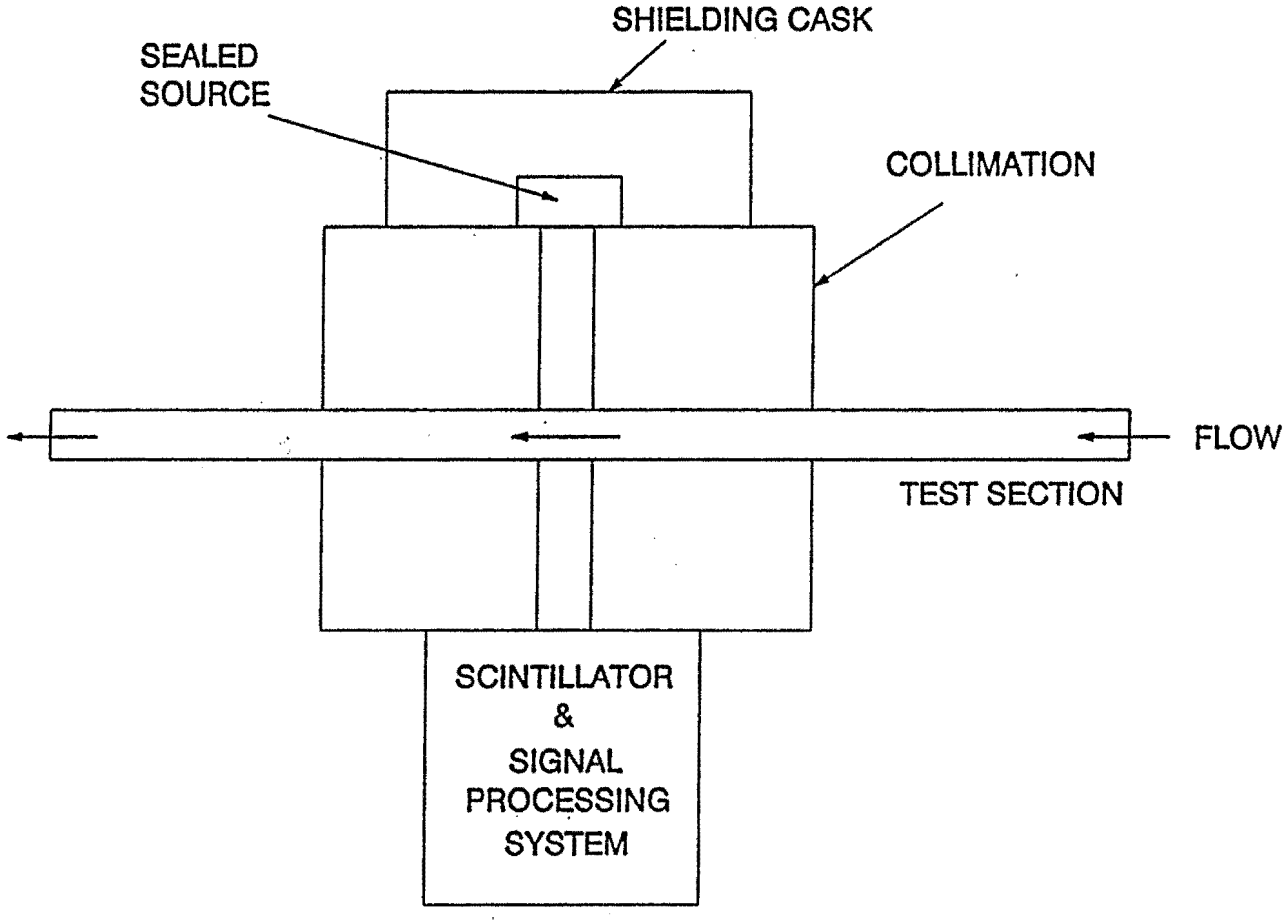

Fig.4.3 Schematic Diagram of a Gamma-Densitometer

passes into the material.

For a test condition under which vapour-liquid mixture refrigerant flows through a stainless steel tube, the measured intensity of the two-phase flow, taking the same character I, may be expressed by:

$$I=I_0 e^{-2\mu_{ss}\delta} e^{-(\mu_g \alpha+\mu_f(1-\alpha))d} \tag{4.18}$$

where μ_{ss} is the absorption coefficient of the tube, δ is the thickness of the tube, μ_g and μ_f are the absorptions of vapour and liquid respectively, d is the inside diameter of the tube and α is the volumetric averaged void fraction.

If the test tube is completely filled with liquid (α = 0) and with vapour (α = 1), then the measured intensities of complete vapour and complete liquid are given by:

$$I_f=I_0 e^{-2\mu_{ss}\delta} e^{-\mu_f d} \tag{4.19}$$

$$I_g=I_0 e^{-\mu_{ss}\delta} e^{-\mu_g d} \tag{4.20}$$

Combining above equations yields the average void fraction as:

$$\alpha=\frac{\ln(\frac{I}{I_f})}{\ln(\frac{I_g}{I_f})} \tag{4.21}$$

For stratified flow, if the gamma beam is parallel to the interface[61], the above equation can be approximated by:

$$\alpha=\frac{I-I_f}{I_g-I_f} \tag{4.22}$$

For the measurements of the gamma ray attenuation intensity in the experiments, I, I_f and I_g are the accumulated counts in a given period of time.

The gamma source used is Cobalt-57 (Co-57) which has principle peak photon energies of 7.0, 14.4, 122.0 and 136.5 keV. The principle photon energy of 122.0 keV was used. The scintillator used for gamma ray detector is NaI(T1), thallium activated sodium iodide. Its high light output yields good energy resolution and its detection efficiency is close to 100% for low energy gamma rays (<200 keV) [32].

For a single beam gamma densitometer operating in the count mode, the errors involved are: 1) geometric and flow regime related errors and 2) statistical error [2]. The first type of error cannot be expressed in a simple mathematic formula. The statistical error is given by Chan and Banerjee [32] as:

$$e=\frac{\sqrt{N}}{S\bar{N}} \tag{4.23}$$

and

$$N=IA_d\theta\eta \tag{4.24}$$

where N is the detector counting rate, A_d is the detector area, θ is the counting interval, η is the detector efficiency, $\overline{N}$ is the average value of the detector counting rate for the complete vapour and complete liquid, S is the sensitivity of the gamma ray to the tested material, and expressed by:

$$S=\frac{I_g-I_f}{\bar{I}}=\frac{I_g-I_f}{\frac{I_g+I_f}{2}} \tag{4.25}$$

The statistical error is inversely proportional to the sensitivity. For a given count rate, the higher the sensitivity, the smaller the error will be.

The sensitivity of the gamma densitometer to refrigerant R-134a was obtained experimentally and equal to about 12% for the present test configuration. The statistical error was less than 2%.

4.3.3 Ultrasonic Pulse-Echo Technique

Application of the ultrasonic techniques to the determination of interfacial parameters and flow regimes in two-phase flow were reported by Chang et al.[21,22]. The advantage of this technique is that it can be used to measure liquid level and void fraction instantaneously. It also can be used to determine two-phase flow regimes. In the present work, the ultrasonic pulse-echo technique is used in both the calibration of the capacitance void meter under static conditions and the determination of the flow patterns under steady state two-phase flow conditions.

A schematic diagram of the ultrasonic pulse-echo technique applied to a horizontal two-phase flow system with a typical ultrasonic waveform corresponding to smooth

stratified vapour-liquid flow are shown in Figure 4.4 (a) and (b) respectively. When an initial pulse waveform from the transducer is propagated through the wall of the tube and meets the wall-liquid interface, both reflection and transmission occur. Part of it is reflected by the wall-liquid interface and received by the transducer. The rest of the pulse wave continues to pass through liquid and is reflected by the liquid-vapour interface and received again by the transducer. Attenuation of the ultrasound wave during passing through solid and liquid is much smaller than that in the vapour or at the liquid-vapour interface for ultrasonics in the MHz range[22]. For the case of the liquid-gas interface, almost 99% of the incident wave is reflected back. This phenomenon is the basis for the application of the ultrasonic technique in two-phase flow systems[23].

The liquid level in the tube can be determined by measuring the time of flight of the pulse wave. Furthermore, the void fraction for the stratified flow also can be determined from the liquid level. Detailed information about the determination of the liquid level by ultrasound method is given in Appendix E.

The flow regime characterization using the ultrasonic technique can be made by continuous determination of the liquid level. Chang et al.[21,22] have developed a data acquisition system for the ultrasonic pulse-echo technique which can detect the instantaneous locations of gas-liquid interface over a period of time and directly output a collection of 1024 data points which indicate the various flow patterns.

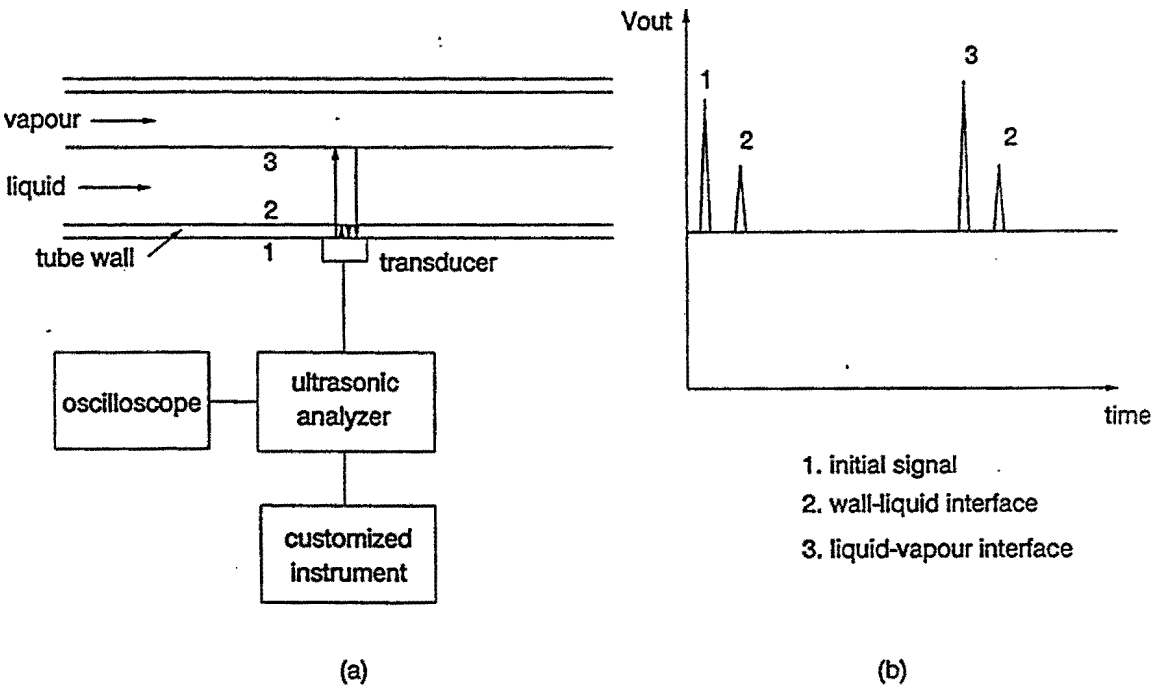

Fig. 4.4 (a) Schematic Diagram of Test Set-up for Horizontal Two-Phase Flow System
(b) Ideal Ultrasonic Waveforms Corresponding to Stratified Two-Phase Flow

CHAPTER 5

EXPERIMENTAL RESULTS AND DISCUSSION

5.1 INTRODUCTION

Experimental determination for refrigerant R-134a two-phase mass flow rate under steady-state flow conditions has been carried out at pressures between 607 kPa to 770 kPa corresponding to saturation temperatures of 22 C to 30 C. Instruments used for the measurement of void fraction were the capacitance transducer and gamma-densitometer. The ultrasonic pulse-echo technique was also used to characterize the flow regime during two-phase flow. The turbine flowmeter and venturi flowmeter were used to determine the two-phase mass flow rate. The individual phase density and the other properties for R-134a used are the saturated liquid and vapour values. Selective analytical models are used for prediction of the experimental results obtained by the turbine and venturi flow

meters. The typical dynamic response of each instrument and the determination of the two-phase mass flow rate by those models are provided and comparisons between the various models are made.

5.2 FLOW PATTERN CHARACTERIZATION

Flow pattern characterization has been made by using the instantaneous output of the ultrasonic transducer. In the present experiments, a collection of 1024 data points in 10 seconds for each test can be stored in the computer and analyzed to indicate different flow patterns.

Figure 5.1 gives a full liquid flow through the transparent tube. The data point fluctuation around 9.7 mm (full with liquid inside the pipe) is probably caused by temperature fluctuations because the sound speed in refrigerant R-134a is temperature dependent. Figure 5.2 shows a strong wavy stratified flow with a low void fraction. Figure 5.3 shows a stable wavy stratified flow with a high void fraction. Figure 5.4 shows a typical plug/slug flow. Figure 5.5 is an enlarged waveform of figure 5.4. As

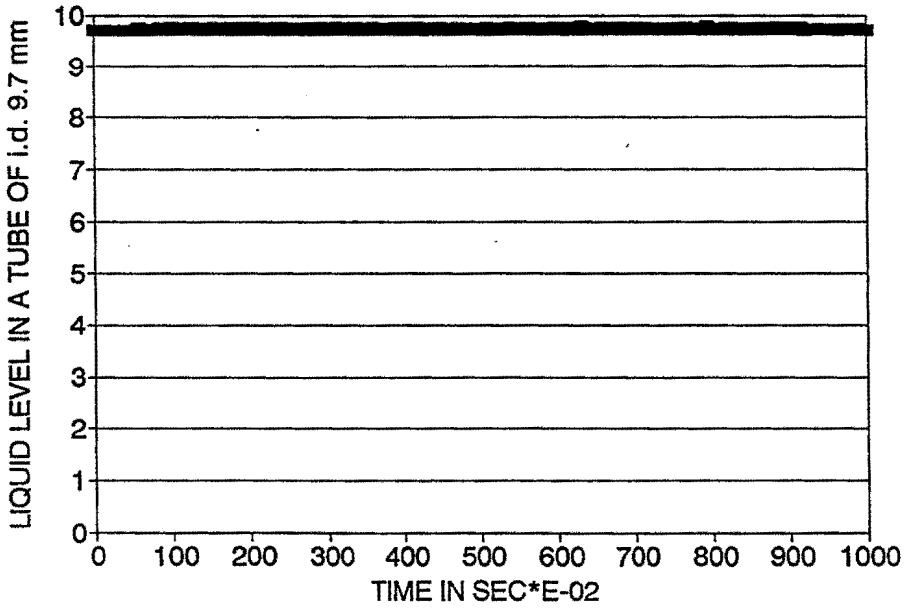

Figure 5.1 Typical liquid single phase flow output signals observed by a pulse-echo ultrasonic technique at M= 0.0 kg/sec, Q= 0.0 kw, T= 26 C

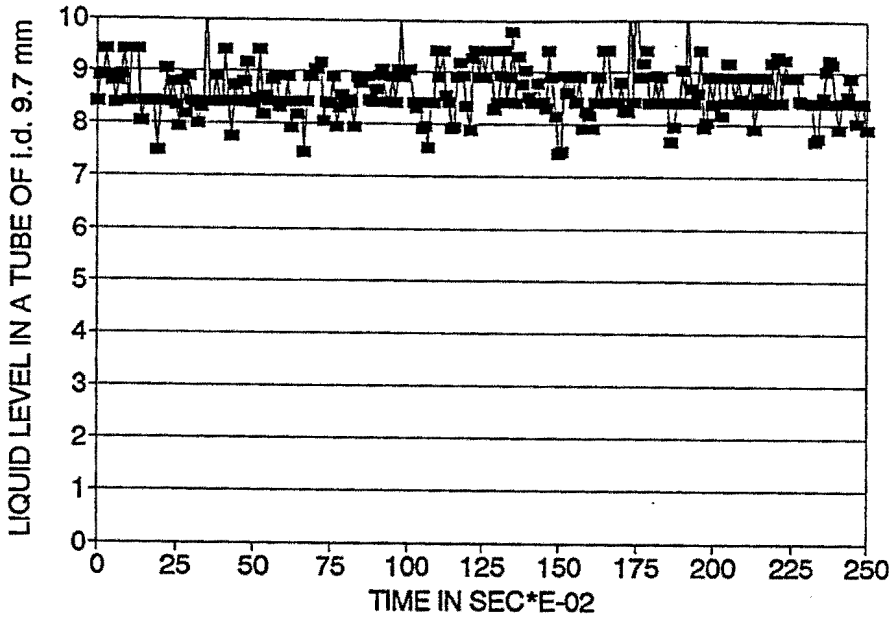

Figure 5.2 Typical stratified wavy flow output signals observed by a pulse-echo ultrasonic technique at M= 0.024 kg/sec, Q= 1.5 kw, Ts= 28.6 C

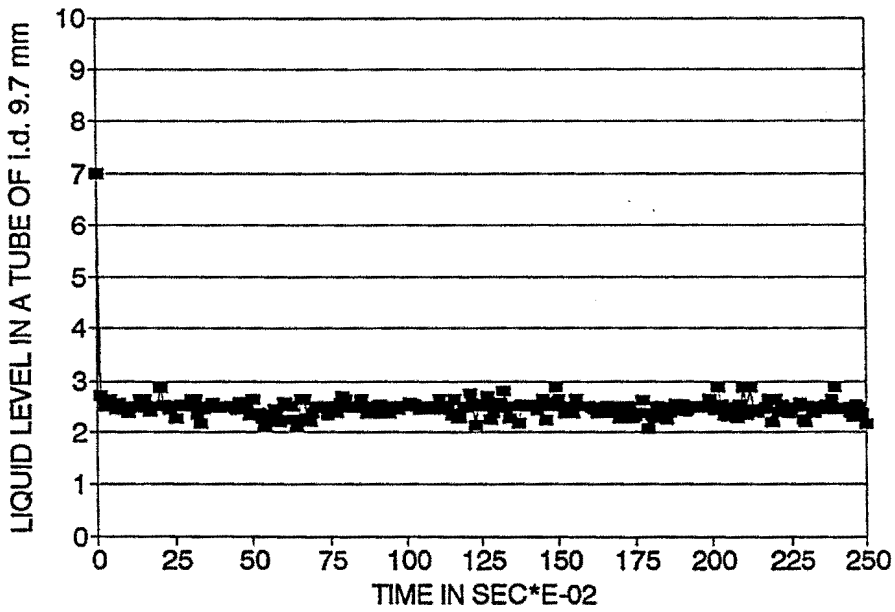

Figure 5.3 Typical stratified wavy flow output signals observed by a pulse-echo ultrasonic technique at M= 0.026 kg/sec, Q= 0.95 kw, Ts= 27 C

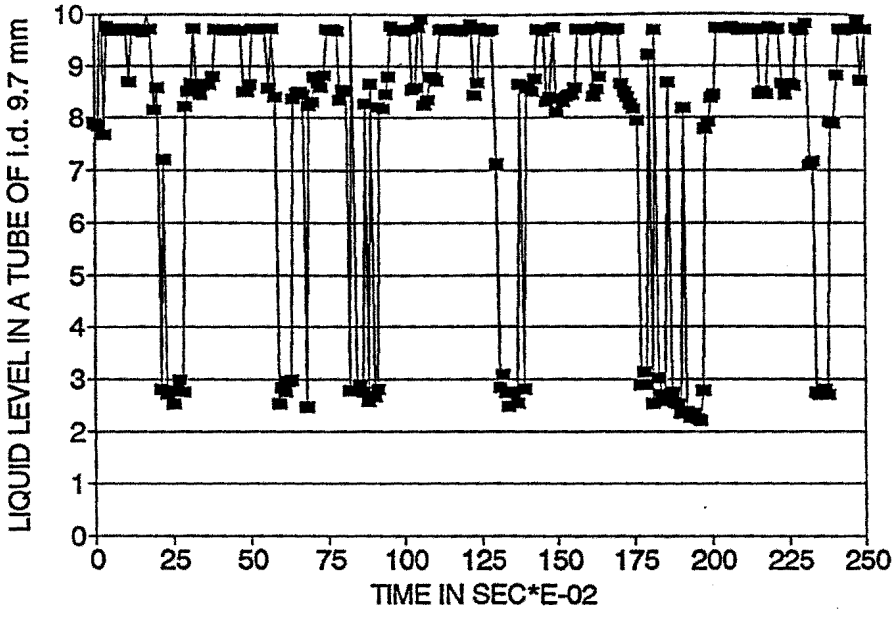

Figure 5.4 Typical slug/plug flow output signals observed by a ultrasonic technique at M= 0.025 kg/sec, Q= 0.6 kw, Ts= 26 C

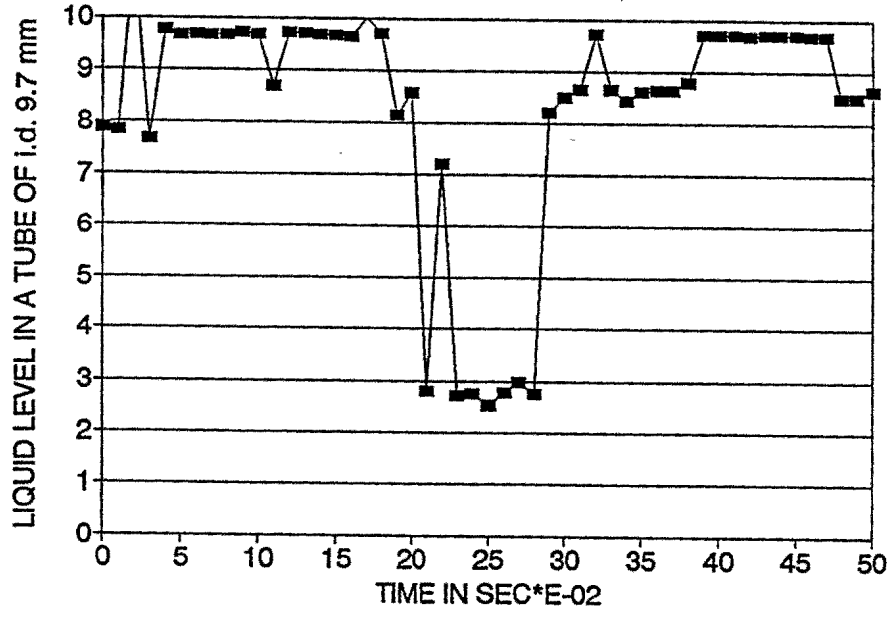

Figure 5.5 Enlarged waveform of slug/plug flow in Figure 5.4

shown, the passage of a complete liquid slug is identified by the time during which a liquid full tube is observed. The measurements of the ultrasonic transducer for flow regime identification were validated by visual observation.

The single beam ultrasonic technique has some limitations in identification of the flow regime and the measurement of void fraction[18,21]. It cannot identify annular flow. In addition, high density droplets entrained by high vapour flow which may contribute to void fraction determination also cannot be detected by the ultrasonic signals[21].

5.3 TYPICAL INSTRUMENTATION RESPONSE

Typical dynamic response of the other instruments is shown here. This is useful in presenting the nature of two-phase flow and can be used for future analysis of the dynamic behaviour of various instruments. The dynamic responses are shown here for a typical steady state experiment. However, the time averaged value are used for further analysis. In all the experiments, the instruments were sampled at a frequency of 10 Hz.

An example of one raw experimental data set for steady state R-134a two-phase flow is given here. The test conditions are given here in averaged values:

power supply: 1.103 kW
system pressure: 0.645 MPa or 93.6 psia (1 kPa = 0.145 psi)
total mass flow rate: 0.03438 kg/sec
inlet temperature: 12.7 C (subcooling condition at the inlet of the heated section)
saturated temperature: 25.1 C (saturated condition in the test section)
thermodynamic quality: 0.0844
output of capacitance void meter: 0.513 pf
void fraction by capacitance transducer: 0.555

void fraction by gamma-densitometer: not available

volumetric flow rate of turbine flowmeter in the test section: 4.5 l/min

density of liquid: 1202.9 kg/m^3

density of vapour: 31.89 kg/m^3

pressure drop through venturi flowmeter: 1.38 kPa or 0.2 psi (1 kPa = 0.145 psi)

The total mass flow rate was measured by the turbine flowmeter under subcooled single phase liquid conditions upstream of the heated section, where Figure 5.6 shows the transient mass flow rate as measured by the turbine flowmeter. In the test section, where two-phase flow existed, the pressure transducer recorded the pressure history as shown in Figure 5.7. Thermodynamic quality calculated based on enthalpy rise is shown in Figure 5.8. The capacitance transducer provided a void fraction transient as shown in Figure 5.9. The two-phase volumetric flow rate measured by the turbine flowmeter is shown in Figure 5.10 where the fluctuation is typical of two-phase flow. The pressure drop across the venturi flowmeter is shown in Figure 5.11. As shown, the fluctuations of the venturi flowmeter output have very large amplitude.

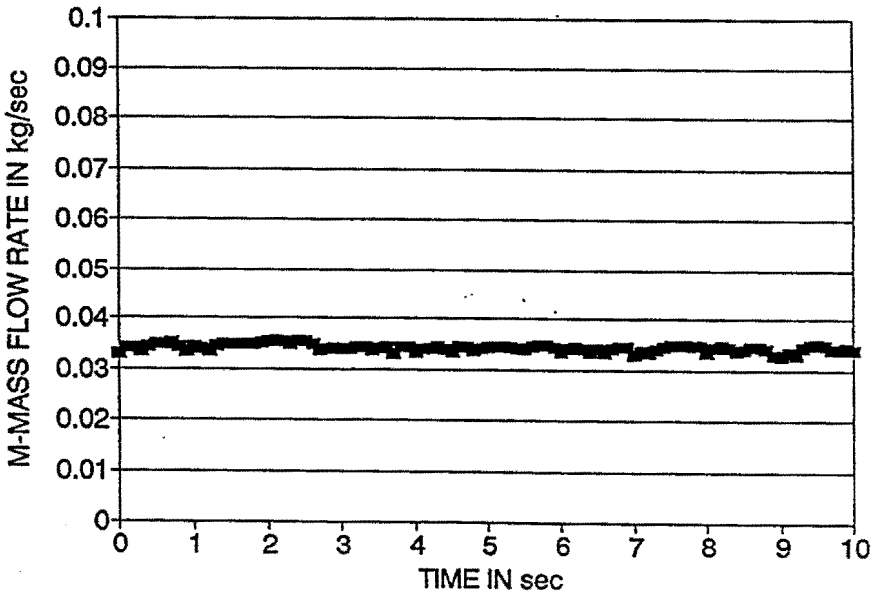

Figure 5.6 Typical mass flow rate transient measured by a turbine flowmeter (#43563) under R-134a two-phase flow

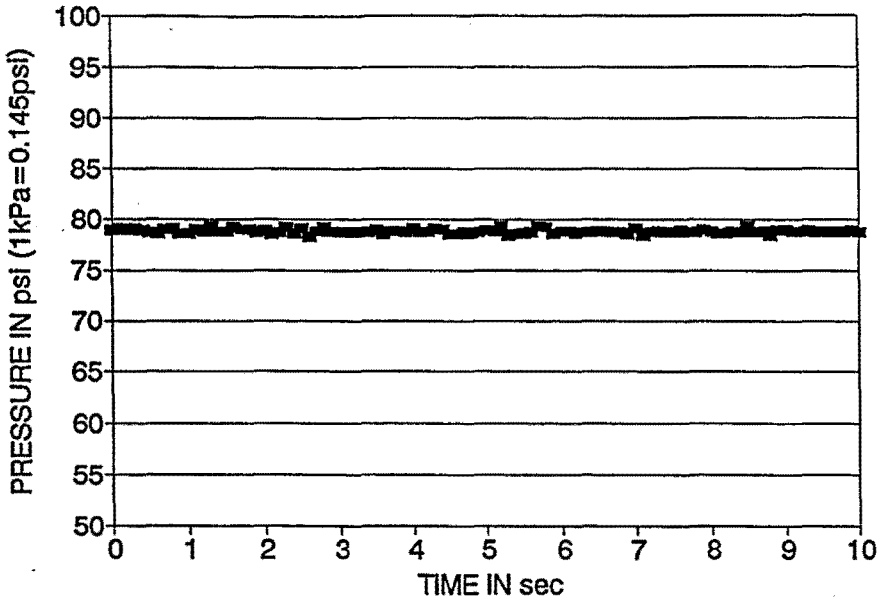

Figure 5.7 Typical transient pressure response measured by a pressure transducer under R-134a two-phase flow

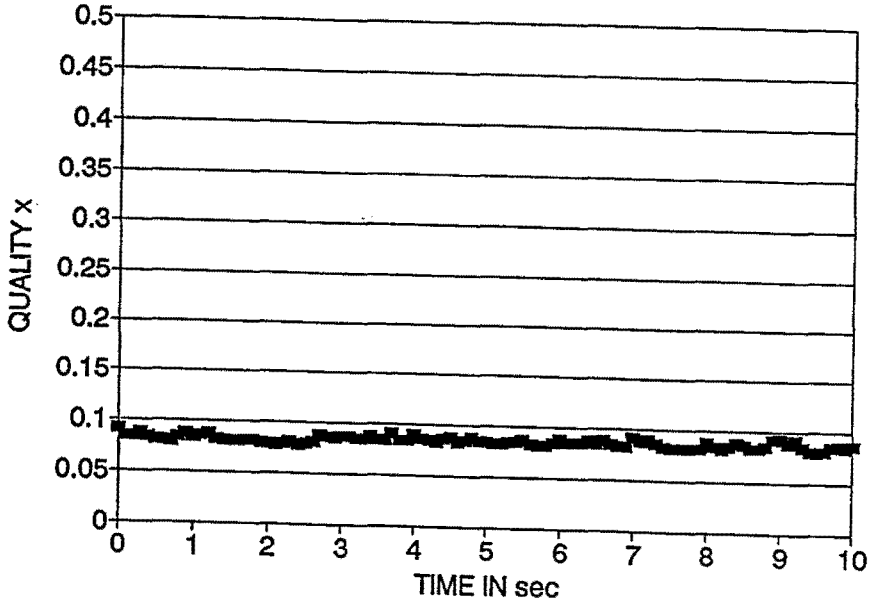

Figure 5.8 Typical thermodynamic quality transient under R-134a two-phase flow

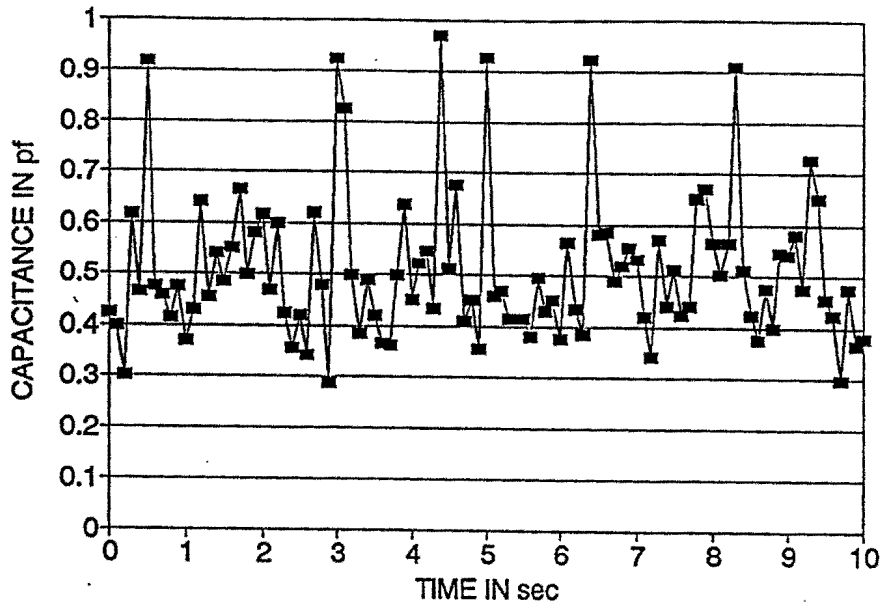

Figure 5.9 Typical capacitance transient measured by a capacitance transducer under R-134a two-phase flow

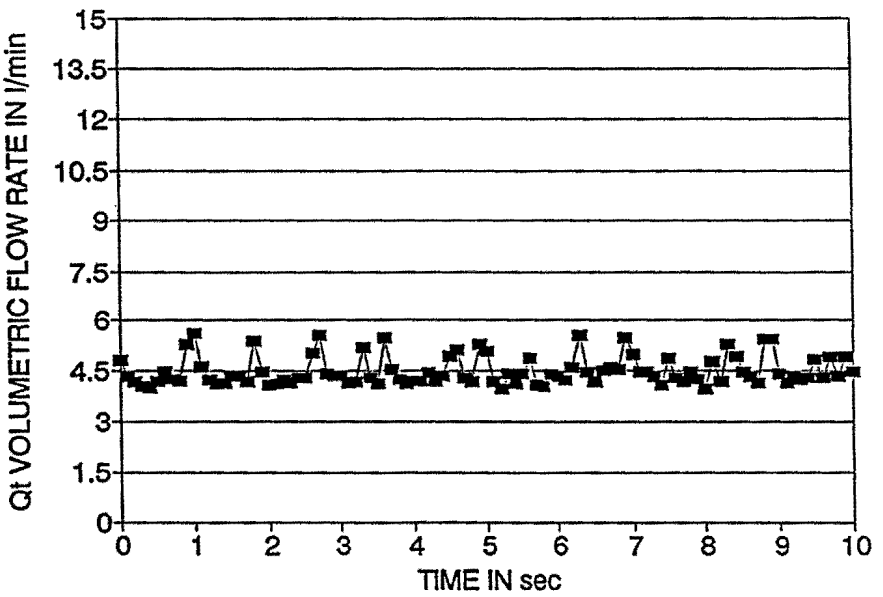

Figure 5.10 Typical volumetric flow rate transient measured by a turbine flowmeter (#44291) under R-134a two-phase flow

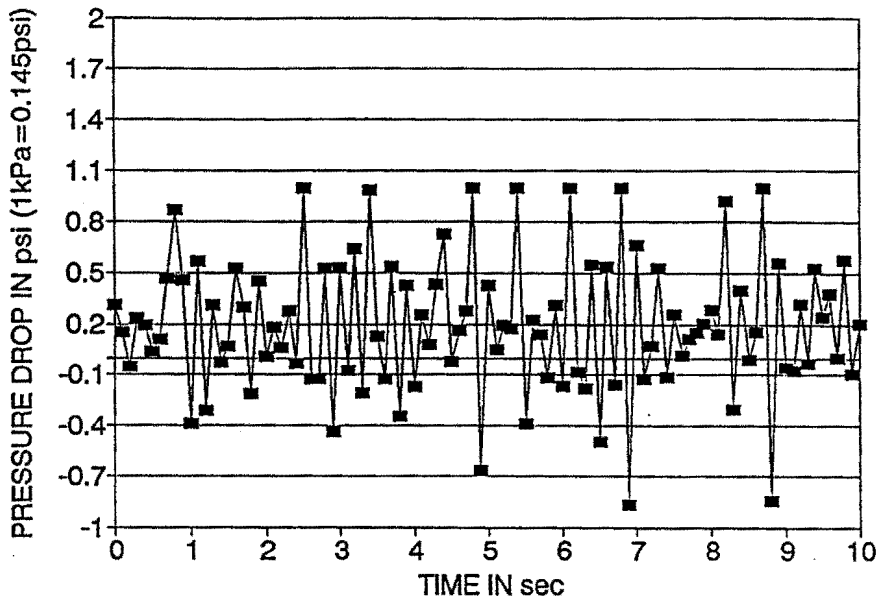

Figure 5.11 Typical pressure drop measured by a venturi flowmeter under R-134a two-phase flow

5.4 VOID FRACTION MEASUREMENT

The calibration of the gamma-densitometer and the capacitance transducer are shown in Appendix E. The theory of operation of the two instruments was discussed earlier. In calculating the time averaged void fraction using the gamma-densitometer, equation (4.21) was used where the counts for the full liquid and full vapour flows were established every day.

A total of 94 experiments were carried out in the present work. The gamma-densitometer was used in 32 of them. A comparison of the time averaged void fraction measured by the capacitance transducer and gamma-densitometer is shown in Figure 5.12. There is a general agreement between the two measurements. However, the time averaged void fraction measured by the capacitance transducer is slightly higher than gamma-densitometer. From experiments we found that the sensitivities of the capacitance transducer in the higher void fraction region were higher than that of gamma-

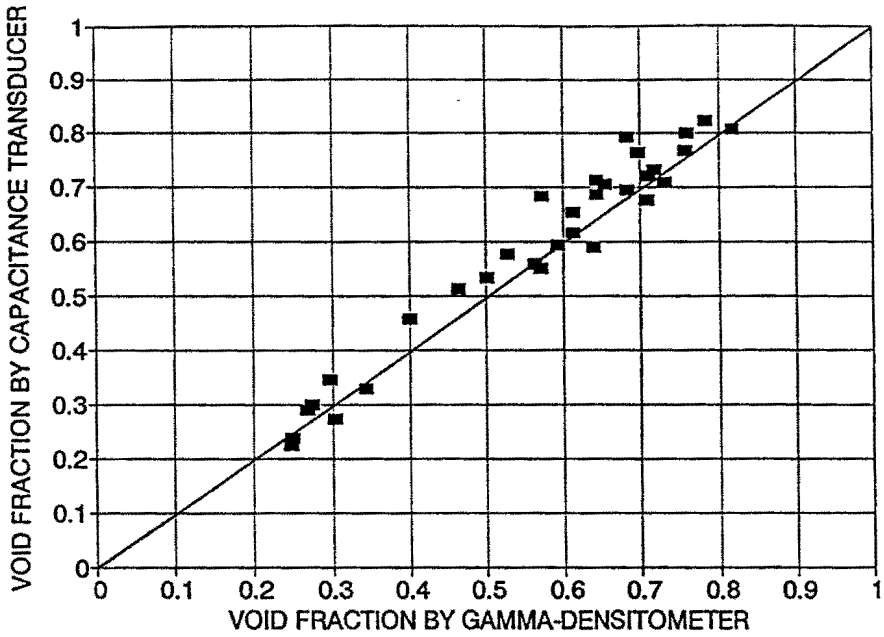

Figure 5.12 Comparison of void fraction measured by gamma-densitometer and capacitance transducer

densitometer.

Since the two void fraction measurements were in general agreement and the gamma-densitometer was not used in all the experiments, the capacitance meter results will be used in conjunction with the mass flow rate measurements discussed below.

5.5 TWO-PHASE MASS FLOW RATE DETERMINATION

Before we discuss the experimental results for the determinations of two-phase mass flow rate using theoretical models, the following definitions are made:

Local void fraction is:

$$\alpha = \frac{A_g}{A} \qquad (5.1)$$

where A is the cross sectional area of the tube and A_g is the part of the cross section occupied by the vapour phase.

Volumetric void fraction is:

$$\alpha = \frac{V_g}{V} \qquad (5.2)$$

where V_g is the volume of vapour occupied in the total volume V which is covered by the void fraction measurement instrument.

In order to obtain the thermodynamic quality for refrigerant R-134a two-phase flow, a steady state saturated flow condition in the test section had to be reached. The test loop was well insulated, and the total heat losses in the test loop were calculated to be less than 5%. The calculation of the total heat loss was made under steady state single liquid phase flow condition. The ratio [(input power) - (heat transferred from R-134a to the water through the condenser)] / (input power) was calculated for the range of operating temperatures of interest and found not to exceed 5%. Moreover, the temperature measured in the outlet of the heated sections was only less than 0.5 C above that in the test section. Therefore, it was assumed that the quality in the outlet of the heated sections should be equal to that in the test section.Detailed error analysis is given in Appendix F.

The heat balance when fluid flows through the heated sections can be expressed by:

$$Q = M_{in}[C_p(T_s - T_i) + x_0 h_{fg}] \qquad (5.3)$$

or

$$Q=M_{in}(h_{fs}-h_{fi}+x_0 h_{fg}) \qquad (5.4)$$

where Q is the power supplied at the heated sections, M_{in} is the single phase liquid mass flow rate at the inlet of the heated sections, C_p is the specific heat at constant pressure, T_{in} is the liquid temperature at the inlet of the heated sections corresponding to the enthalpy h_{fi} , Ts is the temperature of saturated liquid in the test section corresponding to the enthalpy h_{fs} which is considered to be equal to that at the outlet of the heated sections, h_{fg} is the latent heat at the operating condition. Therefore, the thermodynamic quality can be rewritten as:

$$x_0=\frac{\Delta h+h_{fi}-h_{fs}}{h_{fg}} \qquad (5.5)$$

where Δh is the enthalpy rise when the liquid passes the heated sections and equal to:

$$\Delta h=\frac{Q}{M_{in}} \qquad (5.6)$$

Liquid phase velocity is:

$$u_f=\frac{G(1-x)}{\rho_f(1-\alpha)} \qquad (5.7)$$

Vapour phase velocity is:

$$u_g=\frac{Gx}{\rho_g\alpha} \qquad (5.8)$$

Slip ratio:

$$S=\frac{u_g}{u_f}=\frac{(1-\alpha)}{\alpha}\frac{x}{(1-x)}\frac{\rho_f}{\rho_g} \qquad (5.9)$$

Two-phase flow mixture density:

$$\rho_m=\alpha\rho_g+(1-\alpha)\rho_f \qquad (5.10)$$

Two-phase mass flux:

$$G=\alpha\rho_g u_g+(1-\alpha)\rho_f u_f \qquad (5.11)$$

Two-phase mass flow rate:

$$M=GA=\alpha\rho_g u_g A+(1-\alpha)\rho_f u_f A \qquad (5.12)$$

where u_g is the vapour velocity, u_f is the liquid velocity at the test section during two-phase flow, ρ_f is the liquid density and ρ_g is the vapour density.

Experimental results obtained in the present work provided information about the flow conditions of refrigerant R-134a in the horizontal two-phase flow. Figure 5.13 gives the experimental results of quality as a function of void fraction. The void fraction was determined by capacitance transducer. The superimposed lines in Figure 5.13 represent the relationship between the quality and void fraction (equation 5.9) for various slip ratios. From this figure, we may find that for low quality, vapour velocity was slightly higher than liquid velocity and the slip ratio is close to 2. As the quality increased, the volumetric flow rate of vapour was increased, and hence, the slip ratio became higher reflecting the change of flow regime from bubbly to slug/plug and stratified flow regime.

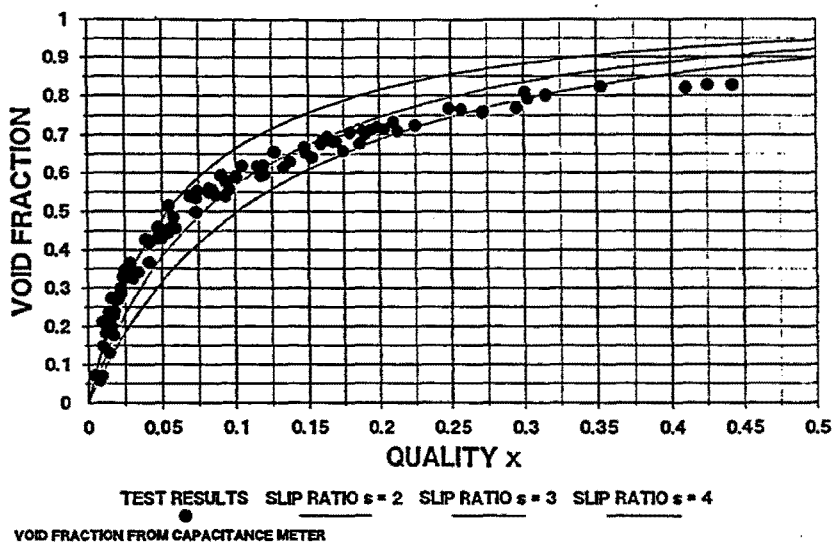

Figure 5.13 Quality as a function of void fraction measured by capacitance transducer under R-134a system pressure: 607 kPa to 770 kPa

5.5.1 Models For Turbine Flowmeter

5.5.1.1 Dispersed Flow Model

Aya[37] proposed a dispersed flow model for the turbine flowmeter under steady two-phase flow conditions. The dispersed flow is defined as the flow in which the two-phases are uniformly distributed at any cross section with constant relative velocity between the phases.

The frictional forces exerted on turbine blades are assumed negligible when compared to the forces due to the momentum changes of the fluids. The vapour phase velocity is usually greater than or equal to the liquid velocity in the dispersed flow. Therefore, a momentum balance on the turbine blade gives:

$$\alpha \rho_g (u_g - u_t)^2 = C_t \rho_f (1-\alpha)(u_t - u_f)^2 \qquad (5.13)$$

where u_t is the velocity of turbine flowmeter which should be a value between the vapour velocity and the liquid velocity, C_t is the ratio of drag coefficients of a turbine blade for the liquid and vapour phases and is equal to (C_{tf}/C_{tg}). C_t is taken as unity for the assumption that the vapour and the liquid velocities exert their forces in the same manner on the turbine blades.

Substituting equations of the vapour velocity and liquid velocity into the above momentum balance equation, one may get a relationship for calculating the two-phase mass flow rate M_{Aya} by the dispersed flow model as follows:

$$M_{Aya} = \frac{(1+Y)\, Q_t}{\frac{x}{\alpha \rho_g} + \frac{(1-x)}{(1-\alpha)\rho_f} Y} \qquad (5.14)$$

and

$$Y = \sqrt{\frac{(1-\alpha)\rho_f}{\alpha \rho_g}} \qquad (5.15)$$

where Q_t is the volumetric flow rate measured by the turbine flowmeter, α is the measured void fraction, x is the thermodynamic quality, ρ_f and ρ_g are from the saturated properties of R-134a.

Time averaged experimental results obtained by the dispersed flow model are compared with the actual mass flow rate in Figures 5.14, 5.15 and 5.16. These three figures were based on the void fraction determined by the capacitance transducer. Figure 5.14 gives the calculated two-phase mass flow rate M_{Aya} against the actual mass flow rate M which was obtained from turbine flowmeter #43563 in subcooled single liquid

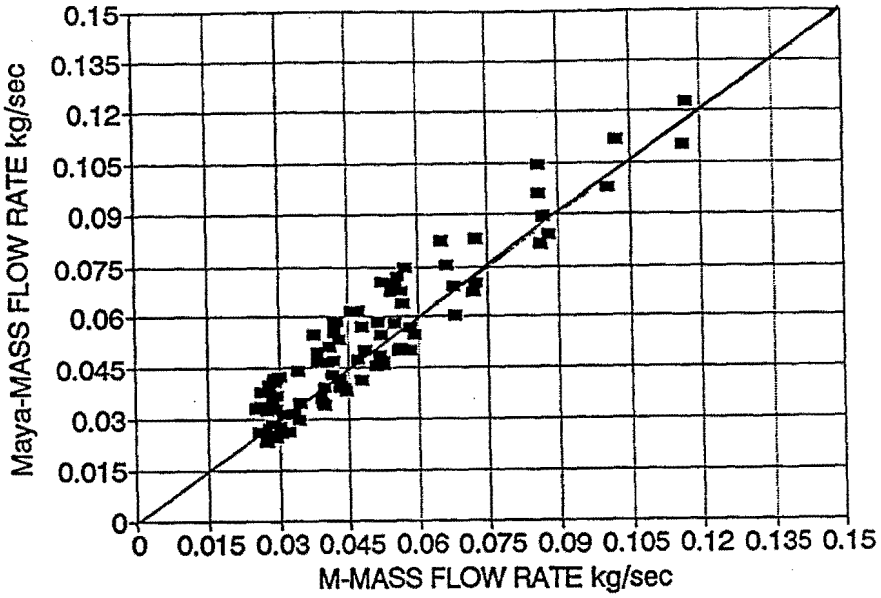

Figure 5.14 Two-phase mass flow rate determined by the dispersed flow model for turbine flowmeter

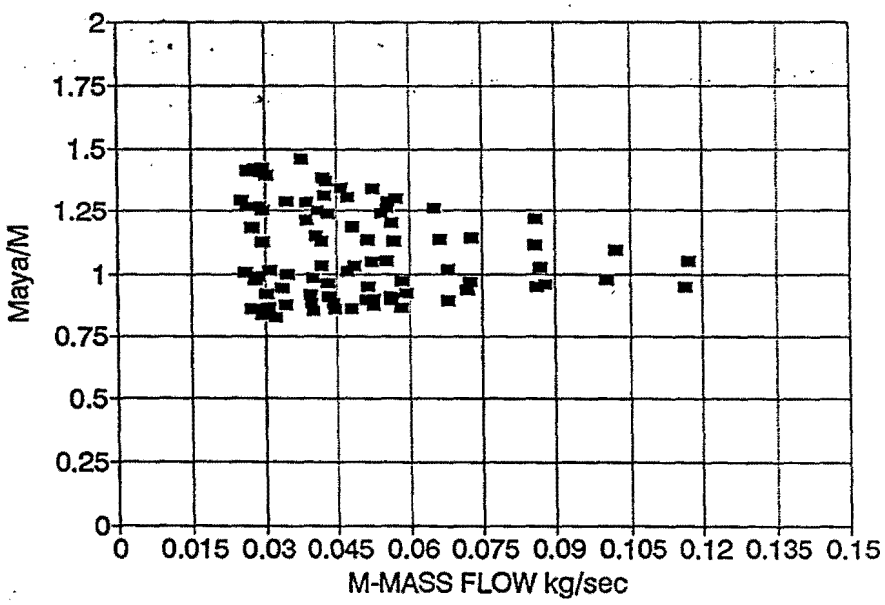

Figure 5.15 Ratio of two-phase mass flow rate determined by the dispersed flow model for turbine flowmeter as a function of the actual mass flow rate

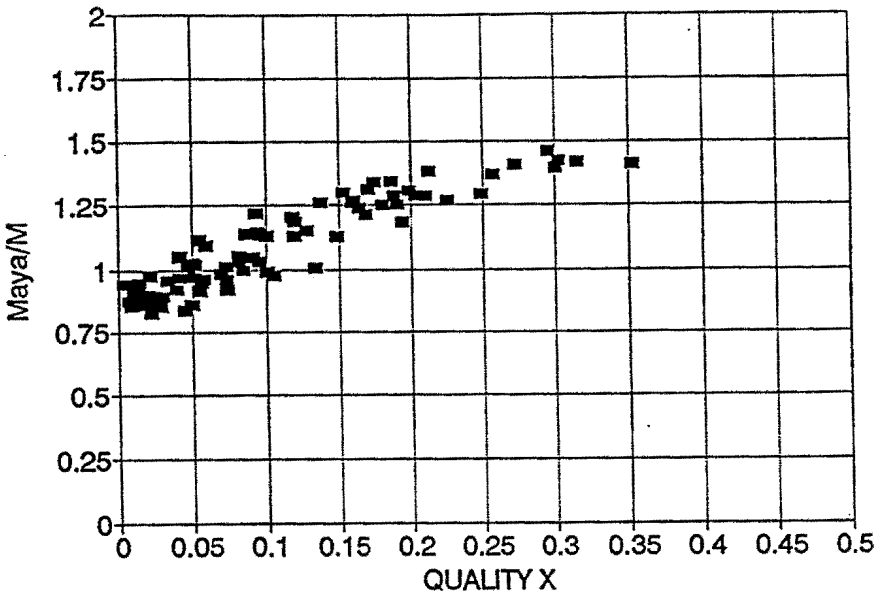

Figure 5.16 Ratio of two-phase mass flow rate determined by the dispersed flow model for turbine flowmeter as a function of quality

phase flow. Figure 5.15 shows the ratio of the calculated mass flow rate to actual mass flow rate as a function of the actual mass flow rate. Most of the experiments were carried out in the range of mass flow rate from 0.02 kg/sec to 0.06 kg/sec where the model overpredicts the mass flow rate. For high mass flow rate range, the results evaluated by this model appear to agree better with the actual mass flow rates and the ratios are between 0.9 and 1.2. Figure 5.16 shows the ratio of the calculated mass flow rate to the actual mass flow rate as a function of thermodynamic quality x. For low qualities less than 5%, this model slightly underestimates the experimental results and the ratios are between 0.8 and 1. For quality higher than 7.5%, the data are overestimated by this model, and the ratios are between 1 and 1.5. The deviation from the actual value increases with increasing the quality. For low quality range below 15%, the results estimated by this model are, in general, satisfactory with respect to the actual mass flow rate.

5.5.1.2 Volumetric Flow Models

In the volumetric flow model the two-phase mass flow rate can be expressed by:

$$M_{vol}=Q_t\rho_m \qquad (5.16)$$

where ρ_m is the mixture density, and Q_t is the volumetric flow rate from the turbine flowmeter. This equation has the same form as in single phase flow. The mixture density in the above equation can be substituted using a number of two-phase flow models as shown below.

5.5.1.2a Homogeneous Flow Model

Homogeneous flow model, which assumes that vapour and liquid are in thermal and mechanical equilibrium, i.e. the two-phase have the same temperature and velocity, can be used to evaluate the experimental data. The mass flow rate can be expressed by:

$$M_{hom}=\rho_h Q_t \qquad (5.17)$$

where ρ_h is the homogeneous density:

$$\rho_h=\frac{1}{\frac{x}{\rho_g}+\frac{(1-x)}{\rho_f}} \qquad (5.18)$$

It should be noted that for the homogeneous model, the slip ratio is one and the relationship between the quality and void fraction is:

$$\alpha = \frac{1}{1 + \frac{(1-x)}{x}\frac{\rho_g}{\rho_f}} \qquad (5.19)$$

Figures 5.17, 5.18 and 5.19 give the experimental results calculated by the homogeneous flow model. This model provides a small data scatter but underestimates the actual mass flow rate values. The ratio between the calculated and the actual mass flow rate is around 0.75 and not influenced very much by the mass flow rate and quality. In the homogeneous flow model, the slip ratio is assumed to be one. As was shown earlier, the actual slip ratio in the present experiments was higher than one. Moreover, the slip ratio increased with increasing quality.

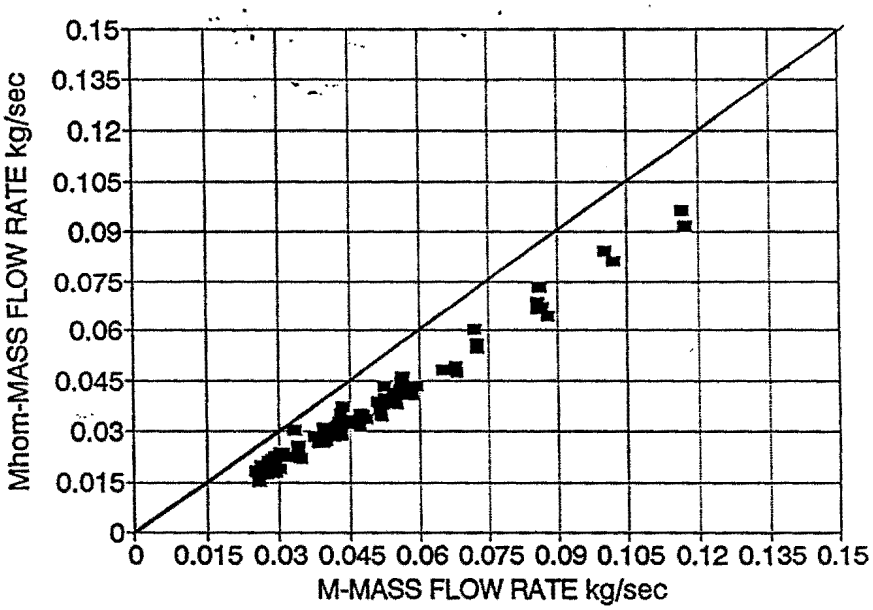

Figure 5.17 Two-phase mass flow rate determined by the homogeneous flow model for turbine flowmeter

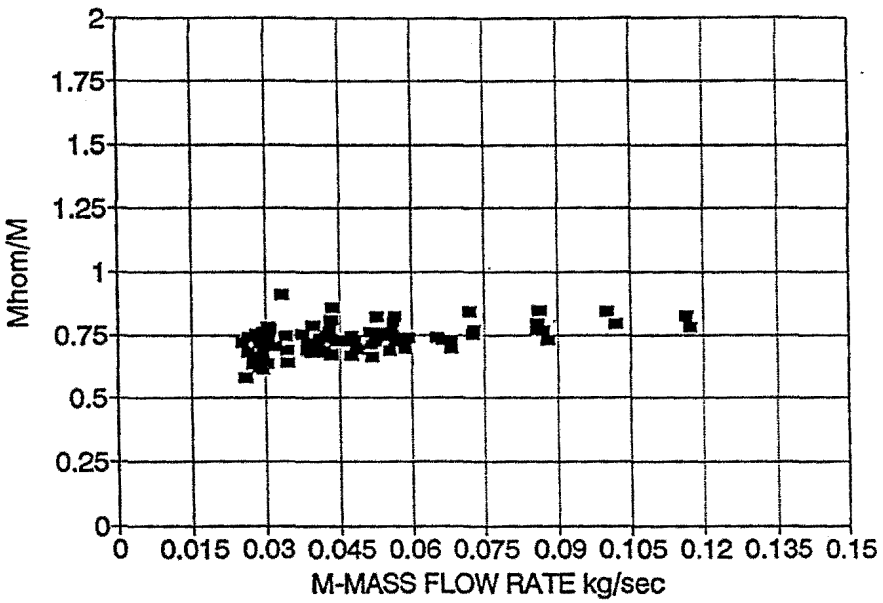

Figure 5.18 Ratio of two-phase mass flow rate determined by the homogeneous flow model for turbine flowmeter as a function of the actual mass flow rate

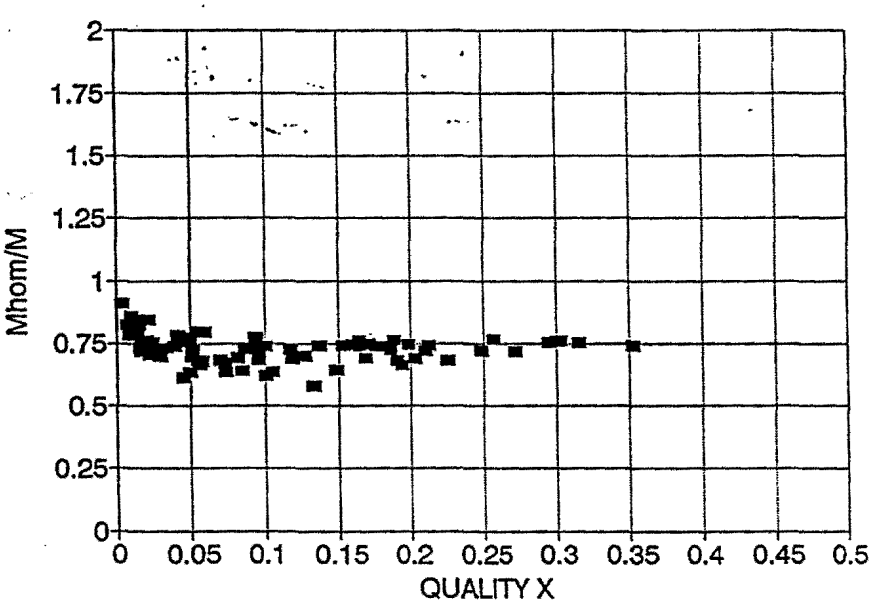

Figure 5.19 Ratio of two-phase mass flow rate determined by the homogeneous flow model for turbine flowmeter as a function of quality

5.5.1.2b Separated Flow Model

In the separated flow model, it is assumed that the vapour and liquid phases are separate with different velocities. The flow coefficient of the turbine meter should be constant in two-phase flow and equal to that in the single liquid phase flow as shown in the calibration curve, and should be independent of the pressure.

In separated flow, the mixture density is defined as:

$$\rho_m = \alpha \rho_g + (1-\alpha)\rho_f \qquad (5.20)$$

and substituting ρ_m into M_{vol}, the separated flow model-1 in volumetric flow models can be rewritten as:

$$M_{vol} = [\alpha \rho_g + (1-\alpha)\rho_f] Q_t \qquad (5.21)$$

where α is the measured results from capacitance void meter or gamma-densitometer.

Figures 5.20, 5.21 and 5.22 provide the results evaluated by this model for time averaged values. In the volumetric separated flow model-1, the two-phase mass flow rate is directly proportional to the mixture density. Void fraction is a dominant factor in this term. Figure 5.20 shows the mass flow rate calculated by this model against the actual mass flow rate. In most of the cases this model overestimates the mass flow rate. Moreover, significant data scatter is shown. Figure 5.22 gives the ratio of the calculated mass flow rate to the actual mass flow rate as a function of the actual mass flow rate. The ratios are between 1 and 2. Figure 5.23 shows the ratio as a function of thermodynamic quality. Although the quality does not appear explicitly in this model, the dependence of the ratio on the quality is obvious. From this figure, data in the quality range less than 7.5% are estimated reasonably well by this model. Most of data in high quality ($x > 7.5\%$) are significantly overestimated by this model.

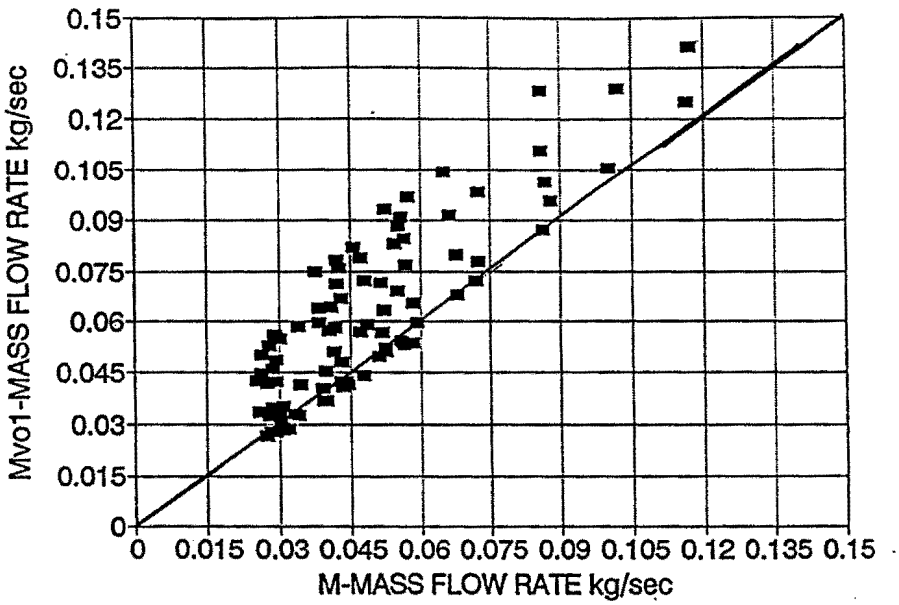

Figure 5.20 Two-phase mass flow rate determined by the separated flow model for turbine flowmeter

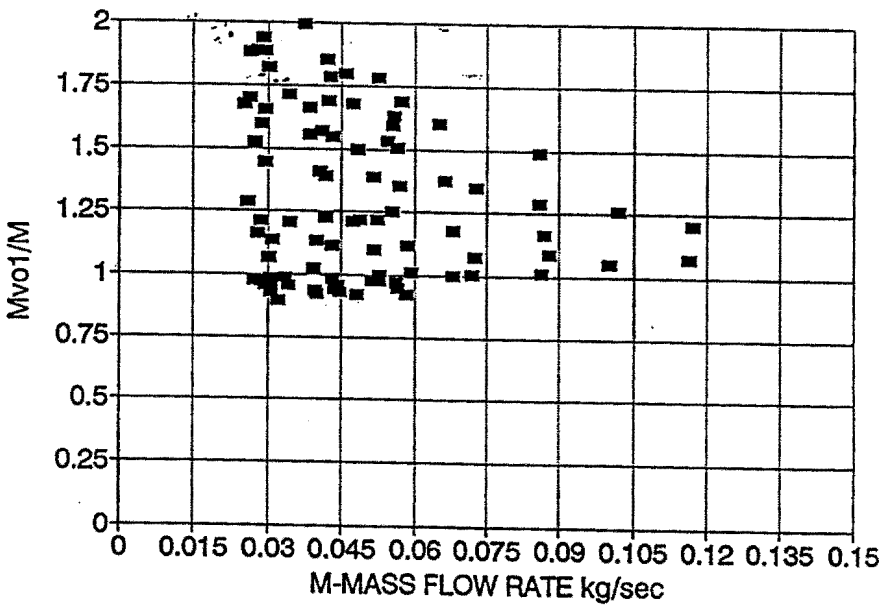

Figure 5.21 Ratio of two-phase mass flow rate determined by the separated flow model for turbine flowmeter as a function of the actual mass flow rate

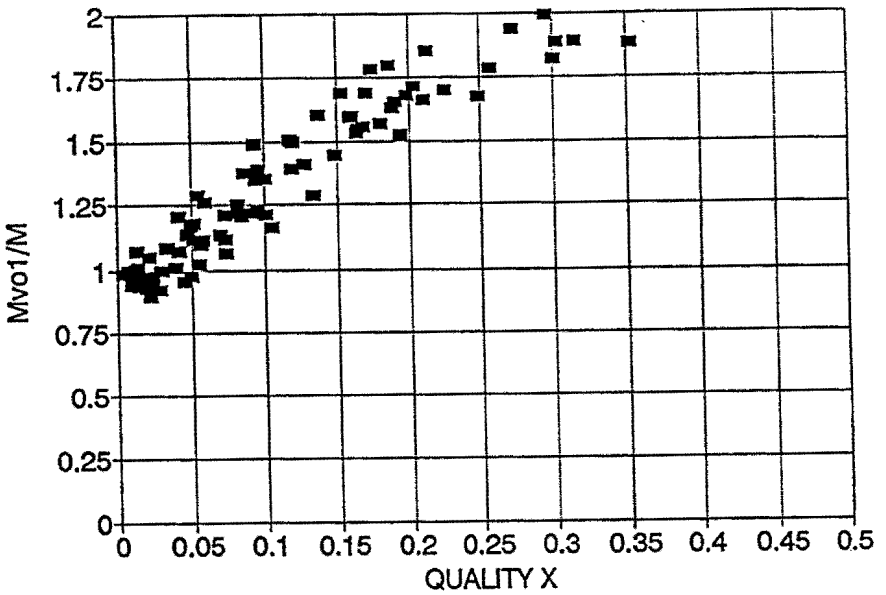

Figure 5.22 Ratio of two-phase mass flow rate determined by the separated flow model for turbine flowmeter as a function of quality

5.5.1.3 Rouhani's Separated Flow Model

Rouhani[35] developed a separated flow model for the modelling of a turbine flowmeter based on the momentum exchange at the turbine blades. The mass fluxes exerting forces on the blades are assumed to be Mx and M(1-x) for vapour and liquid phases respectively. In Rouhani's model, three main assumptions are made:

a. The turbine flowmeter rotation velocity is determined by the momentum exchange of each phase with the turbine blades, with different velocities, densities and volumetric fraction of each phase establishing the balance.

b. Flow entry is in the axial direction only, i.e. no prerotation of entering fluid.

c. Bearing friction is neglected.

The momentum exchange of the vapour and liquid phases can be explained as follows. When the vapour liquid mixture comes in contact with the turbine blades, the vapour phase with higher velocity imparts some momentum to the blades, so that the turbine rotates at a speed too high for the liquid phase to contact the front side of the blades. Consequently, the slower liquid phase will be hit by the back side of the blades, in effect, causing a momentum exchange between vapour and liquid phases to take place. The rotational speed of the turbine in steady-state conditions will be so balanced that the relative velocities of the two phases will result in no excess momentum on the blades. The steady state momentum balance acting on the turbine blades may be expressed by:

$$M(1-x)\,(u_t-u_f)=Mx(u_g-u_t) \qquad (5.22)$$

Substituting the equations of the vapour and liquid velocities, the calculated result for two-phase mass flow rate M_{Rou} may be expressed as:

$$M_{Rou}=\frac{Q_t}{\frac{x^2}{\alpha\rho_g}+\frac{(1-x)^2}{(1-\alpha)\rho_f}} \qquad (5.23)$$

The inverse of the bottom term is considered as the momentum density.

Figures 5.23, 5.24 and 5.25 show the results calculated by this model based on the void fraction measured using the capacitance transducer. Generally speaking, Rouhani's separated flow model has the same basic characteristics as the dispersed flow model because both of them are based on the momentum balance on the turbine blades. However, Rouhani's separated flow model illustrates a direct form of mass flow rate for a turbine flowmeter using momentum density. From Figure 5.23 one may find that most of the data are overestimated by this model but the scatter is very narrow. The ratios of

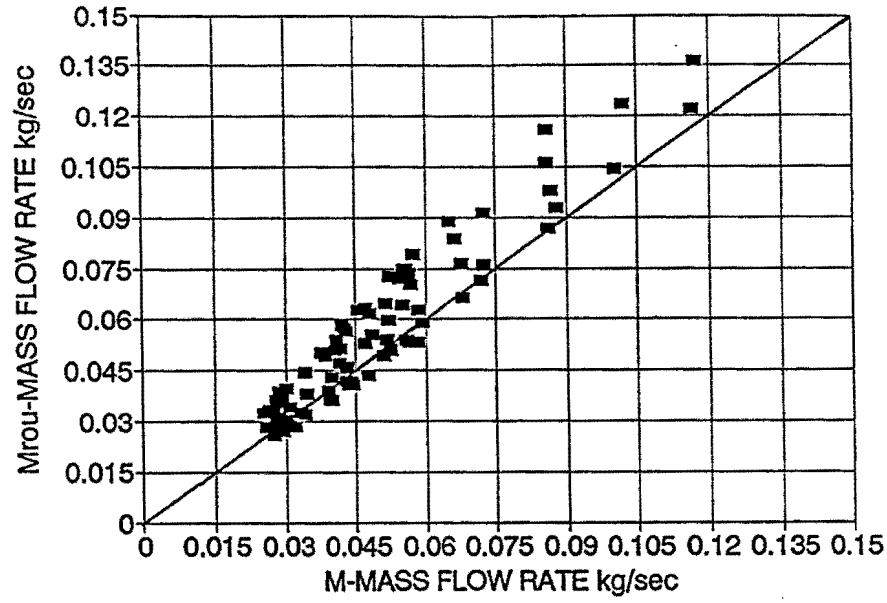

Figure 5.23 Two-phase mass flow rate determined by the Rouhani's separated flow model for turbine flowmeter

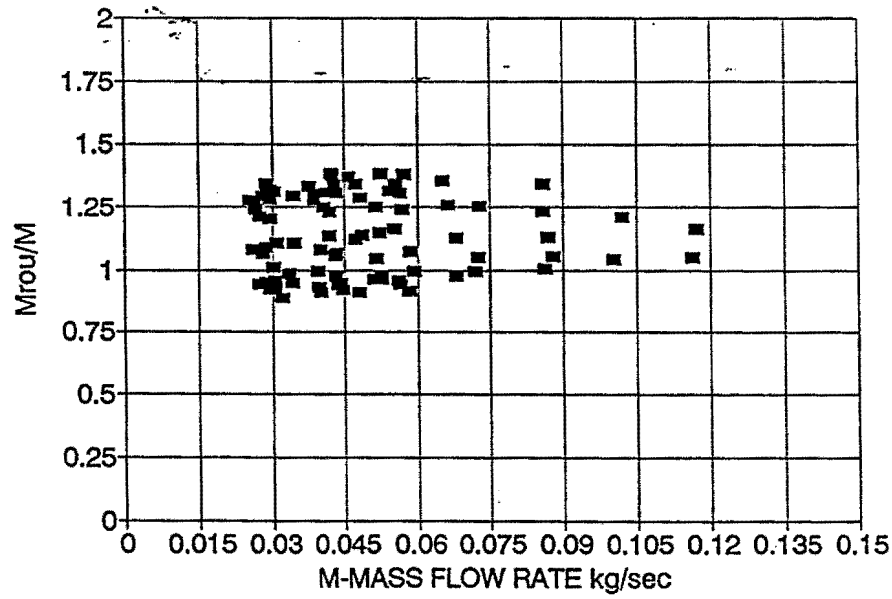

Figure 5.24 Ratio of two-phase mass flow rate determined by the Rouhani's separated flow model for turbine flowmeter as a function of the actual mass flow rate

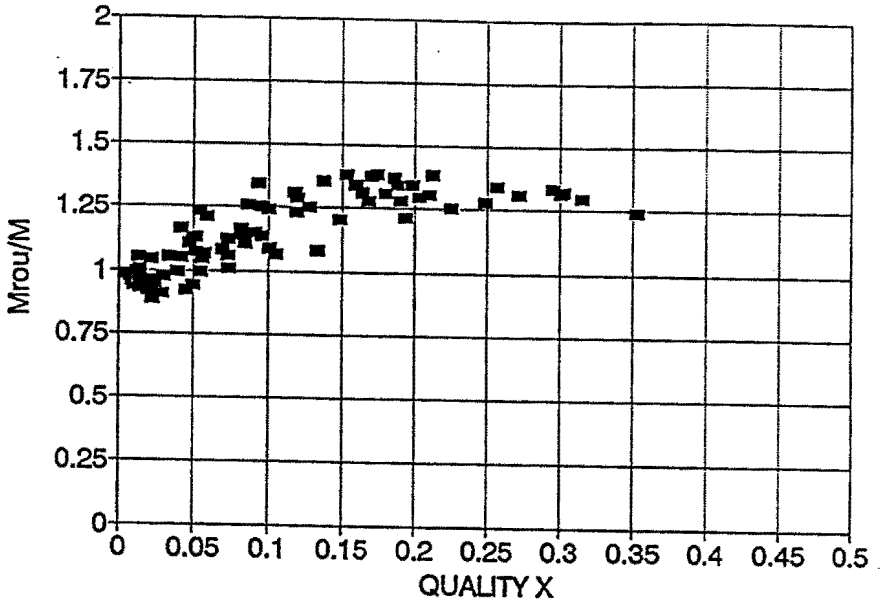

Figure 5.25 Ratio of two-phase mass flow rate determined by the Rouhani's separated flow model for turbine flowmeter as a function of quality

the calculated mass flow rate to the actual mass flow rate as a function of the actual mass flow rate and quality are between 0.85 and 1.35. The data scatter in this model is a little bit better than using the dispersed flow model. Like the dispersed flow model, this model overestimates the data at qualities higher than 5%.

5.5.2 Models for Venturi Flowmeter

5.5.2.1 Chisholm's Model for Momentum Density

Chisholm[39] established a model for pressure drop devices to be applied to two-phase flow. When a vapour-liquid mixture flows through the device, the density change of the vapour or the liquid phase is assumed negligible. Taking into account the drag force between the vapour and liquid phases, the ratio of the two-phase pressure drop over the single liquid pressure drop is a function of the Lockhart-Martinelli parameter, density ratio and slip ratio:

$$\frac{\Delta P_{2\phi}}{\Delta P_f} = 1 + \left[s\sqrt{\frac{\rho_g}{\rho_f}} + \frac{1}{s}\sqrt{\frac{\rho_f}{\rho_g}} \right] \frac{1}{X} + \frac{1}{X^2} \qquad (5.24)$$

where X is the Lockhart-Martinelli parameter[40], s is the slip ratio defined in terms of the vapour velocity over liquid velocity, ρ_g and ρ_f are the vapour density and liquid density respectively, $\Delta P_{2\phi}$ is the two-phase pressure drop through venturi flowmeter when the vapour-liquid mixture passes the device and ΔP_f is the pressure drop when single phase liquid passes through the device.

In separated flow in a pipe, the parameter X is[40]:

$$X = \sqrt{\frac{\Delta P_f}{\Delta P_g}} \qquad (5.25)$$

where ΔP_g is the pressure drop when vapour flows through the device alone. Therefore, the above equations may be rewritten as:

$$\frac{\Delta P_{2\phi}}{\Delta P_f} = 1 + \left[s\sqrt{\frac{\rho_g}{\rho_g}} + \frac{1}{s}\sqrt{\frac{\rho_f}{\rho_g}} \right] \sqrt{\frac{\Delta P_g}{\Delta P_f}} + \frac{\Delta P_g}{\Delta P_f} \qquad (5.26)$$

If the Reynolds numbers of the vapour and liquid at the throat of the venturi flowmeter are in the range over 10^4 [36], then the flow coefficients for the vapour and liquid can be considered equal and constant.

For single phase vapour and single phase liquid flow in venturi flowmeter, the pressure drop can be expressed by:

$$\Delta P_f = K_v \frac{M^2 (1-x)^2}{\rho_f} \qquad (5.27)$$

$$\Delta P_g = K_v \frac{M^2 x^2}{\rho_g} \qquad (5.28)$$

where K_v is the dimensional flow coefficient of the venturi flowmeter, M is the mass flow rate, x is the quality calculated from the thermodynamic quality. Substituting those two equations into the equation of the two-phase mixture pressure drop:

$$\Delta P_{2\phi} = K_v M^2 \left[\frac{x^2}{\alpha \rho_g} + \frac{(1-x)^2}{(1-\alpha)\rho_f} \right] \qquad (5.29)$$

where α is the void fraction introduced from following general equation:

$$\alpha = \frac{1}{1 + S \frac{(1-x)}{x} \frac{\rho_g}{\rho_f}} \qquad (5.30)$$

Rearranging the above equations, the two-phase mass flow rate through the venturi flowmeter can be expressed by:

$$M_{Chi} = K \sqrt{\Delta P_{2\phi} \rho_{2\phi}} \qquad (5.31)$$

where K is the dimensional flow coefficient for a particular venturi flowmeter and equal to:

$$K=\frac{1}{\sqrt{K_v}} \qquad (5.32)$$

K is actually a calibration constant which depends on the geometry of the venturi flowmeter, Reynolds number, discharge coefficient and expansion coefficient, $\rho_{2\phi}$ contributes as the momentum density of the mixture as follow:

$$\rho_{2\phi}=\frac{1}{\frac{x^2}{\alpha\rho_g}+\frac{(1-x)^2}{(1-\alpha)\rho_f}} \qquad (5.33)$$

The time averaged experimental mass flow rate evaluated by Chisholm's model for the venturi flowmeter is presented in Figure 5.26, 5.27 and 5.28 based on the void fraction measured by the capacitance transducer. Using the time averaged pressure drop through the device, this model seems to give the best agreement with the actual values. Figure 5.26 shows the calculated mass flow rate against the actual mass flow rate. The data scatter is quite small. Figures 5.27 and 5.28 show the ratio of the calculated mass flow rate to the actual mass flow rate as a function of the actual mass flow rate and quality respectively. From the above two figures, it is found that for high mass flow rate, this model estimates the experimental data quite well. The ratios are between 0.9 and 1.2 except at lower mass flow rate (M < 0.035 kg/sec). For quality higher than 10%, this model overestimated the data slightly. There is no appreciable dependency observed on the mass flow rate and quality. The results obtained with this model are very satisfactory with respect to mass flow rate determination for the refrigerant R-134a two-phase flow compared with the models discussed before.

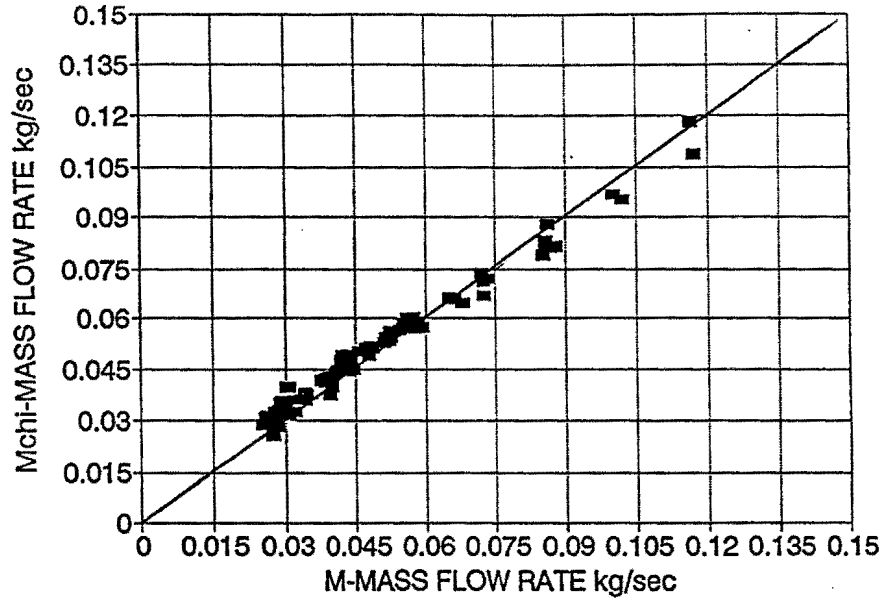

Figure 5.26 Two-phase mass flow rate determined by the Chisholm's model for venturi flowmeter

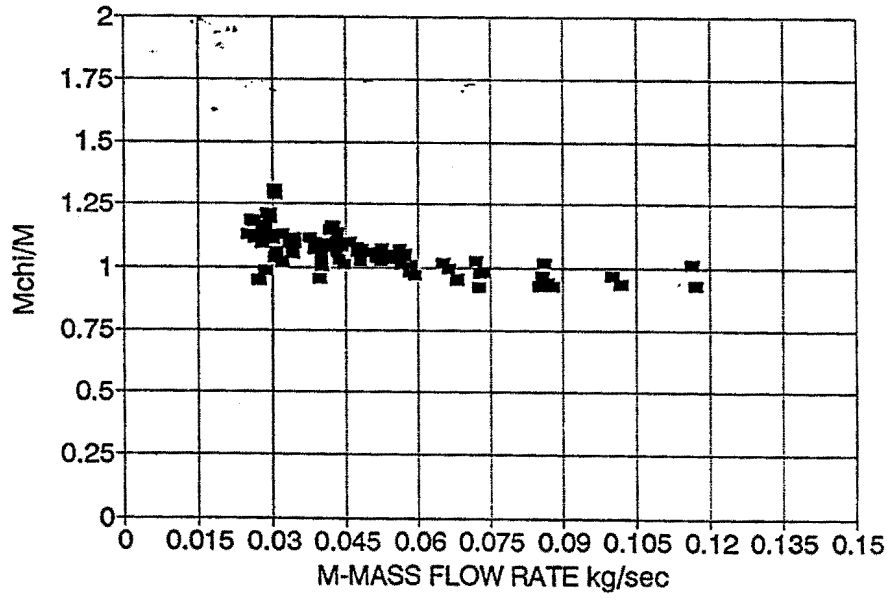

Figure 5.27 Ratio of two-phase mass flow rate determined by the Chisholm's model for venturi flowmeter as a function of the actual mass flow rate

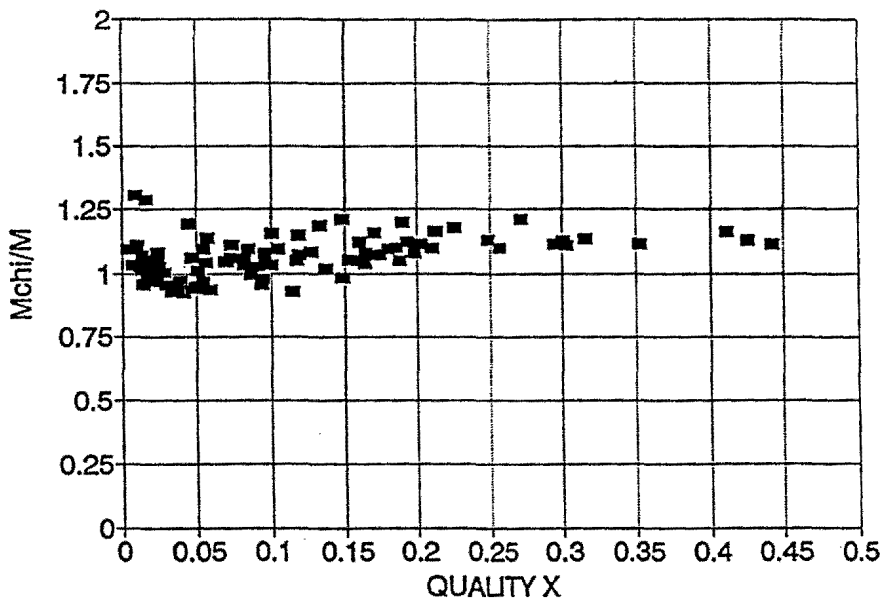

Figure 5.28 Ratio of two-phase mass flow rate determined by the Chisholm's model for venturi flowmeter as a function of quality

5.5.2.2 Mixture Density Models

A simple approach can be made in the determination of two-phase mass flow rate for the venturi meter. Since the void fraction and two-phase pressure drop were determined experimentally, the two-phase mass flow rate can be calculated with an appropriate mixture density instead of single phase density in the equation:

$$M = K\sqrt{\Delta P_{2\phi}\rho_m} \qquad (5.34)$$

Equation (5.34) is equivalent to Chisholm's model in which the mixture density is substituted by the momentum density defined by equation (5.33).

5.5.2.2a Homogeneous Density

Similar to the homogeneous flow model used for the turbine flowmeter when homogeneous flow is assumed, homogeneous density can be used in the equation of the venturi device instead of single phase density. The two-phase mass flow rate can be rewritten as:

$$M_{hov}=K\sqrt{\frac{\Delta P_{2\phi}}{\frac{x}{\rho_g}+\frac{(1-x)}{\rho_f}}} \qquad (5.35)$$

Figures 4.29, 4.30 and 4.31 show the results calculated by this equation. The data are underestimated by the homogeneous density model for the venturi flowmeter but they are predicted better than those for the turbine flowmeter. The ratio is between 0.75 and 1, except for several data points, without showing much dependence on the mass flow rate and quality.

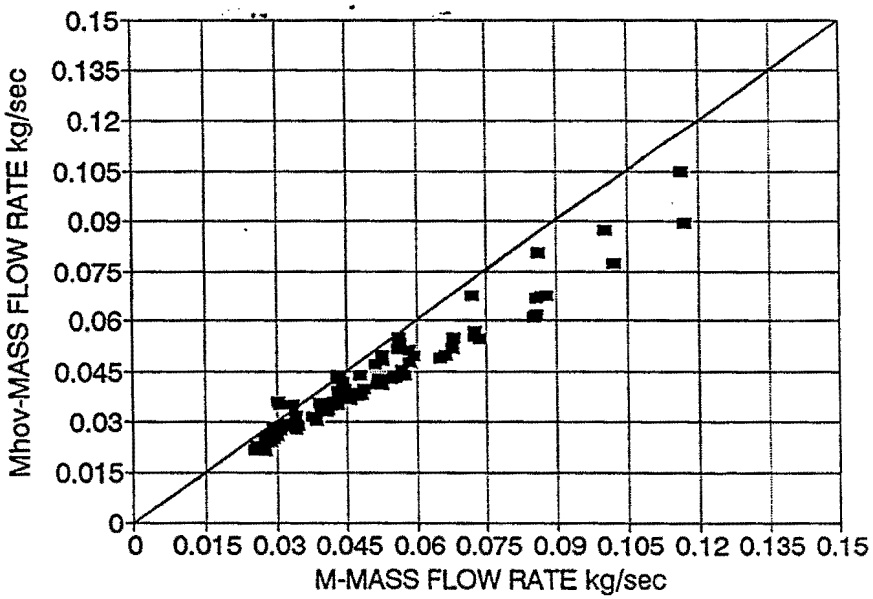

Figure 5.29 Two-phase mass flow rate determined by the homogeneous density for venturi flowmeter

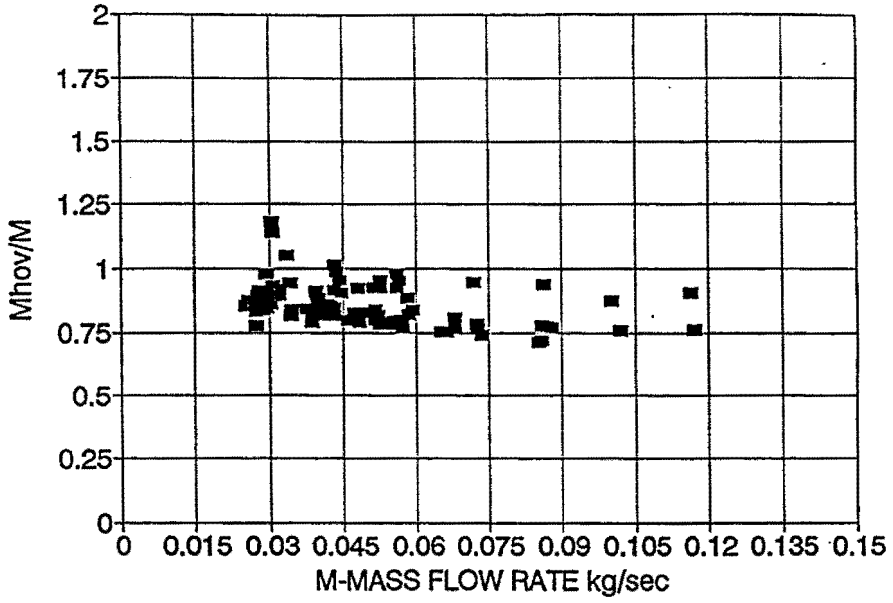

Figure 5.30 Ratio of two-phase mass flow rate determined by the homogeneous density for venturi flowmeter as a function of the actual mass flow rate

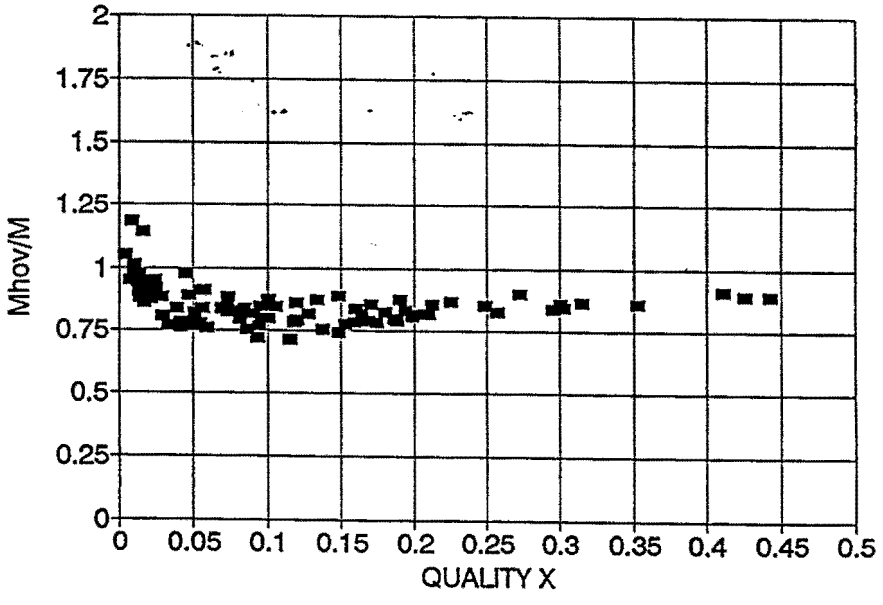

Figure 5.31 Ratio of two-phase mass flow rate determined by the homogeneous density for venturi flowmeter as a function of quality

5.5.2.2b Separated Flow Model

Taking the mixture density from the separated flow model, given in section 5.5.1.2b, and substituting it into the equation for the venturi device, one may obtain an equation to calculate two-phase mass flow rate when the mixture flows through the venturi device:

$$M_{msv}=K\sqrt{\Delta P_{2\phi}\,(\alpha\rho_g+(1-\alpha)\rho_f)} \qquad (5.36)$$

The results calculated by this equation are shown in Figure 5.32, 5.33 and 5.34 for the data based on the void fraction determined from the capacitance transducer. This equation overestimates the mass flow rate in the low mass flow rate range (M < 0.06 kg/sec) for qualities higher than 0.1. The ratios of the calculated mass flow rate to the actual mass flow rate are between 0.9 and 1.5. Most of the ratios are less than 1.3.

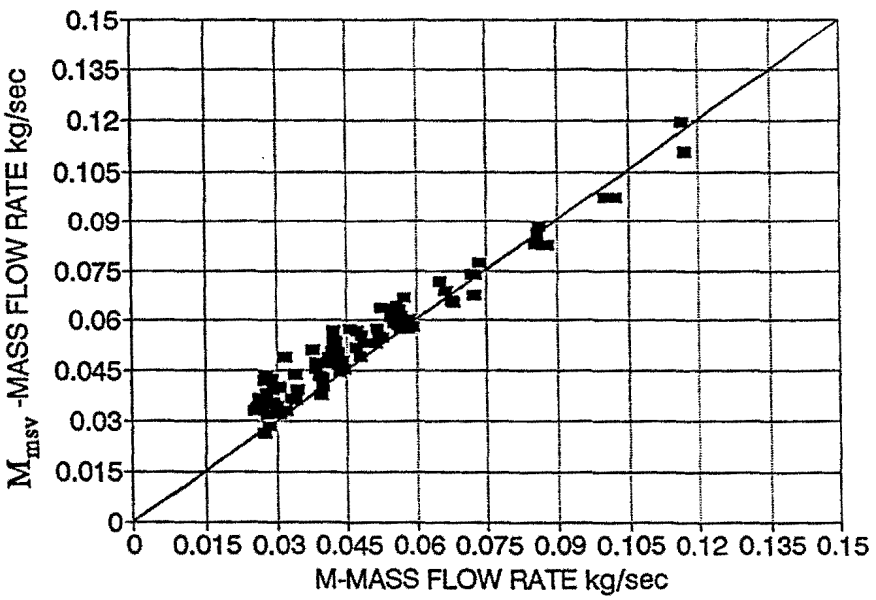

Figure 5.32 Two-phase mass flow rate determined by the mixture density for venturi flowmeter

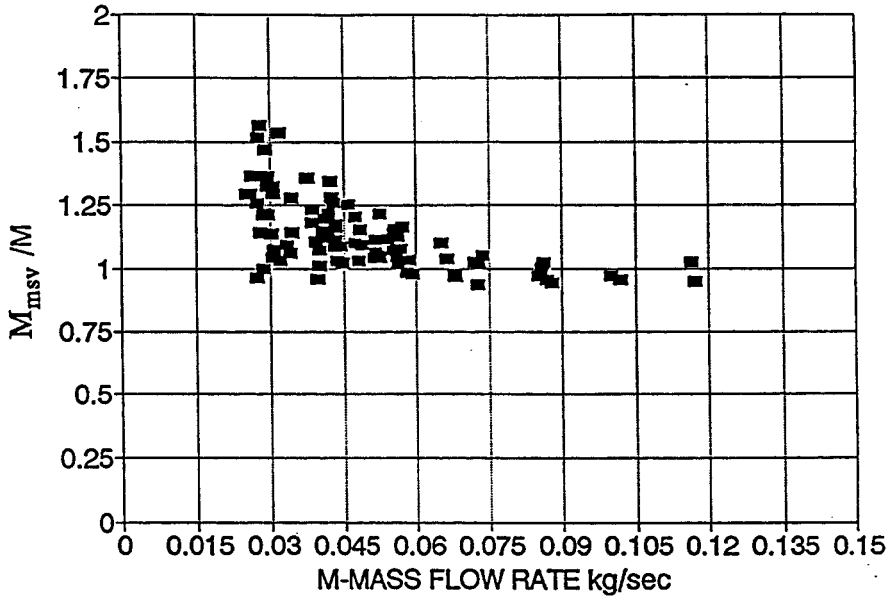

Figure 5.33 Ratio of two-phase mass flow rate determined by the mixture density for venturi flowmeter as a function of the actual mass flow rate

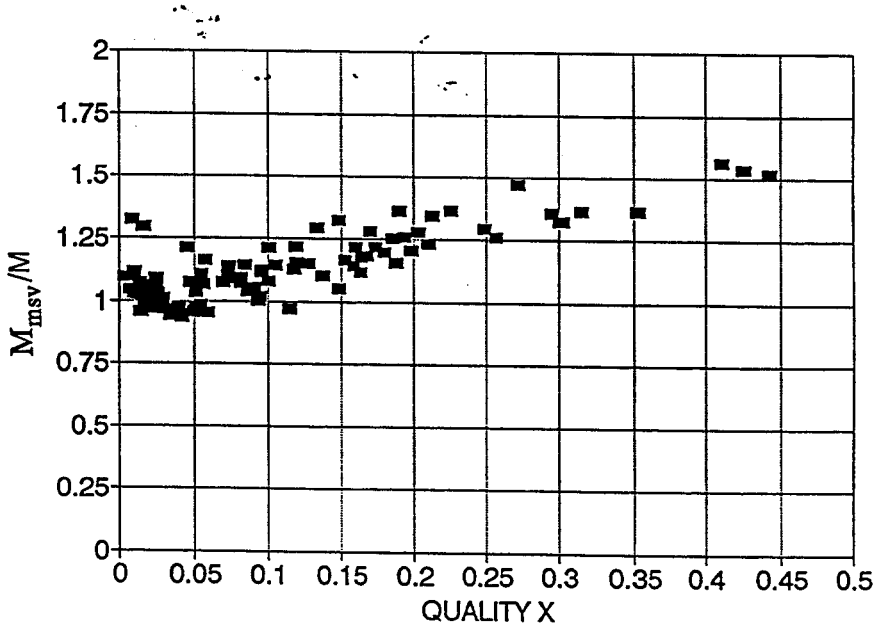

Figure 5.34 Ratio of two-phase mass flow rate determined by the mixture density for venturi flowmeter as a function of quality

5.5.2.3 Equal Pressure Drop Model

This model is based on the separated flow approach as applied to flow in venturi meters, or other pressure drop devices. It is assumed that the two phases are flowing in the venturi flowmeter independent from each other, which means that:

(i) no interaction occurs between the phases;
(ii) each phase is occupying a distinct portion of the flow area, i.e. A_f and A_g for the liquid and vapour respectively;
(iii) the venturi coefficient K is the same for each phase.

Based on the above assumptions, the total mass flow rate M_{mev} in the venturi flowmeter can be written as:

$$M_{msv}=M_g+M_f \tag{5.37}$$

$$M_{mev}=K[\alpha\sqrt{\rho_g \Delta P_g}+(1-\alpha)\sqrt{\rho_f \Delta P_f}] \tag{5.38}$$

If it is also assumed that the pressure drop of the two phases are the same, then:

$$M_{mev}=K\sqrt{\Delta P_{2\phi}(\alpha \rho_g^{1/2}+(1-\alpha)\rho_f^{1/2})^2} \tag{5.39}$$

It should be noted that this model is similar to the typical venturi model if the fluid density is replaced by an effective mixture density defined by:

$$\rho_m^{1/2}=\alpha \rho_g^{1/2}+(1-\alpha)\rho_f^{1/2} \tag{5.40}$$

Results calculated by this model are given in Figure 5.35, 5.36 and 5.37 based on

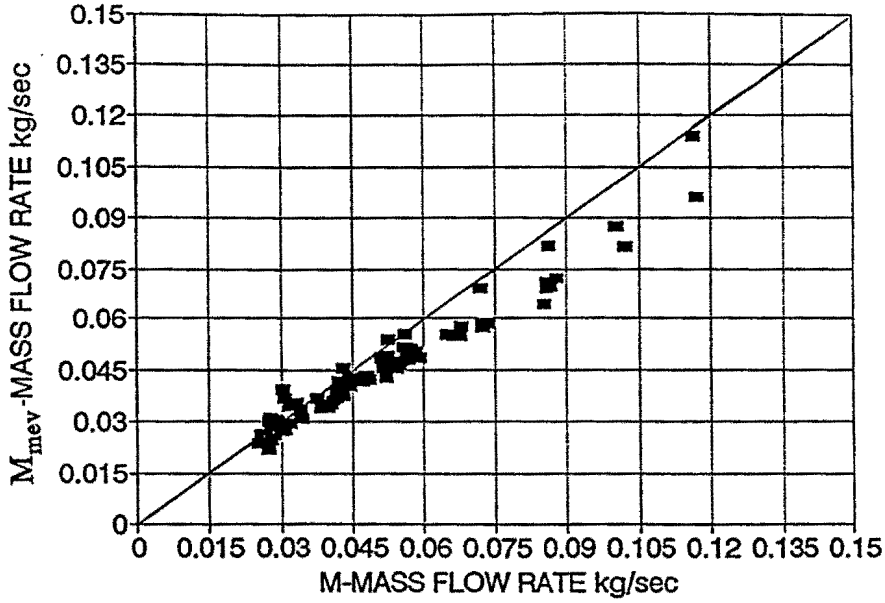

Figure 5.35 Two-phase mass flow rate determined by the equal pressure drop model for venturi flowmeter

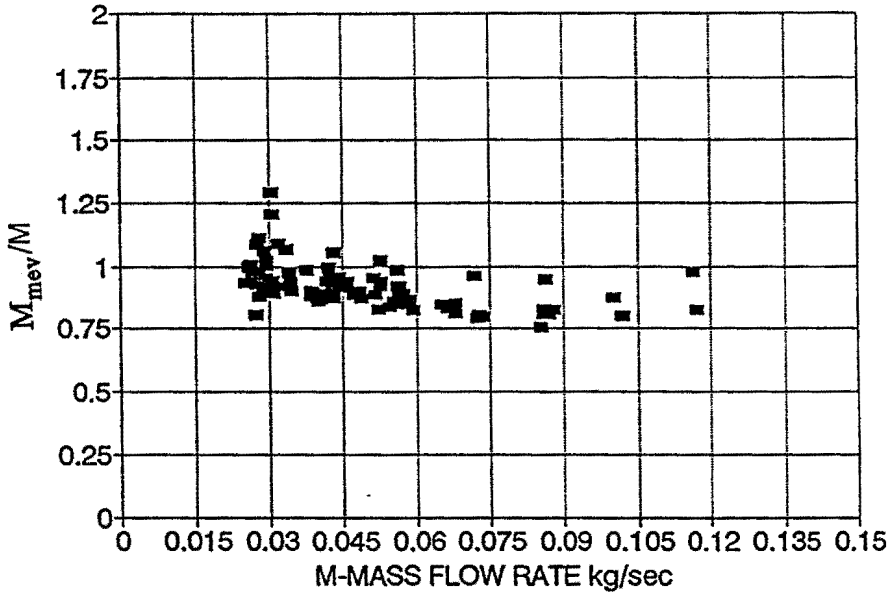

Figure 5.36 Ratio of two-phase mass flow rate determined by the equal pressure drop model for venturi flowmeter as a function of the actual mass flow rate

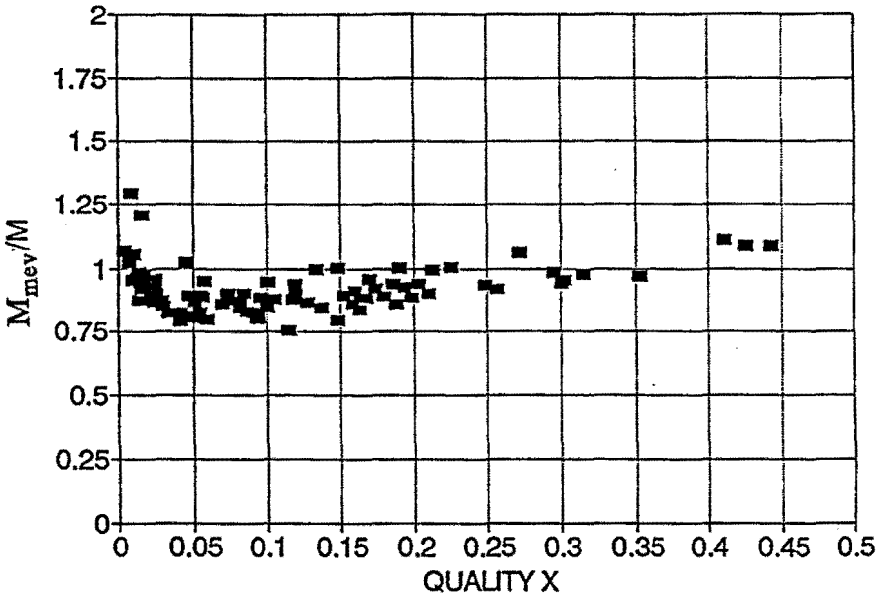

Figure 5.37 Ratio of two-phase mass flow rate determined by the equal pressure drop for venturi flowmeter as a function of quality

the void fraction determined from the capacitance transducer. From these figures, one may find that for the low mass flow rate range ($M < 0.06$ kg/sec), this equation predicts the data very well and the data scatter is quite small. The ratios of the calculated mass flow rate to the actual mass flow rate are between 0.85 and 1.05 except few data points. But in the high mass flow rate range ($M > 0.06$ kg/sec), the mass flow rates predicted are slightly low. The ratios are between 0.75 and 1. There is no obvious dependence on the quality and mass flow rate.

Covering a relatively wide range of mass flow rate and quality are important considerations in selecting an appropriate flowmeter for two-phase mass flow rate measurement. Flow meters which are limited in their operation to a given range of volumetric flow rate, i.e. turbine flowmeter, will tend to cover a small range of mass flow rate and qualities. This is particularly true in two-phase flow applications where the

liquid to vapour density ratio is high. For R-134a at room temperature, the liquid density is approximately 45 times higher than that of the vapour. Accordingly, if a flowmeter is expected to cover the entire quality range $0 < x < 1$, even for a given single mass flow rate, the corresponding increase of the volumetric flow rate will be 45 folds, a range which is beyond the normal linear range of commercial turbine flow meters. In order to measure two-phase mass flow rate under high quality conditions, several turbine flow meters of different flow rate ranges may be required. Venturi devices do not have this limitation. They can be applied to the measurement of pressure drop for a wide quality range.

5.5.3 Combined Model for Turbine and Venturi Flow Meters

A simple model for two-phase mass flow rate based on the combined output from the turbine and venturi flow meters is derived here. The model is based on an assumption that the mixture density does not change when the mixture passes through the turbine and venturi flow meters under steady-state flow conditions.

In two-phase vapour-liquid flow the mass flow rate related to the turbine flowmeter and venturi flowmeter can be expressed individually as follows:

$$M=\rho_{2\phi}Q_t \tag{5.41}$$

$$M=K\sqrt{\rho_{2\phi}\Delta P_{2\phi}} \tag{5.42}$$

where $\rho_{2\phi}$ is mixture density, Q_t is the volumetric flow rate of the turbine flowmeter, $\Delta P_{2\phi}$ is the two-phase flow pressure drop through the venturi flowmeter and K is the calibrated flow coefficient. Combining the two equations and eliminating the density, the two-phase mass flow rate $M_{V\text{-}T}$ for the combined model can be written as:

$$M_{V-T}=K^2\frac{\Delta P_{2\phi}}{Q_t} \qquad (5.43)$$

Figures 5.38, 5.39 and 5.40 show the results calculated by this model. Figure 5.38 gives the calculated mass flow rate against the actual mass flow rate. For the low mass flow rate (M < 0.06 kg/sec), this model predicts the mass flow rate very well, and the data scatter is quite small. For the high mass flow rates (M > 0.06 kg/sec), the mass flow rate is underestimated by this model. Figures 5.39 and 5.40 show the ratios of the calculated mass flow rate to the actual mass flow rate as a function of the actual mass flow rate and the pressure drop through venturi device respectively. These two figures provide the same information because the pressure drop is proportional to the mass flow rate. The ratios are between 0.75 and 1.25. As the pressure drop increases, the ratios decreased slowly. This model is not as good as the Chisholm's model for venturi flowmeter but is better than the other models based on the data scatter. The results evaluated by this model are still acceptable for the determination of refrigerant R-134a two-phase mass flow rate.

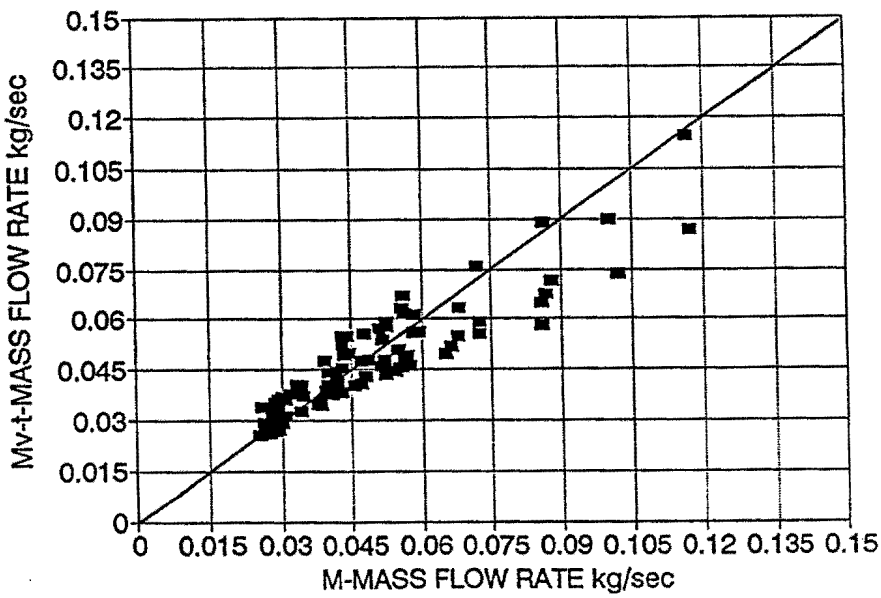

Figure 5.38 Two-phase mass flow rate determined by the combined model for turbine and venturi meters

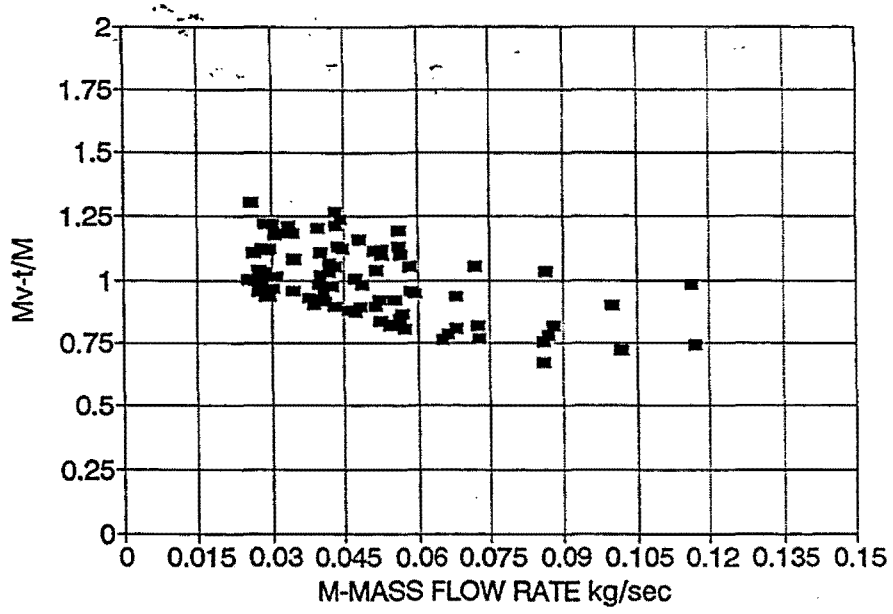

Figure 5.39 Ratio of two-phase mass flow rate determined by the combined model for turbine and venturi meters as a function of the actual mass flow rate

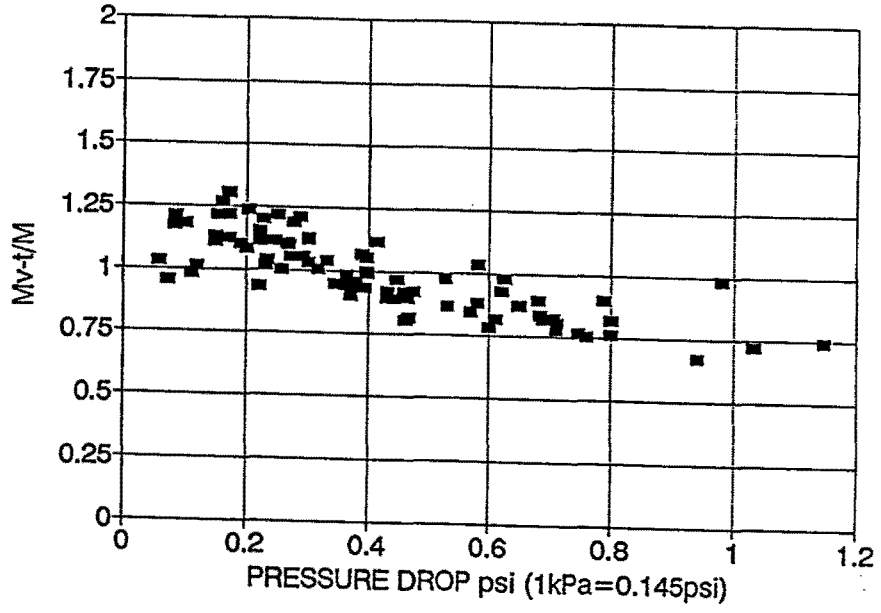

Figure 5.40 Ratio of two-phase mass flow rate determined by the combined model for turbine and venturi meters as a function of pressure drop

5.6 COMPARISONS BETWEEN DIFFERENT TECHNIQUES

Evaluation of the experimental results for refrigerant R-134a two-phase mass flow rate have been made for the turbine and the venturi flow meters based on the void fraction measured by the capacitance transducer for the different predictive models used. In assessing the various models, the relative error is calculated.

To evaluate the various models for each of the two flow meters on a common basis, the mean error and standard deviation for each were calculated.

The relative error is defined by:

$$\varepsilon = \frac{(M_{calculated} - M_{actual})}{M_{actual}} \qquad (5.44)$$

The mean error and standard deviation are calculated by:

$$\bar{\varepsilon} = \frac{1}{N}\sum \varepsilon_i \qquad (5.45)$$

and

$$\sigma = \sqrt{\frac{1}{N}\sum \varepsilon_i^2} \qquad (5.46)$$

The results of this quantitative evaluation of the methods used for two-phase R-134a mass flow rate measurement are given below:

For the turbine flowmeter:

Model	$\bar{\varepsilon}$	σ
Dispersed flow model	0.07633	0.19886
Homogeneous flow model	-0.26814	0.27418
Separated flow model	0.29565	0.43295
Rouhani's model	0.13886	0.21066

For the venturi flowmeter:

Model	$\bar{\varepsilon}$	σ
Chisholm's model	0.06369	0.10112
Homogeneous density model	-0.14461	0.16540
Separated flow model	0.13838	0.20013
Equal pressure drop model	-0.08210	0.12044

For the turbine and venturi flow meters:

Model	$\bar{\varepsilon}$	σ
Combined model	-0.00862	0.14596

The above results clearly show that for the turbine flowmeter, the dispersed flow model is superior to the others based on both the mean error and standard deviation. However, as can be seen in Figure 5.16, this model tends to consistently overestimate the actual mass flow rate in the higher quality region. This issue needs to be examined in detail before one can recommend this method.

For the venturi meter, Chisholm's model is clearly the best. Figures 5.26 to 5.28 confirm the adequacy of this model over the ranges of mass flow rates and qualities tested in this work. The use of the combined outputs of the turbine and venturi flow meters is acceptable. However, based on the above results, the use of the venturi flowmeter in conjunction with Chisholm's model is recommended for the determination of two-phase refrigerant mass flow rate.

CHAPTER 6

CONCLUSIONS AND RECOMMENDATIONS

(1) An experimental apparatus for the determination of mass flow rate for refrigerant R-134a two-phase flow has been constructed and steady state experiments have been conducted. Various combinations of a turbine flowmeter and/or a venturi flowmeter with the measurement of void fraction by a capacitance transducer and/or a gamma-densitometer have demonstrated successful measurement techniques capable of being applied to refrigerating and air-conditioning equipment.

(2) For the time averaged void fraction measurements obtained by the capacitance transducer and gamma-densitometer, the results were in agreement within the present range of test conditions. The capacitance transducer also provided an instantaneous response for void fraction measurement. The ultrasonic pulse-echo has been used to characterize the flow patterns successfully. The flow pattern measurements were in agreement with visual observations.

(3) In applying the turbine flowmeter for measuring refrigerant two-phase mass flow rate, a number of models were assessed. It is shown that the dispersed flow model is better able to predict the mass flow rate as compared to other models tested. The predicted values, however, tended to be consistently higher than the actual mass flow rate for qualities above 15%.

(4) The venturi flow meter was also used and a number of models for estimating the actual mass flow rate were tested. The results show that Chisholm's model is the best to be used for estimating the flow rate measurements for the venturi flowmeter.

(5) The combination of turbine and venturi flow meter also is able to measure two-phase mass flow rate, although greater scatter was encountered in the data.

(6) Based on the present results, the use of the venturi flowmeter, in conjunction with Chisholm's model, is recommended for R-134a refrigerant two-phase mass flow rate measurements.

(7) The present data covered a quality range of $0 < x < 50\%$. In order to complete the evaluation of methods for two-phase mass flow rate measurements, the data base needs to be extended up to 100% quality.

REFERENCE

[1] Z.M. Ayub and W.W. Seaton, 1991 "Measurement of Two-Phase Refrigerant Liquid-Vapour Mass Flow Rate", ASHRAE research project. 722-TRP.

[2] S. Banerjee and R.T. Lahey Jr. 1981 "Advances in Two-Phase Flow Instrumentation", In Advances in Nuclear Science and Technology, Vol.13, Plenum Press, New York.

[3] C.W. Snoek, 1990 "A Selection of New Developments in Multiphase Flow Measurement Techniques", Experimental Thermal and Fluid Science. Vol.3, pp 60-73.

[4] J.M. Delhaye, 1981, "Instrumentation in Two-Phase Flow and Heat Transfer in the Power and Process Industries", A.E. Bergles, J.G. Collier, J.M. Delhaye, G.F. Hewitt and F.Mayinger, Edited. Chapter 15, pp 453-488. Hemisphere, Washington, D.C.

[5] G.F. Hewitt, 1978, Measurement of Two-Phase Flow Parameters. Academic Press, London.

[6] M. Shoukri, J.S. Chang and A. Abdul-Razzak, 1992, "Measurement of Two-Phase Refrigerant Liquid-Vapour Mass Flow Rate", McMaster University, Review Report to ASHREA. No. 722-TRP.

[7] K. Hashizume, 1983 "Flow Pattern, Void Fraction and Pressure Drop of Refrigerant Two-Phase Flow in a Horizontal Pipe, I: Experimental Data", Int. J. Multiphase Flow, Vol.9, No.4, pp 399-410.

[8] V.C. Mei, 1990 "Two-Phase Refrigerant Flow Measurement with Liquid and Vapour Separation Technique", ASHRAE Transaction. Vol.94, No.3161, pp 238-242.

[9] P.J. Hawken, P.F. Hearty and C. Lemal, 1990 "The Influence of Two-Phase Flow on a Coriolis Effect Mass Flow Meter", ASHRAE Transaction, Vol.94, No.2878, pp 310-320.

[10] Z. Lin, 1982 "Two-Phase Flow Measurements with Sharp-Edged Orifices", Int. J. Multiphase Flow, Vol.8, pp

[11] J.S. Chang, Y. Ichikawa and G.A. Irons, 1983 "Flow Regime Characterization and Liquid Film Thickness Measurement in Horizontal Gas-Liquid Two-Phase Flow by an Ultrasonic Method", Mass Flow Measurement-1984, ASME Press, New York pp. 7-12.

[12] J.S. Chang, R. Girard, R. Raman and F.B.P. Tran, 1984 "Measurement of Void Fraction in Vertical Gas-Liquid Two-Phase Flow by Ring Type Capacitance Transducers", Mass Flow Measurements-1984, edited by T.R. Hedrick and R.M. Reimer. ASME Press, New York. pp 93-99.

[13] H. Auracher and J. Daubert, 1985 "A Capacitance Method for Void Fraction Measurements in Two-Phase Flow", 2nd International Conference on Multiphase Flow. London, England, June 19-21, pp 425-441.

[14] C.G. Xie, A. Plaskowski and M.S. Beck, 1989 "8-Electrode Capacitance System for Two-Component Flow Identification, Part 1: Tomographic Flow Imaging; Part 2: Flow Regime Identification", IEE Proceedings, Vol.136, No.4, pp 173-190.

[15] S.M. Huang, A.B. Plaskowski, C.G. Xie and M.S. Beck, 1989 "Tomographic Imaging of Two-Component Flow Using Capacitance Sensors", J. Phys. E, Sci. Instrum., 22, pp 173-177.

[16] L.C. Lynnworth, 1989 Ultrasonic Measurements for Process Control. Academic Press.

[17] W.J.G. Brimley and J.S. Chang, 1982 "Flow Diagnostics and Monitoring", Chapter 9 of Thermalhydraulics for CANDU Reactors - An Intensive Short Course in McMaster University, edited by R. Bonalumi et al.

[18] J.S. Chang, Y. Ichikawa, G.A. Irons, E.C. Morala and P.T. Wan, 1983 "Void Fraction Measurement by an Ultrasonic Transmission Technique in Bubbly Gas-Liquid Two-Phase Flow", Measurement Techniques in Gas-Liquid Two-Phase Flows, IUTAM Symposium, Springer Pub. Berlin. pp 319-335.

[19] E.C. Morala, D. Cheong, P.T. Wan, G.A. Irons and J.S. Chang, 1983, "Ultrasonic Wave Propagation in a Bubbly Gas-Liquid Two-Phase Flow", Proceedings of 3rd Multiphase Flow and Heat Transfer Int. Symp. Hemisphere Pub. Washington.

[20] L.A. Xu, D. Leonard and R.G. Green, 1985 "A Pulsed Ultrasound Transducer System for Two-Component Flow", J. Phys. E, Sci. Instrum., 22, pp 609-613.

[21] J.S. Chang, 1988 "Determination of Two-Phase Interfacial Parameters by an Ultrasonic Technique", 3rd Int. Topical Meeting on NUPTHO-3, Vol.1: Thermal Hydraulics, edited by C.N. Hee and J.K. Hho. Seoul, Korea, pp A9.1-8.

[22] J.S. Chang, T.A.Myint, N.Hayashi, M.W.Wu, D. Galicki and K. Brodowicz, 1991 "Development of Non-Intrusive Capacitance Transducer Techniques for Void Fraction, Velocity and Flow Regime Measurements in Two-Phase Gas-Powder Flow", Proceedings of Int. Conf. on Multiphase Flows, Vol.2, '91-Tsukuba, Japan. pp 265-268.

[23] E.C. Morala, 1986 Master Thesis. McMaster University, Canada.

[24] A. Plaskowski, M.S. Beck and J.S. Krowaczynski, 1987 "Flow Imaging for Multi-Component Flow Measurement", Tran. Inst. M. C. Vol.9, No.2, pp 108-112.

[25] S. Banerjee, A.M.C. Chan, N. Ramanathan and P.S.L. Yuen, 1978 "Fast Neutron Scattering and Attenuation Technique for Measurement of Void Fractions and Phase Distributions in Transient Flow Boiling", Proc. 6th Int. Heat Transfer Conference. 1, pp 351-355.

[26] S. Banerjee, P.S.L. Yuen and M.A. Vandenbroek, 1979 "Calibration of a Fast Neutron Scattering Technique for Measurement of Void Fraction in Rod Bundles", J. Heat Transfer, Vol.101, pp 295-299.

[27] S. Banerjee, E. Hussein and D.A. Meneley, 1978 "Simulation of a Neutron Scattering Method for Measuring Void Fraction in Two-Phase Flow", Nuclear Engineering and Design. Vol.53, pp 393-405.

[28] P.S.L. Yuen, D.A. Meneley and S. Banerjee, 1988 "Measurement of Void Fraction by a Neutron Scattering Technique with Portable Sources: Effect of The Incident Energy Spectrum", Int. J. Multiphase Flow, Vol.14, No.4, pp 401-412.

[29] J.S. Chang, W.H. Fairholm and G.D. Harvel, 1991 "Visualization of Two-Phase Interfaces in a Natural Circulation Loop by a Real-Time Neutron Radiography Imaging System", ANS Proceedings for 1991 National Heat Transfer Conference, July, Minneapolis, Minnesota. pp 199-206.

[30] N. Takenaka, T. Fujii, A. Ono, K. Sonoda, H. Asano and H. Nagata, 1991 "Two-Dimensional Void Fraction Measurement of Dispersed Flow in a Nozzle by Neutron Radiography", Proceedings of Int. Conf. on Multiphase Flows, Vol.1, '91-Tsukuba, Japan. pp 237-240.

[31] T. Narabayashi, T. Ishiyama, H. Miyano and H. Nei, 1991 "Measurement of Void Distribution in High Pressure Steam-Water Two-Phase Flow Using High Speed X-Ray Scanner", Proceedings of Int. Conf. on Multiphase Flows, Vol.1, '91-Tsukuba, Japan, pp 241-246.

[32] A.M.C. Chan and S. Banerjee, 1981 "Design Aspects of Gamma Densitometers For Void Fraction Measurements in Small Scale Two-Phase Flows", Nuclear Instruments and Methods, 190, North-Holland Publishing Co. pp 135-148,

[33] A.M.C. Chan, 1980 Ph.D Thesis, McMaster University, Canada.

[34] A.M.C. Chan and D. Bzovey, 1988 "Measurement of Mass Flux in High Temperature High Pressure Steam-Water Two-Phase Flow Using A Combination of Pitot Tubes and A Gamma Densitometer", 3rd Int. Topical Meeting on NUPTHO-3, Vol.1: Thermal Hydraulics, edited by C.N. Hee and J.K. Hho. Seoul, Korea, pp A9.9-16.

[35] Rouhani, 1964, "Application of the Turbine Type Flowmeters in the Measurement of Steam Quality and Void", Symposium on In Core Instrumentation, Oslo, June.

[36] R. Frank, J. Mazars and R. Ricque, 1977 "Determination of Mass Flow Rate and Quality Using A Turbine Meter and A Venturi", Heat and Fluid Flow in Water Reactor Safety, Manchester, September 13-15, pp 63-69.

[37] I. Aya, 1975 "Model to Calculate Mass Flow Rate and Other Quantities of Two-Phase Flow in A Pipe with A Densitometer, A Drag Disk, and A Turbine Meter", ORNL-TM-4759.

[38] Fluid Meters: Their Theory and Application, Report of ASME Research Committee on Fluid Meters, Fifth Edition, 1959.

[39] D. Chisholm, 1967 "Flow of Incompressible Two-Phase Mixtures Through Sharp-Edged Orifices", Journal Mechanical Engineering Science, Vol.9, No.1, pp 72-77.

[40] J.G. Collier, 1972, "Convective Boiling and Condensation", McGraw-Hill.

[41] D.B. Collins and M. Gacesa, 1971 "Measurement of Steam Quality in Two-Phase Upflow with Venturi meters and Orifice Plates", Journal of Basic Engineering, March, pp 11-21

[42] A. Fouda and E. Rhodes, 1978 "Total Mass Flow and Quality Measurement in Gas-Liquid Flow", Two-Phase Transport and Reactor Safety, edited by T.N. Veziroglu and S. Kakac, Hemisphere Publishing Co., Vol.IV, pp 1331-1355.

[43] P.T. Wan, 1985 "Two-Phase Flow Measurement with Flow Nozzles", Details are not available.

[44] J. Reimann, H. John and R. Frank, 1983 "Measurement of Mass Flow Rate and Quality with a Venturi Nozzle and a Turbine Meter in Steam-Water Flow", Transient Two-phase Flow. edited by M.S. Plesset, N. Zuber and I. Catton, Hamisphere Publishing Co., pp 77-84.

[45] J. Reimann, H. John and U. Muller, 1982 "Measurement of Two-Phase Flow Rate: A Comparison of Different Techniques", Int. J. Multiphase Flow. Vol. 8. No.1, pp 33-46.

[46] K. Kose, 1991 "Flow Visualization by NMR Imaging", Proceeding of The International Conference on Multiphase Flows. '91-Tsukuba, Sept. 24-27. Tsukuba, Japan.

[47] H. John, J. Reimann and G. Eisele, E. Ohlmer and W. Schulze, 1984 "Test of a Mass Flow Rate Measuring Spool Piece Involving Drag Body, Gamma Densitometer, Local Flow Turbines and Full Flow Turbine in Transient Two-Phase Flow", Mass Flow Measurement-1984, edited by T.R. Hedrick and R.M. Reimer. ASME Press. pp 113-121.

[48] J.T. Grumski and R.A. Bajura, 1984 "Performance of a Coriolis-Type Mass Flow Meter in the Measurement of Two-Phase Air-Liquid Mixtures", Mass Flow Measurements-1984, edited by T.R. Hedrick and R.M. Reimer. ASME Press. pp 64-75.

[49] R.N. Bernier and C.E. Brennen, 1983, "Use of The Electromagnetic Flowmeter in a Two-Phase Flow", Int. J. Multiphase Flow, Vol.9, No.3, pp 251-257.

[50] J.E. Cox and C.R. Miro, 1992 "U.S. Phases Out CFCs Early", ASHRAE Journal. April, pp 10-19.

[51] A. Kamei, C.C. Piao, H. Sato and K. Watanabe, 1990 "Thermodynamic Charts and Cycle Performance of FC-134a and FC-152a", ASHRAE Transaction. Vol.96, part 1, No.3318, pp 141-149.

[52] C. Piao, H. Sato and K. Watanabe, 1991, "Thermodynamic Charts, Tables, and Equations for Refrigerant HFC-134a", ASHRAE Transaction, Vol.97,part 2. pp 268-283.

[53] C. Piao, H. Sato and K. Watanabe, 1990, "An Experimental Study for PVT Properties of CFC Alternative Refrigerant R-134a", ASHRAE Transaction.Vol.96,part 1.pp132-140.

[54] M.O. McLinden et al, 1989, "Measurement and Formulation of the Thermodynamic Properties of Refrigerants R-134a and R-123", ASHRAE Transaction. Vol.95, part 2, pp363-283.

[55] S.M. Sami and T.N. Duong, 1991, "Dynamic Performance of Heat Pumps using Refrigerant R-134a", ASHRAE Transaction. Vol.97, part 2, pp41-47.

[56] J.R. Sand, E.A. Vineyard and R.J. Nowak, 1990, "Experimental Performance of Ozone Safe Alternative Refrigerants", ASHRAE Transaction. Vol.96, pp 173-182.

[57] FTB-100 and FTB-200 Turbine Flow Meter Operator's Manual, M389/0787. 1992.

[58] P.B. Whalley, 1987 Boiling, Condensation and Gas-Liquid Flow. Oxford Science Publications.

[60] A. Abdul-Razzak, 1993, Private communication, September, 1993.

APPENDIXES

APPENDIX A. R-134a PROPERTIES OF SATURATED LIQUID AND SATURATED VAPOR

The properties of saturated liquid and saturated vapour for refrigerant R-134a are shown in Table A-1. These tables were provided directly by ASHRAE. Using Tables A-1 and A-2, the thermophysical properties in the present experimental range were correlated as shown in Figures A.1 to A.9. These correlations were used in analyzing the data.

Table A.1 Refrigerant 134a properties of saturated liquid and vapour (SI units)

Refrigerant 134a (1,1,1,2-tetrafluoroethane) Properties of Saturated Liquid and Saturated Vapor

Temp.* °C	Pressure, MPa	Density, kg/m³ Liquid	Volume, m³/kg Vapor	Enthalpy, kJ/kg Liquid	Enthalpy, kJ/kg Vapor	Entropy, kJ/(kg·K) Liquid	Entropy, kJ/(kg·K) Vapor	Specific Heat c_p, kJ/(kg·K) Liquid	Specific Heat c_p, kJ/(kg·K) Vapor	c_p/c_v Vapor	Velocity of Sound, m/s Liquid	Velocity of Sound, m/s Vapor	Viscosity, μPa·s Liquid	Viscosity, μPa·s Vapor	Thermal Cond, mW/(m·K) Liquid	Thermal Cond, mW/(m·K) Vapor	Surface Tension, mN/m	Temp, °C
−103.30a	0.00039	1591.2	35.263	71.89	335.07	0.4143	1.9638	1.147	0.585	1.163	1135.	127.	2186.6	6.63	—	—	28.15	−103.30
−100.00	0.00056	1581.9	25.039	75.71.	337.00	0.4366	1.9456	1.168	0.592	1.161	1111.	128.	1958.2	6.76	—	—	27.56	−100.00
−90.00	0.00153	1553.9	9.7191	87.59	342.94	0.5032	1.8975	1.201	0.614	1.155	1051.	131.	1445.6	7.16	—	—	25.81	−90.00
−80.00	0.00369	1526.2	4.2504	99.65	349.03	0.5674	1.8505	1.211	0.637	1.151	999.	134.	1109.9	7.57	—	—	24.11	−80.00
−70.00	0.00801	1498.6	2.0528	111.78	355.23	0.6286	1.8069	1.215	0.660	1.148	951.	137.	879.6	7.97	125.8	—	22.44	−70.00
−60.00	0.01594	1471.0	1.0770	123.96	361.51	0.6871	1.8016	1.220	0.685	1.146	904.	139.	715.4	8.38	121.1	—	20.81	−60.00
−50.00	0.02948	1443.1	0.60560	136.21	367.83	0.7432	1.7812	1.229	0.712	1.146	858.	142.	594.3	8.79	116.5	7.12	19.22	−50.00
−40.00	0.05122	1414.8	0.36095	148.57	374.16	0.7973	1.7649	1.243	0.740	1.148	812.	144.	502.2	9.20	111.9	8.19	17.66	−40.00
−30.00	0.08436	1385.9	0.22596	161.10	380.45	0.8498	1.7519	1.260	0.771	1.152	765.	145.	430.4	9.62	107.3	9.16	16.13	−30.00
−28.00	0.09268	1380.0	0.20582	163.62	381.70	0.8601	1.7497	1.264	0.778	1.153	756.	145.	418.0	9.71	106.3	9.35	15.83	−28.00
−26.07b	0.10132	1374.3	0.19016	165.87	382.90	0.8701	1.7476	1.268	0.784	1.154	747.	146.	406.4	9.79	105.4	9.52	15.54	−26.07
−26.00	0.10164	1374.1	0.18961	166.16	382.94	0.8704	1.7476	1.268	0.785	1.154	747.	146.	406.0	9.79	105.4	9.53	15.53	−26.00
−24.00	0.11127	1368.2	0.17410	168.70	384.19	0.8806	1.7455	1.273	0.791	1.155	738.	146.	394.6	9.88	104.5	9.71	15.23	−24.00
−22.00	0.12160	1362.2	0.16010	171.26	385.43	0.8908	1.7436	1.277	0.798	1.156	728.	146.	383.6	9.96	103.6	9.89	14.93	−22.00
−20.00	0.13268	1356.2	0.14744	173.82	386.66	0.9009	1.7417	1.282	0.805	1.157	719.	146.	373.1	10.05	102.6	10.07	14.63	−20.00
−18.00	0.14454	1350.2	0.13597	176.39	387.89	0.9110	1.7399	1.286	0.812	1.159	710.	146.	363.0	10.14	101.7	10.24	14.33	−18.00
−16.00	0.15721	1344.1	0.12556	178.97	389.11	0.9211	1.7383	1.291	0.820	1.160	700.	147.	353.3	10.22	100.8	10.42	14.04	−16.00
−14.00	0.17074	1338.0	0.11610	181.56	390.33	0.9311	1.7367	1.296	0.827	1.162	691.	147.	344.0	10.31	99.9	10.59	13.74	−14.00
−12.00	0.18516	1331.8	0.10749	184.16	391.55	0.9410	1.7351	1.301	0.835	1.164	682.	147.	335.0	10.40	99.0	10.76	13.45	−12.00
−10.00	0.20052	1325.6	0.09963	186.78	392.75	0.9509	1.7337	1.306	0.842	1.166	672.	147.	326.3	10.49	98.0	10.93	13.16	−10.00
−8.00	0.21684	1319.3	0.09246	189.40	393.95	0.9608	1.7323	1.312	0.850	1.168	663.	147.	318.0	10.58	97.1	11.10	12.87	−8.00
−6.00	0.23418	1313.0	0.08591	192.03	395.15	0.9707	1.7310	1.317	0.858	1.170	654.	147.	309.9	10.67	96.2	11.28	12.58	−6.00
−4.00	0.25257	1306.6	0.07991	194.68	396.33	0.9805	1.7297	1.323	0.866	1.172	644.	147.	302.2	10.76	95.3	11.45	12.29	−4.00
−2.00	0.27206	1300.2	0.07440	197.33	397.51	0.9903	1.7285	1.329	0.875	1.175	635.	147.	294.7	10.85	94.3	11.62	12.00	−2.00
0.00	0.29269	1293.7	0.06935	200.00	398.68	1.0000	1.7274	1.335	0.883	1.178	626.	147.	287.4	10.94	93.4	11.79	11.71	0.00
2.00	0.31450	1287.1	0.06470	202.68	399.84	1.0097	1.7263	1.341	0.892	1.180	616.	147.	280.4	11.03	92.5	11.96	11.43	2.00
4.00	0.33755	1280.5	0.06042	205.37	401.00	1.0194	1.7252	1.347	0.901	1.183	607.	147.	273.6	11.13	91.6	12.13	11.14	4.00
6.00	0.36186	1273.8	0.05648	208.08	402.14	1.0291	1.7242	1.353	0.910	1.187	598.	147.	267.0	11.22	90.7	12.31	10.86	6.00
8.00	0.38749	1267.0	0.05284	210.80	403.27	1.0387	1.7233	1.360	0.920	1.190	588.	147.	260.6	11.32	89.7	12.48	10.58	8.00
10.00	0.41449	1260.2	0.04948	213.53	404.40	1.0483	1.7224	1.367	0.930	1.193	579.	146.	254.3	11.42	88.8	12.66	10.30	10.00
12.00	0.44289	1253.3	0.04636	216.27	405.51	1.0579	1.7215	1.374	0.939	1.197	569.	146.	248.3	11.52	87.9	12.84	10.02	12.00
14.00	0.47276	1246.3	0.04348	219.03	406.61	1.0674	1.7207	1.381	0.950	1.201	560.	146.	242.5	11.62	87.0	13.02	9.74	14.00
16.00	0.50413	1239.3	0.04081	221.80	407.70	1.0770	1.7199	1.388	0.960	1.206	550.	146.	236.8	11.72	86.0	13.20	9.47	16.00
18.00	0.53706	1232.1	0.03833	224.59	408.78	1.0865	1.7191	1.396	0.971	1.210	541.	146.	231.2	11.82	85.1	13.39	9.19	18.00
20.00	0.57159	1224.9	0.03603	227.40	409.84	1.0960	1.7183	1.404	0.982	1.215	532.	145.	225.8	11.92	84.2	13.57	8.92	20.00
22.00	0.60777	1217.5	0.03388	230.21	410.89	1.1055	1.7176	1.412	0.994	1.220	522.	145.	220.5	12.03	83.3	13.76	8.65	22.00
24.00	0.64566	1210.1	0.03189	233.05	411.93	1.1149	1.7169	1.420	1.006	1.226	512.	145.	215.4	12.14	82.4	13.96	8.38	24.00
26.00	0.68531	1202.6	0.03003	235.90	412.95	1.1244	1.7162	1.429	1.018	1.231	503.	144.	210.4	12.25	81.4	14.15	8.11	26.00
28.00	0.72676	1194.9	0.02829	238.77	413.95	1.1338	1.7155	1.438	1.031	1.238	493.	144.	205.5	12.36	80.5	14.35	7.84	28.00
30.00	0.77008	1187.2	0.02667	241.65	414.94	1.1432	1.7149	1.447	1.044	1.244	484.	143.	200.7	12.48	79.6	14.56	7.57	30.00
32.00	0.81530	1179.3	0.02516	244.55	415.90	1.1527	1.7142	1.457	1.058	1.251	474.	143.	196.0	12.60	78.7	14.76	7.31	32.00
34.00	0.86250	1171.3	0.02374	247.47	416.85	1.1621	1.7135	1.467	1.073	1.259	465.	142.	191.4	12.72	77.7	14.97	7.05	34.00
36.00	0.91172	1163.2	0.02241	250.41	417.78	1.1715	1.7129	1.478	1.088	1.267	455.	142.	186.9	12.84	76.8	15.19	6.78	36.00
38.00	0.96301	1154.9	0.02116	253.37	418.69	1.1809	1.7122	1.489	1.104	1.276	445.	141.	182.5	12.97	75.9	15.41	6.52	38.00
40.00	1.0165	1146.5	0.01999	256.35	419.58	1.1903	1.7115	1.500	1.120	1.285	436.	140.	178.2	13.10	75.0	15.64	6.27	40.00
42.00	1.0721	1137.9	0.01890	259.35	420.44	1.1997	1.7108	1.513	1.138	1.295	426.	140.	174.0	13.24	74.1	15.86	6.01	42.00
44.00	1.1300	1129.2	0.01786	262.38	421.28	1.2091	1.7101	1.525	1.156	1.306	416.	139.	169.8	13.38	73.1	16.10	5.76	44.00
46.00	1.1901	1120.3	0.01689	265.42	422.09	1.2185	1.7094	1.539	1.175	1.318	407.	138.	165.7	13.52	72.2	16.34	5.51	46.00
48.00	1.2527	1111.3	0.01598	268.49	422.88	1.2279	1.7086	1.553	1.196	1.331	397.	137.	161.7	13.67	71.3	16.59	5.26	48.00
50.00	1.3177	1102.0	0.01511	271.59	423.63	1.2373	1.7078	1.569	1.218	1.345	387.	137.	157.7	13.83	70.4	16.84	5.01	50.00
52.00	1.3852	1092.6	0.01430	274.71	424.35	1.2468	1.7070	1.585	1.241	1.360	377.	136.	153.8	13.99	69.5	17.10	4.76	52.00
54.00	1.4553	1082.9	0.01353	277.86	425.03	1.2562	1.7061	1.602	1.266	1.377	367.	135.	149.9	14.16	68.5	17.36	4.52	54.00
56.00	1.5280	1073.0	0.01280	281.04	425.68	1.2657	1.7051	1.621	1.293	1.395	358.	134.	146.1	14.33	67.6	17.63	4.28	56.00
58.00	1.6033	1062.8	0.01212	284.25	426.29	1.2752	1.7041	1.641	1.322	1.416	348.	133.	142.3	14.51	66.7	17.91	4.04	58.00
60.00	1.6815	1052.4	0.01146	287.49	426.86	1.2847	1.7031	1.663	1.354	1.438	338.	132.	138.6	14.71	65.8	18.19	3.81	60.00
62.00	1.7625	1041.7	0.01085	290.77	427.37	1.2943	1.7019	1.686	1.388	1.463	328.	131.	134.9	14.91	64.9	18.48	3.57	62.00
64.00	1.8464	1030.7	0.01026	294.08	427.84	1.3039	1.7007	1.712	1.426	1.490	318.	129.	131.2	15.12	63.9	18.78	3.34	64.00
66.00	1.9334	1019.4	0.00970	297.44	428.25	1.3136	1.6993	1.740	1.468	1.522	308.	128.	127.5	15.35	63.0	19.09	3.12	66.00
68.00	2.0234	1007.7	0.00917	300.84	428.61	1.3234	1.6979	1.772	1.515	1.557	298.	127.	123.9	15.59	62.1	19.40	2.89	68.00
70.00	2.1165	995.6	0.00867	304.29	428.89	1.3332	1.6963	1.806	1.567	1.597	287.	126.	120.3	15.85	61.2	19.72	2.67	70.00
72.00	2.2130	983.1	0.00818	307.79	429.10	1.3430	1.6945	1.846	1.626	1.642	277.	124.	116.7	16.12	60.3	20.05	2.46	72.00
74.00	2.3127	970.0	0.00772	311.34	429.23	1.3530	1.6926	1.890	1.693	1.695	267.	123.	113.1	16.41	59.3	20.39	2.24	74.00
76.00	2.4159	956.5	0.00728	314.96	429.27	1.3631	1.6905	1.941	1.770	1.757	256.	121.	109.4	16.73	58.4	20.74	2.03	76.00
78.00	2.5227	942.3	0.00686	318.65	429.20	1.3733	1.6881	2.000	1.861	1.830	246.	120.	105.8	17.08	57.5	21.09	1.83	78.00
80.00	2.6331	927.4	0.00646	322.41	429.02	1.3837	1.6855	2.069	1.967	1.917	235.	118.	102.1	17.46	56.6	21.46	1.63	80.00
85.00	2.9259	886.2	0.00550	332.27	427.91	1.4105	1.6775	2.313	2.348	2.231	207.	113.	92.7	18.59	54.3	22.41	1.15	85.00
90.00	3.2445	836.9	0.00461	343.01	425.48	1.4392	1.6663	2.766	3.064	2.832	178.	108.	82.6	20.15	—	—	0.72	90.00
95.00	3.5916	771.6	0.00374	355.43	420.60	1.4720	1.6490	3.961	4.942	4.424	145.	102.	70.9	22.59	—	—	0.33	95.00
100.00	3.9721	646.7	0.00265	374.02	407.08	1.5207	1.6093	—	—	—	105.	94.	53.0	28.86	—	—	0.03	100.00
101.03c	4.0560	513.3	0.00195	389.79	389.79	1.5593	1.5593	∞	∞	∞	0	0	—	—	∞	∞	0	101.03

*temperatures are on the ITS-90 scale a = triple point b = boiling point c = critical point

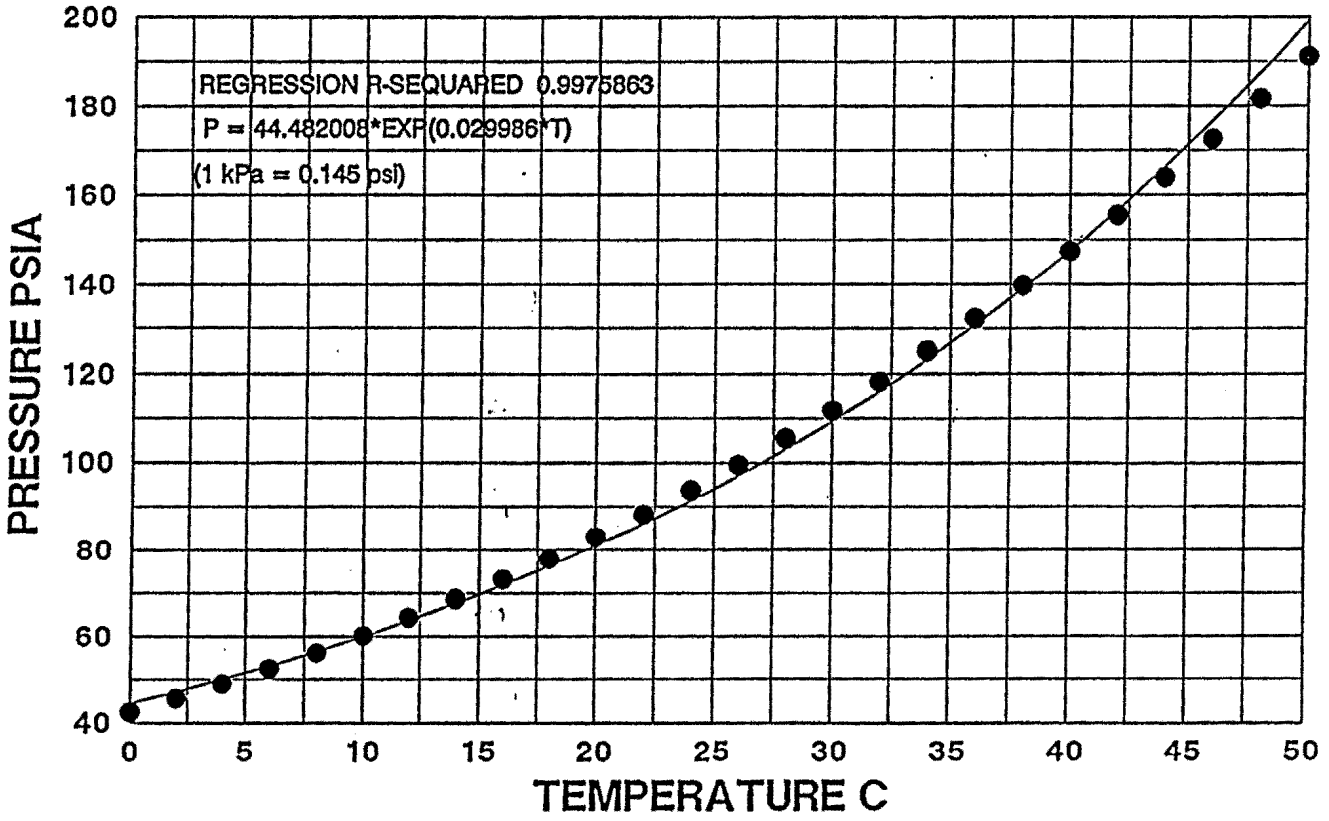

Figure A.1 R-134a property: pressure as a function of temperature

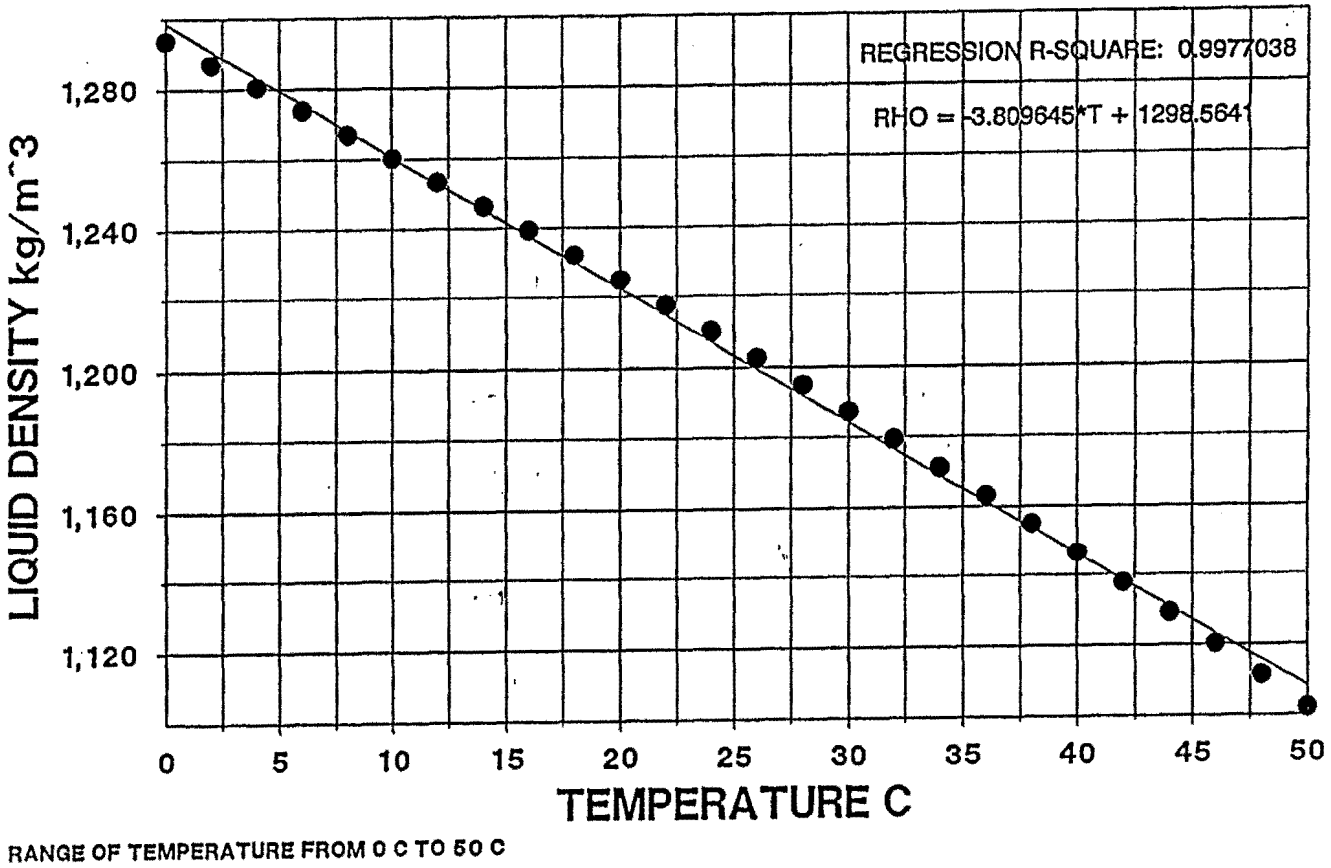

Figure A.2 R-134a property: liquid density as a function of temperature

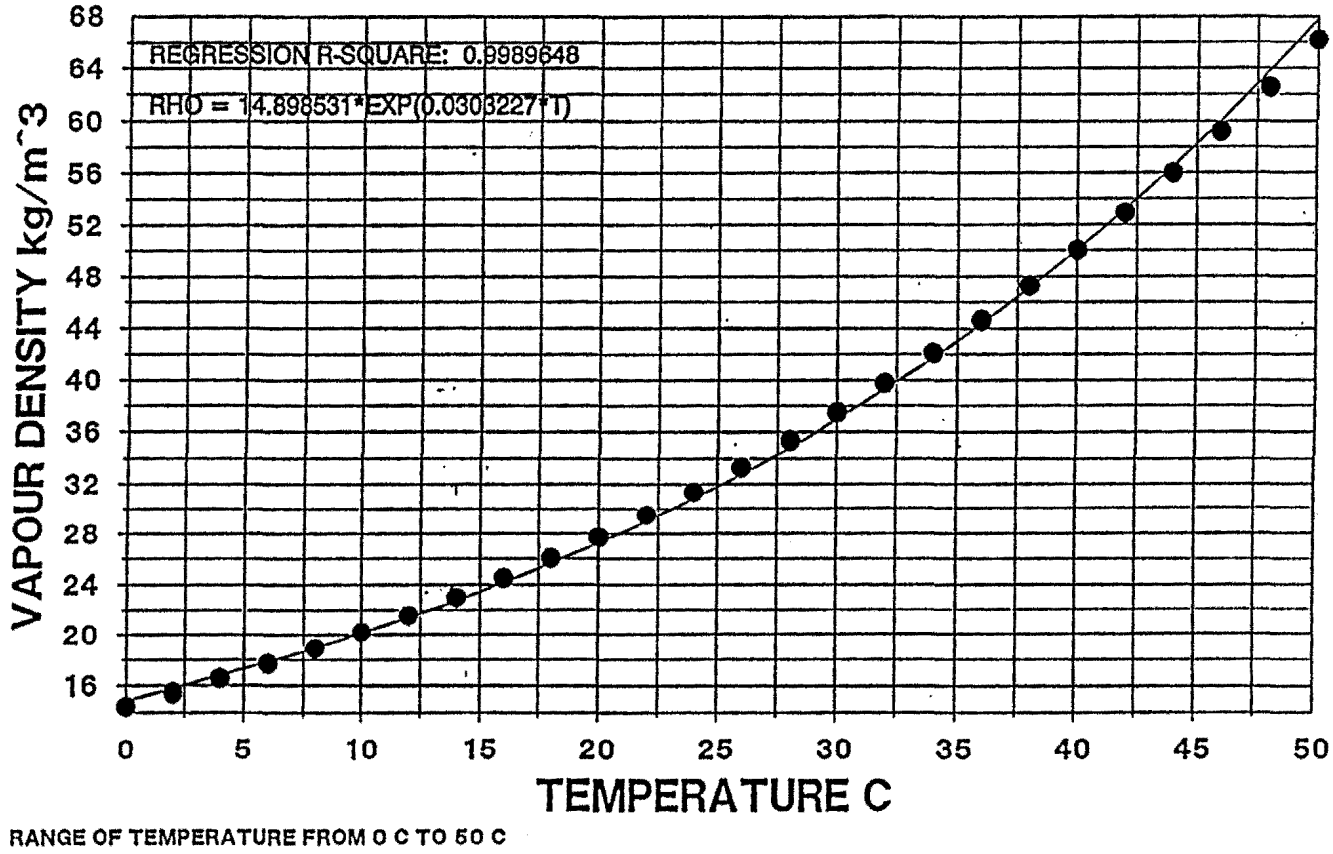

Figure A.3 R-134a property: vapour density as a function of temperature

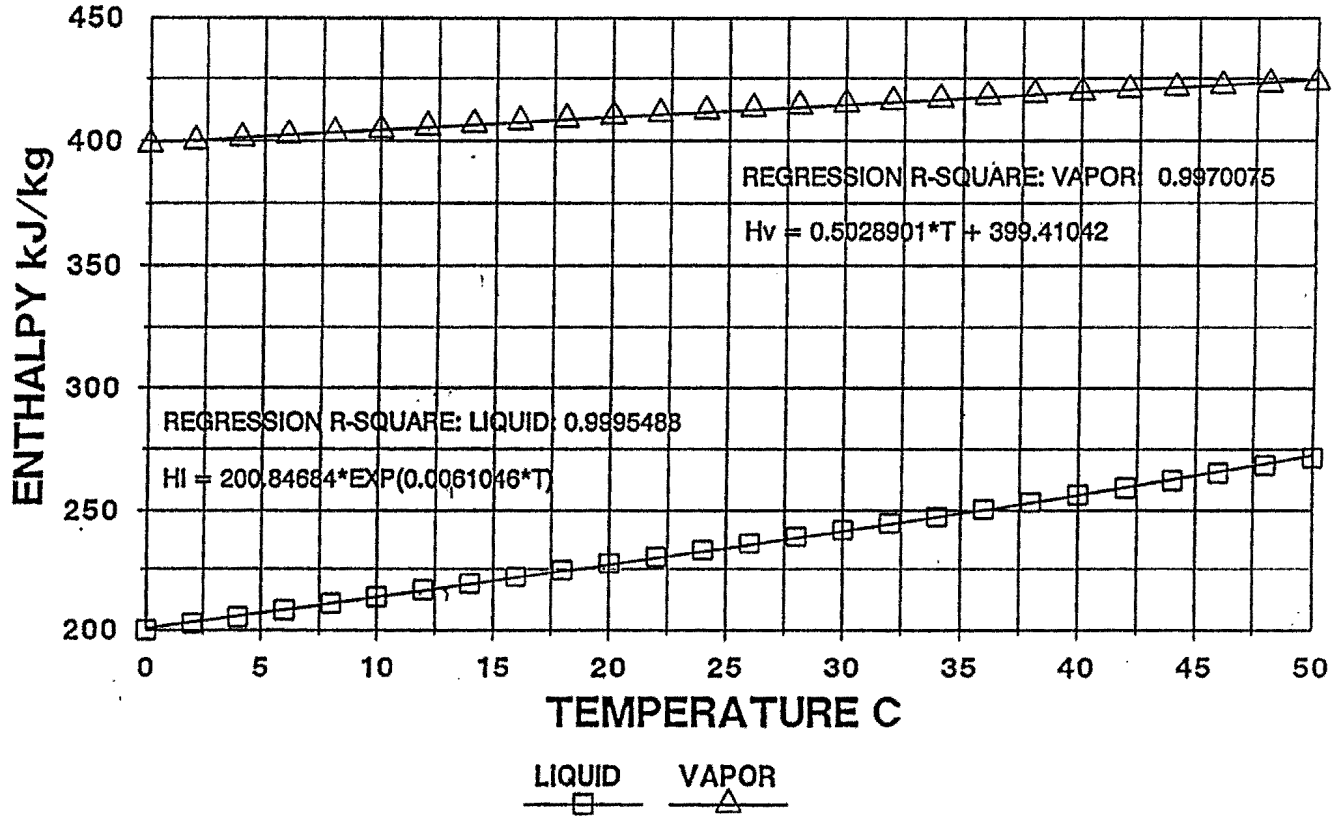

Figure A.4 R-134a property: liquid and vapour enthalpy as a function of temperature

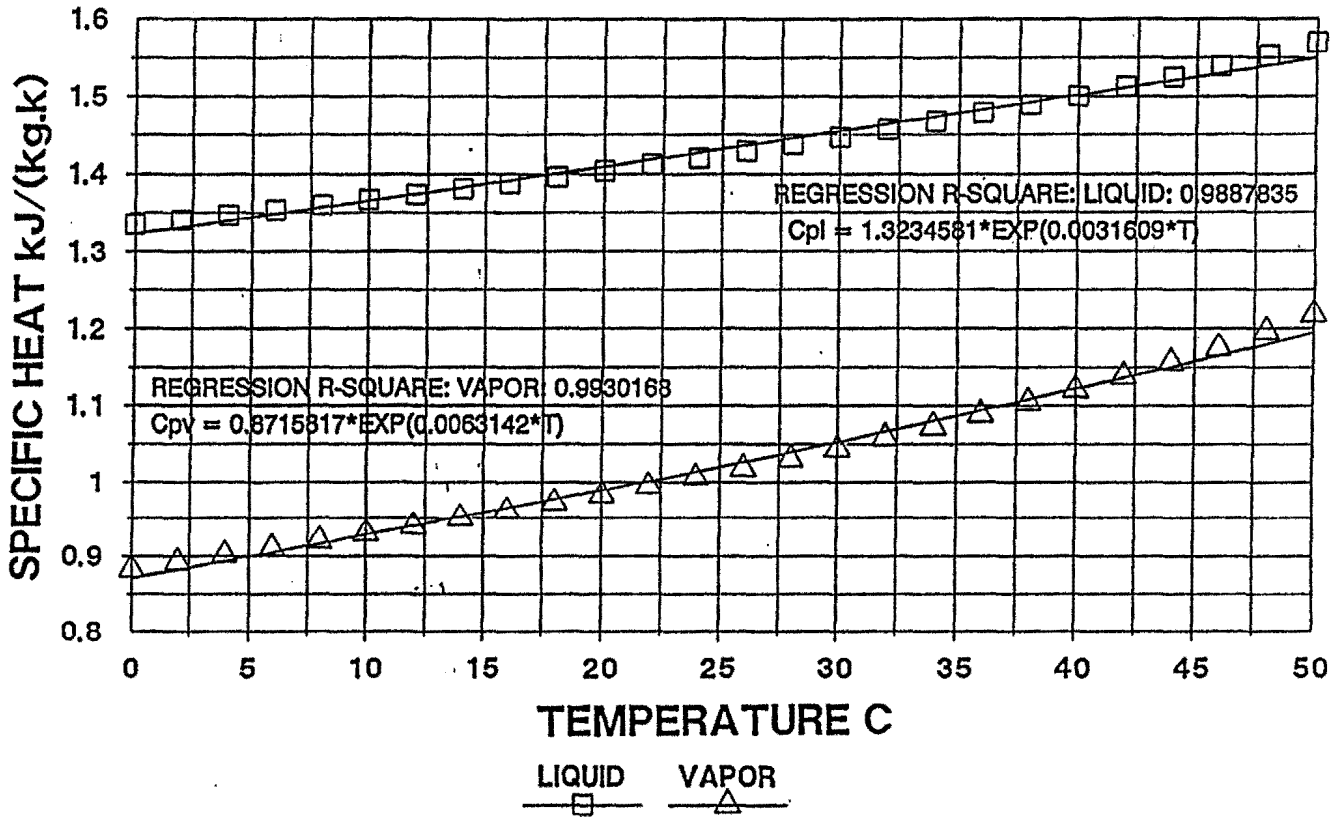

Figure A.5 R-134a property: liquid and vapour specific heat as a function of temperature

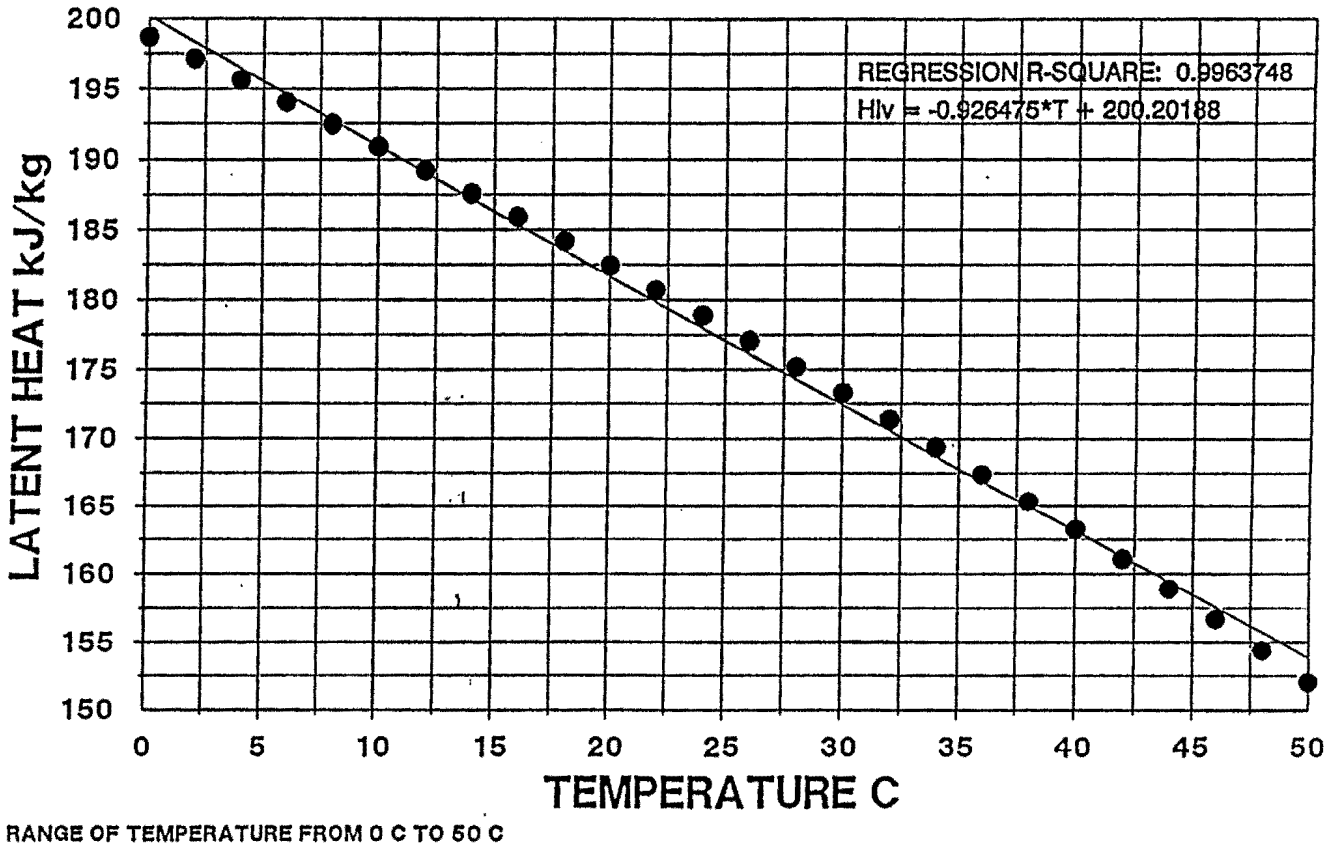

Figure A.6 R-134a property: latent heat as a function of temperature

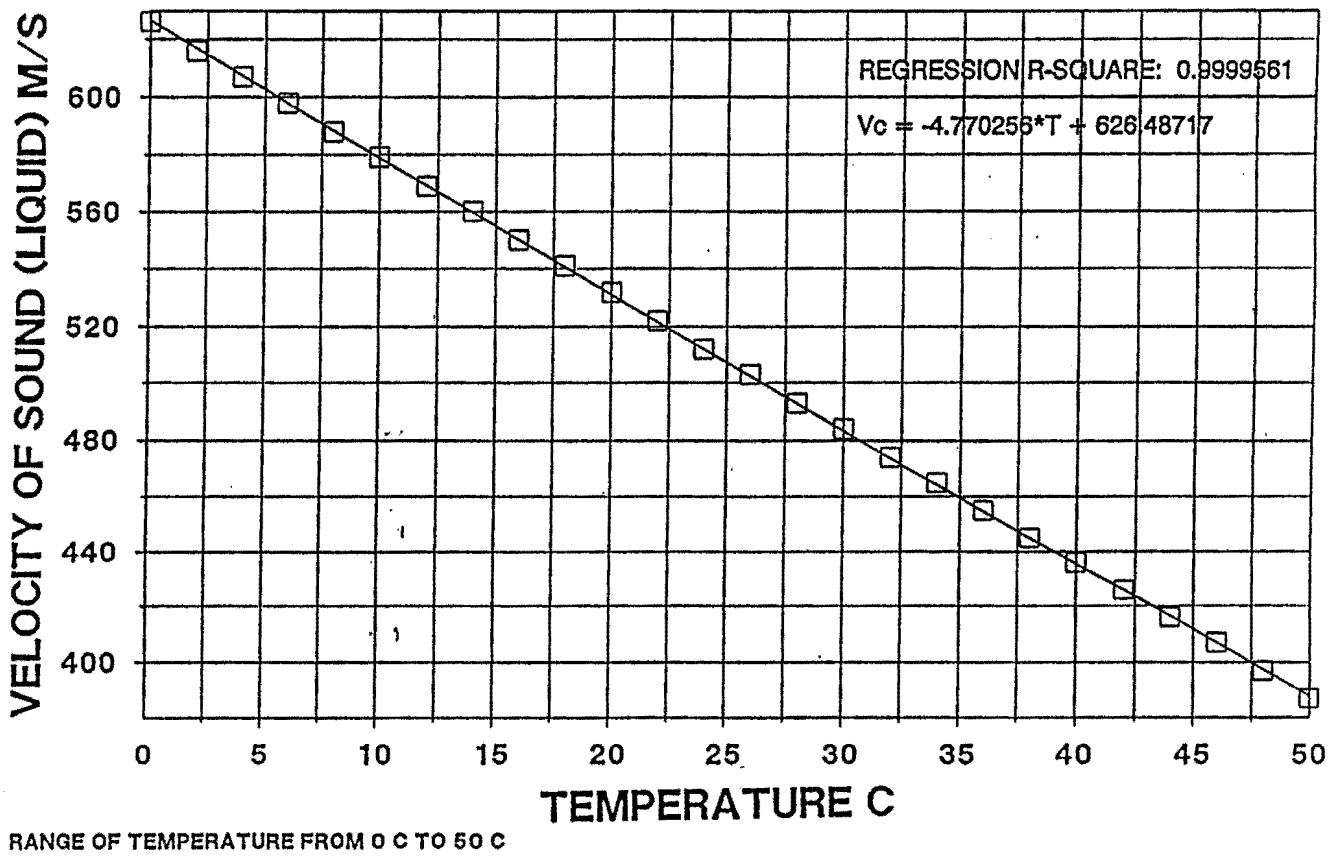

Figure A.7 R-134a property: sound velocity of liquid as a function of temperature

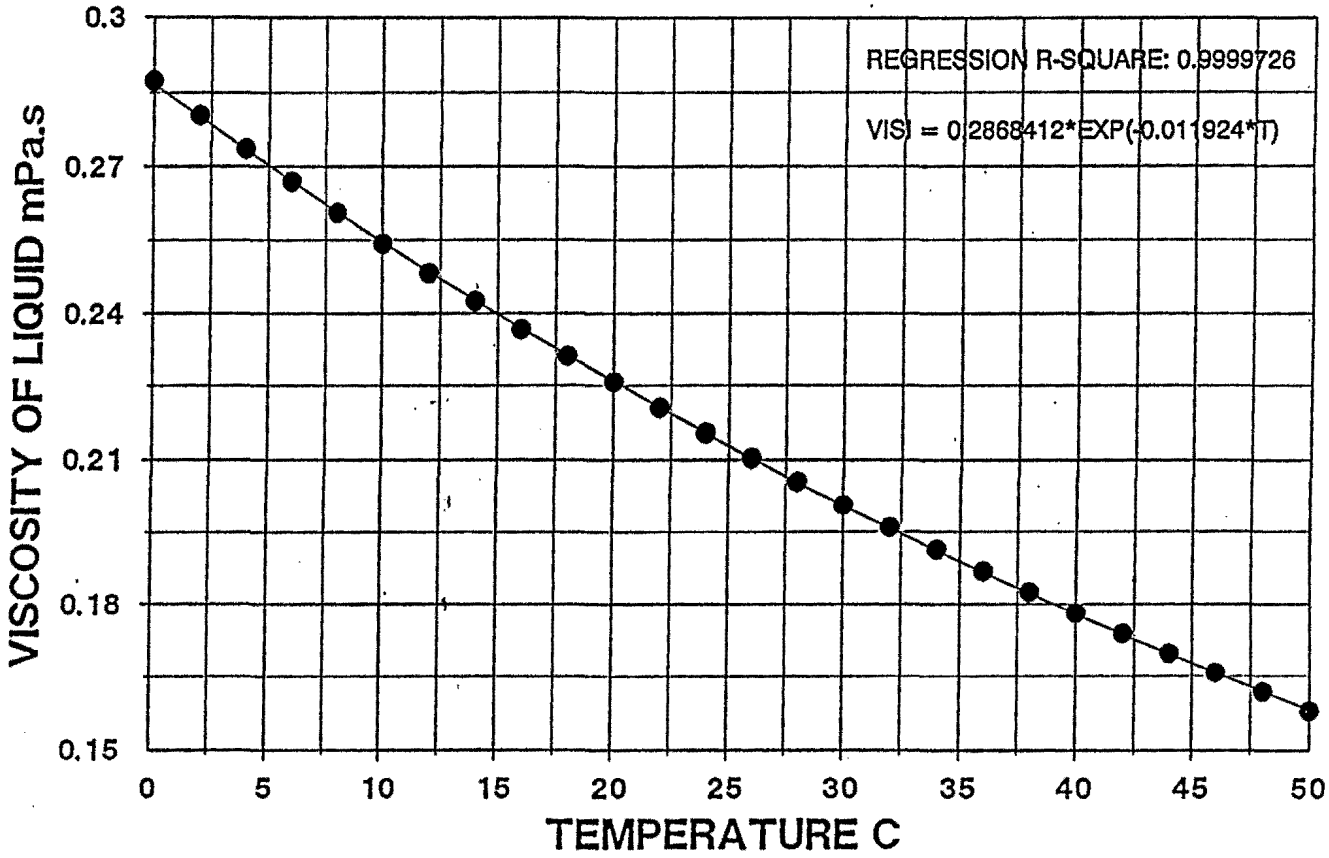

Figure A.8 R-134a property: viscosity of liquid as a function of temperature

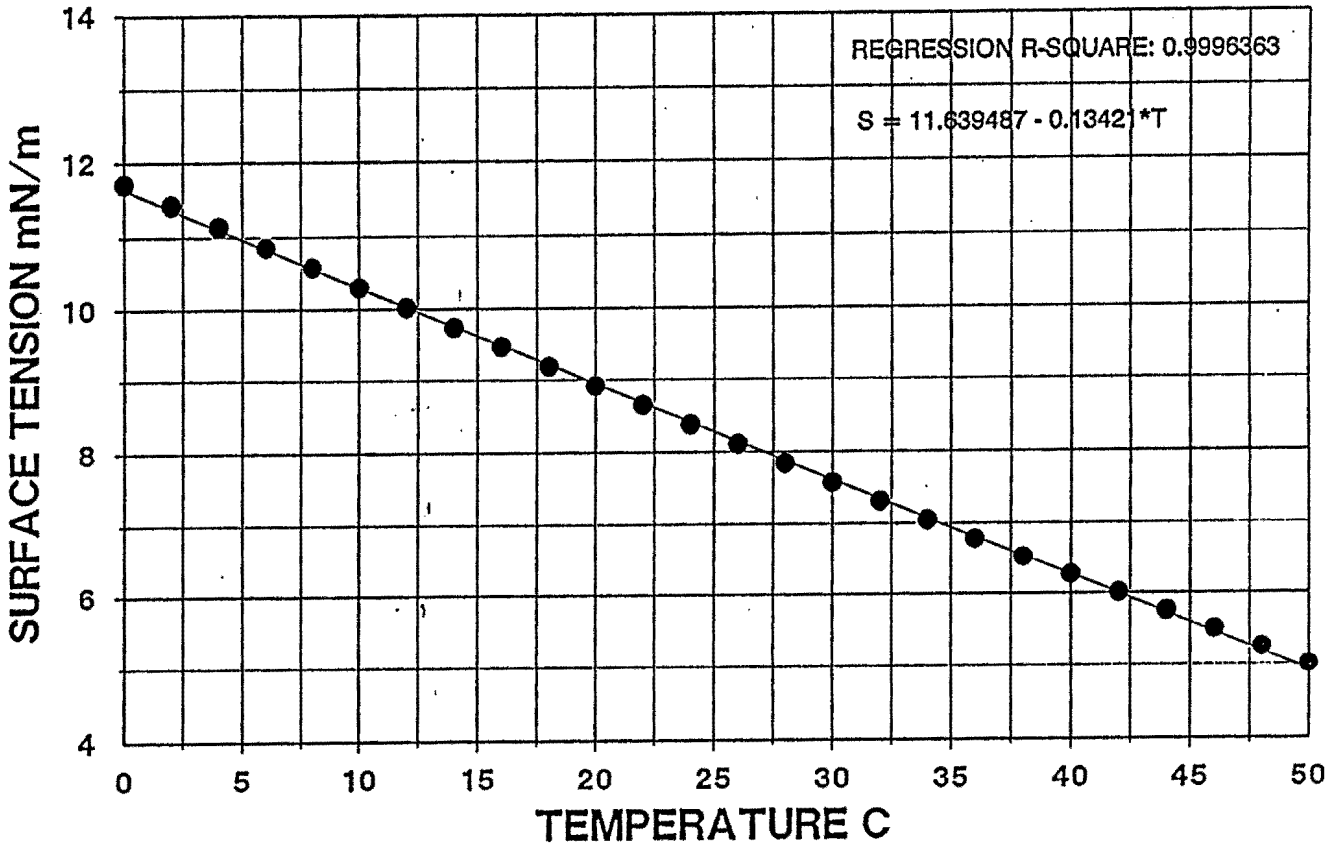

Figure A.9 R-134a property: surface tension as a function of temperature

APPENDIX B. CALIBRATION OF ROTAMETERS

Two Fischer & Porter rotameters were used to measure flow rate of cold water flowing through the condenser. The calibration curve is shown in Figure B. The rotameters have a strictly linear behaviour as can be observed from Figure B.

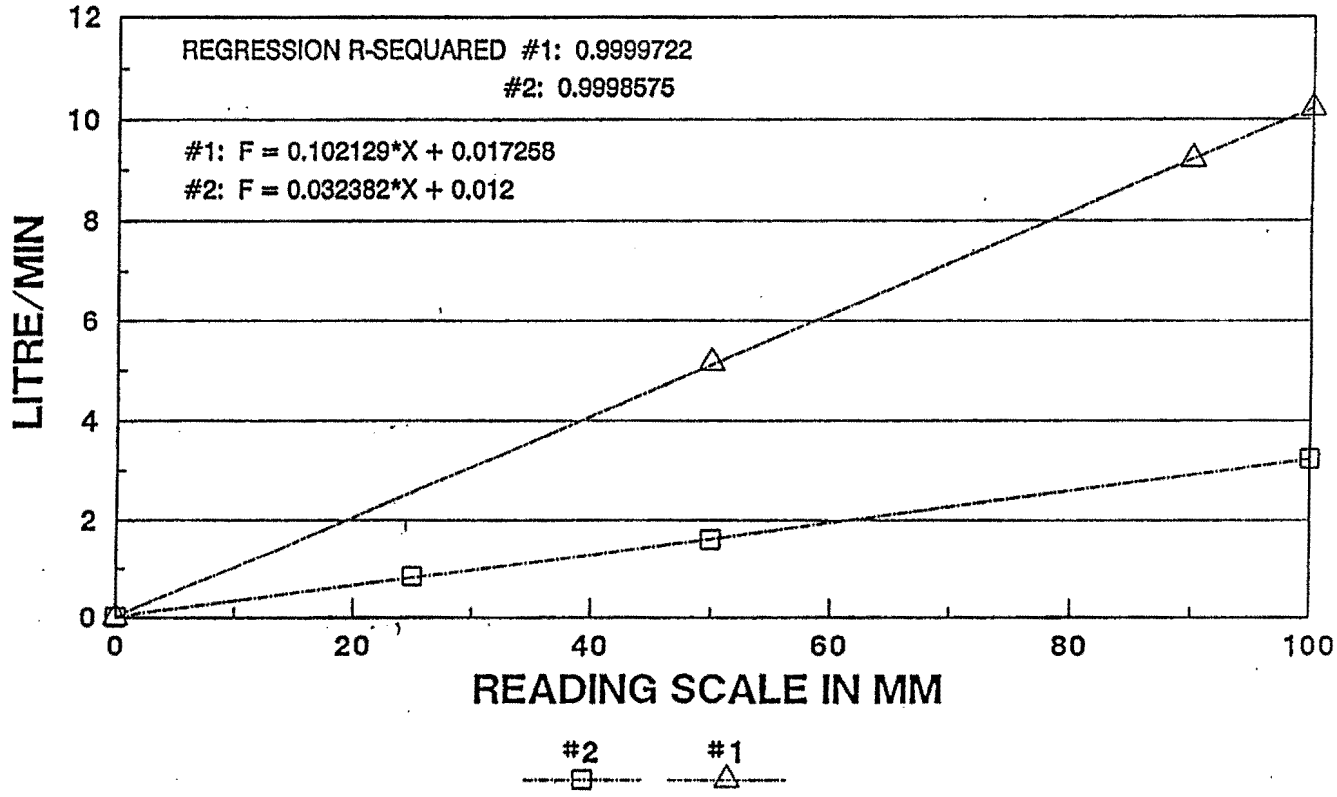

Figure B Calibration of rotameters #1 and #2

APPENDIX C. CALIBRATION OF TURBINE FLOW METERS

Two factory calibrated OMEGA FTB-101 Turbine Flowmeters were used in the present work. One (serial# 43563) was used for single phase flow measurement and the second (serial# 44291) for two-phase flow conditions. The general features listed by the manufacturer are given in Table C-1, and the calibration curves based on water provided by manufacturer are shown in Table C-2 and Figure C.1.

Recalibration of these turbine flowmeters for water was carried out by collecting water. Calibration curves are shown in Figure C.2. The curves of both meters gave perfectly linear behaviour.

A frequency-to-voltage converter, model 4702 provided by TELEDYNE PHILBRICK, was used to convert the output frequency of turbine transducer to a voltage signal. The output range of the converter is $\pm$ 10 volts. With 4 decades of dynamic range and high linearity the transfer characteristic is:

$$Eo = 10\ V \times FREQ\ IN / 10{,}000$$

The high linearity of the device makes it an excellent choice for applications such as measuring flow rate from sine wave or pulse type transducers. However, the accuracy was determined by the transducer itself, not the V/F converter.

Table C-1. General Features of Model# FTB-101 Turbine Meter[57]

Linear Flow Range (US GPM)	NPT End Fittings	Maximum Operating Pressure (PSIG)	Maximum Pressure Drop (PSID)	Length	Nominal K-Factor Cycle/Gal
0.35-3.5	1/2"	5000	3.0	2.45"	13,000

ACCURACY: ± 1/2% of reading

REPEATABILITY: ± 0.1% of reading

MAX. TEMPERATURE RANGE: -232 C to +232 C

MAX. INTERMITTENT OVERRANGE: 150% of max. range

MATERIALS OF CONSTRUCTION: Body: 304 SS; Rotor: 17-4 pH steel

BEARINGS: 440C stainless steel

Table C-2. Calibration Data Sheet of FTB-101 Turbine Meter[57]

MODEL#: FTB-101

SERIAL#: 43563

TEST RANGE: 0.37451 to 3.36994 GPM

TEST FLUID: water at 25.4 C degrees

TEST STAND: 2 weight #1

SPECIFIC GRAVITY: 0.998

COIL TYPE: PC24-45G min. 18 mV output

DATE: 04/15/92

Run#	Frequency Hz	GPM	K, Cycle/GAL
1	100.51	0.37451	16103.19
2	152.18	0.56303	16217.01
3	198.55	0.73453	16219.03
4	298.83	1.11261	16115.28
5	400.02	1.49268	16079.02
6	501.67	1.87212	16078.01
7	626.84	2.33048	16138.45
8	701.71	2.61259	16115.28
9	802.71	2.99573	16077.00
10	904.56	3.36994	16105.21

K-value average: 16124.75

Linearity $\pm$ 0.4398

TABLE C-2 (Continue)

MODEL#: FTB-101

SERIAL#: 44291

TEST RANGE: 0.32753 to 3.47857 GPM

TEST FLUID: water at 24.5 C degree

TEST STAND: 2 weight #1

SPECIFIC GRAVITY: 0.998

COIL TYPE: PC24-45G min. 10 mV output

DATE: 08/11/92

Run#	Frequency Hz	GPM	K Cycle/GAL
1	75.77	0.32753	13880.15
2	96.95	0.41893	13885.19
3	149.36	0.64555	13882.17
4	196.62	0.84991	13880.15
5	297.80	1.29691	13777.41
6	397.20	1.73231	13757.26
7	498.79	2.17525	13758.27
8	593.31	2.58821	13754.24
9	701.28	3.05943	13753.23
10	797.48	3.47857	13755.25

K-value average: 13808.33

Linearity $\pm$ 0.4774

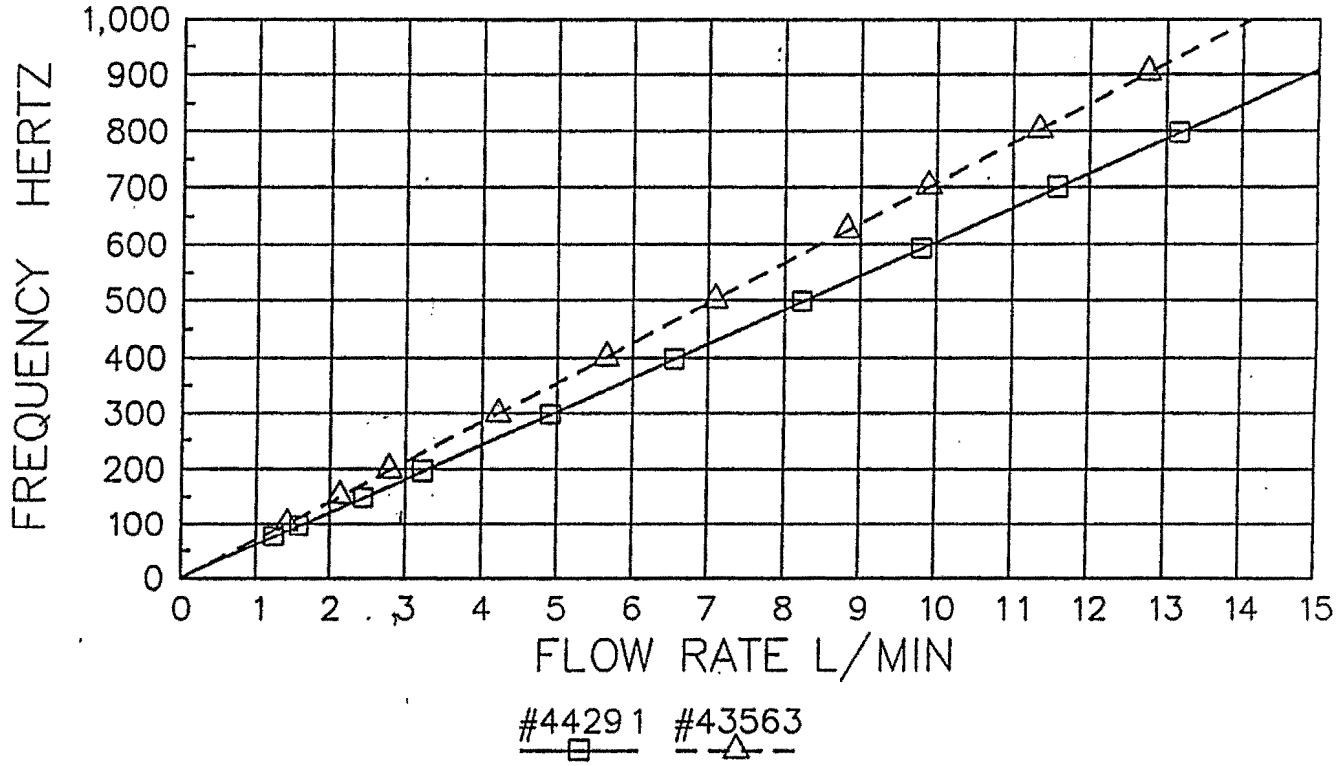

Figure C.1 Calibration of turbine meters #44291 & #43563 in terms of frequency

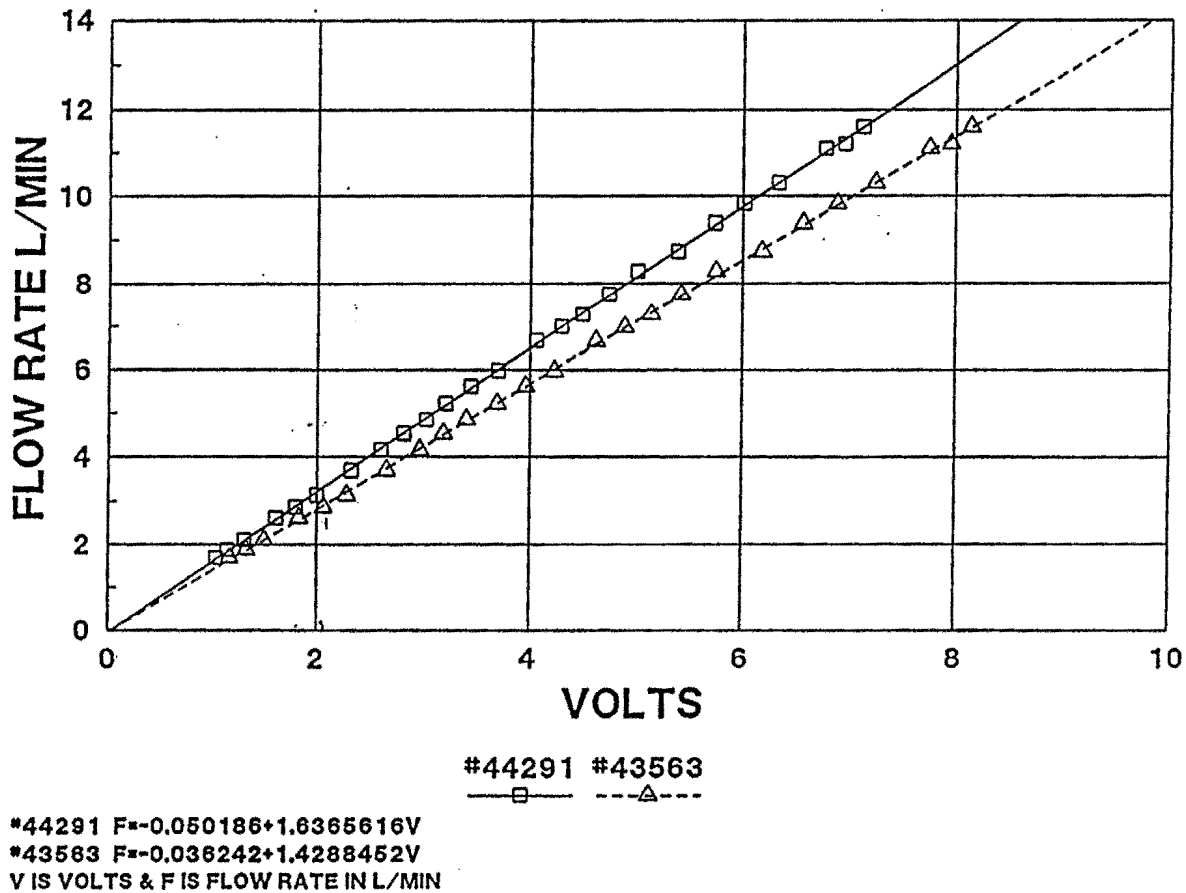

Figure C.2 Calibration of turbine meters #44291 & #43563 in terms of volt

APPENDIX D. CALIBRATION OF VENTURI FLOW METER

The venturi flowmeter was machined from a 38 mm diameter solid brass rod. It was manufactured according to the ASME recommended standards given in the book: Fluid Meters: Their Theory and Application[38]. A schematic diagram of the venturi meter is shown in Figure D.1. Four pressure taps were located around the circumference at each of the inlet and throat section as shown. However, only the bottom taps were connected to the pressure transducers in the present experiments.

Arrangement of the pressure transducers for the venturi flowmeter measurement is shown in Figure D.2. All of the three pressure transducers are Validyne type products which have high accuracy of 0.1% of reading. Calibrations against water and mercury manometers were made. All transducers have strictly linear performance and the output voltage from 0 to 10 volts was set by two demodulators in order to be recorded by the data acquisition system. A cold water jacket was used to maintain liquid phase in the lines to the pressure transducers.

The relationship between the single-phase mass flow rate and the pressure drop in a venturi flowmeter is given by:

$$G=(\frac{\pi d^2}{4})\frac{C}{\sqrt{1-\beta^4}}\sqrt{2\rho\Delta P} \qquad \text{(D.1)}$$

where β = d/D, d is the throat diameter of venturi, D is the tube diameter, C is an empirical constant which depends on the Reynolds number, discharge coefficient and expansion coefficient if the fluid is compressible.

The present venturi flowmeter was calibrated in-situ against the turbine flowmeter. The calibration curve is shown in Figure D.3 for which the constant C = 0.9299:

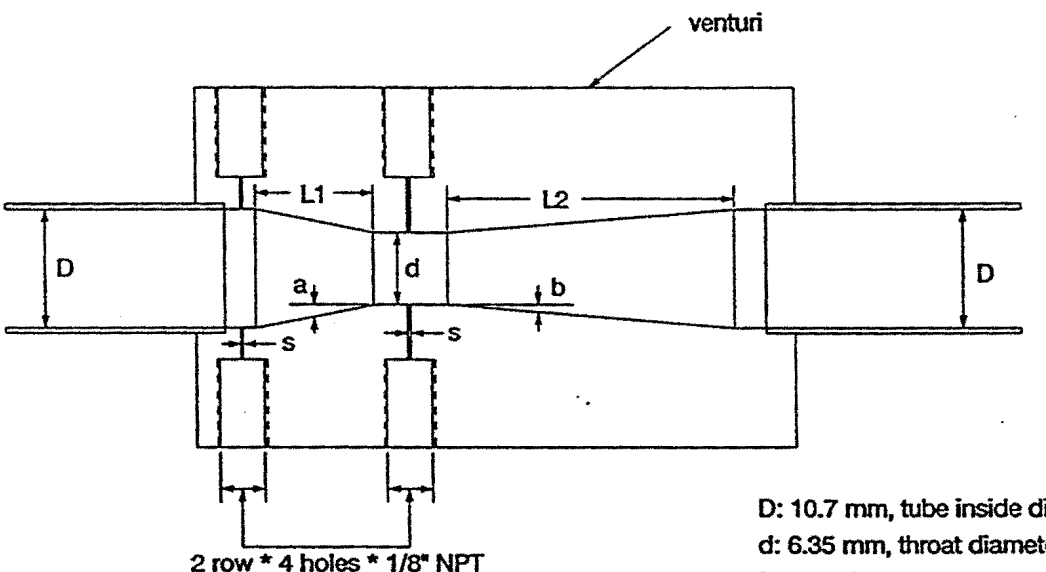

D: 10.7 mm, tube inside diameter
d: 6.35 mm, throat diameter
L1: 10.69 mm
L2: 24.86 mm
a: 11.5° ± 1°
b: 5° ± 0.5°
s: 1/16" (1.59 mm)
Venturi : 1 1/2" brass bar (38 mm)

Fig. D.1 Designed Venturi Flowmeter

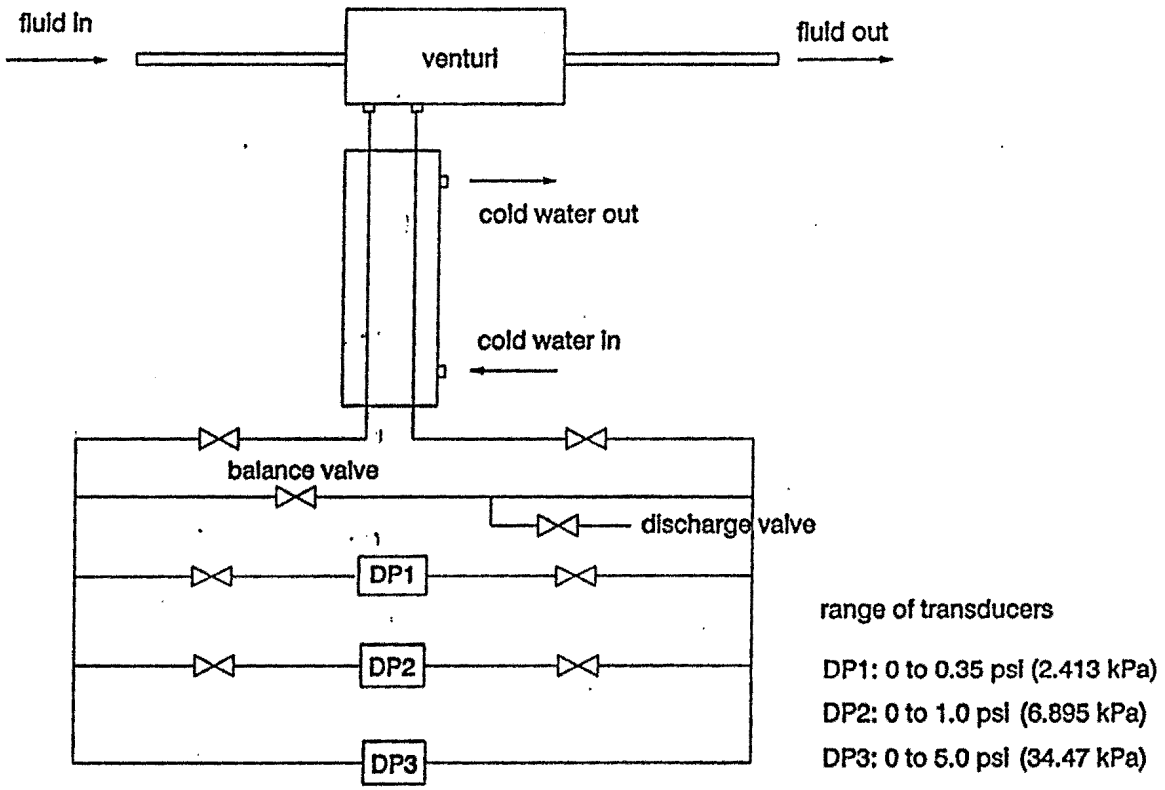

Fig. D.2 Arrangement of Transducer on Venturi Meter

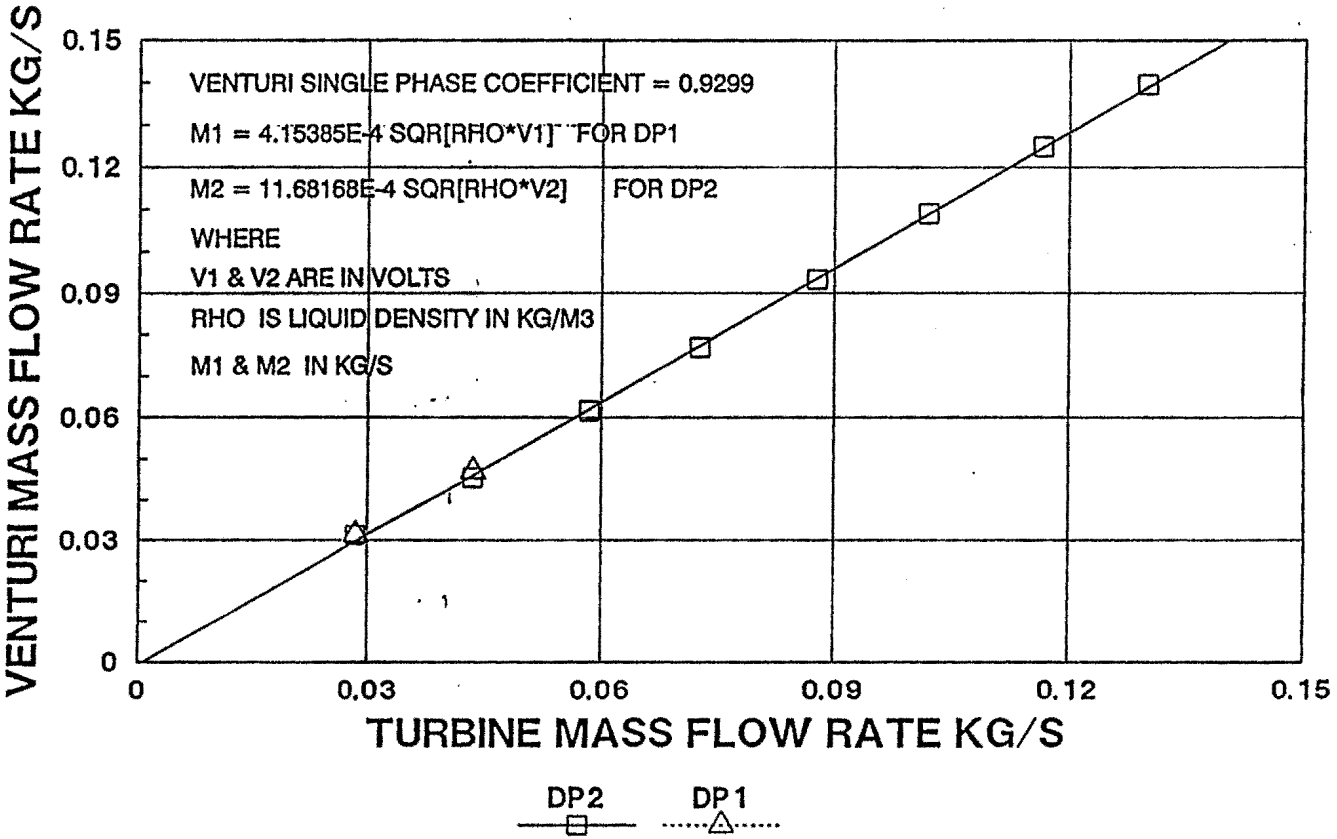

Figure D.3 Calibration of venturi vs. turbine meter

APPENDIX E. CALIBRATIONS OF CAPACITANCE TRANSDUCER AND GAMMA-DENSITOMETER

E.1 CALIBRATION OF CAPACITANCE TRANSDUCER

A multi-ring type capacitance tranducer was used to measure the void fraction in the two-phase refrigerant flow. A schematic diagram of the transducer is shown in Figure E.1. Each ring is 6 mm wide and they are spaced by 8 mm apart. The transducer is covered by a grounded copper sheet to shield it from electromagnetic interferences.

The capacitance transducer was connected to a capacitance meter, (Boonton Model-72B) which has an accurency of $\pm$ 0.5% of full scale reading and the output voltage was recorded by the data acquisition system.

The capacitance transducer was calibrated in-situ for static stratified liquid of various levels. The test section was isolated allowing the flow through the bypass line. Incremental amounts of liquid were allowed into the test section to generate a range of liquid levels. The capacitance transducer output was calibrated against the liquid level measurement obtained using the ultrasonic pulse-echo technique. The measurement of the liquid level H was obtained by a 10 MHz ultrasonic transducer with Panametrics ultrasonic analyser and an oscilloscope. The liquid level was determined by:

$$H=(\frac{t}{2}-\frac{\delta_L}{V_{CL}})V_{CR} \qquad \text{(E.1)}$$

where t is the total propagation time of the pulsed ultrasound wave from the transducer to pass through the transparent tube and the liquid and to be reflected back to the ultrasound transducer δ_L is the thickness of transparent tube, V_{CL} is the speed of sound in the lucite tube, lucite, V_{CR} is the sound speed of R-134a which is temperature dependent.

From the liquid level H, the void fraction occupied in the cross section of the tube can be calculated by:

$$\alpha = 1 - \frac{A_f}{A} = 1 - \frac{\frac{D^2}{4}\arccos\left(1 - \frac{2H}{D}\right) - \left(\frac{D}{2} - H\right)\sqrt{H(D-H)}}{\frac{1}{4}\pi D^2} \qquad \text{(E.2)}$$

where D is the inside diameter of the tube, A_f is the liquid fraction in the cross section of the tube, and A is the area of the cross section.

Finally, the calibration curve of the capacitance transducer is shown in Figure E.2 and a correlation of void fraction and capacitance reading is given by:

$$\alpha = 0.990773 - 0.62797 Cp^* - 0.57575 Cp^{*2} + 0.211382 Cp^{*3} \qquad \text{(E.3)}$$

where Cp^* is the dimensionless capacitance and should be equal to :

$$Cp^* = \frac{Cp}{Cp_{sat}} \qquad \text{(E.4)}$$

where Cp_{sat} is the single phase liquid value as a function of temperature in pf. Separate tests were carried out to measure the liquid capacitance as a function of temperature. The data was corrected by:

$$Cp_{sat} = 1.116766 - 0.00392 T_{sat} \qquad \text{(E.5)}$$

where T_{sat} is the saturated temperature of refrigerant R-134a in C.

In order to certify the calibration curve of the capacitance transducer for R-134a, a calibration of the transducer with water at room temperature was also conducted as shown in Figure E.3. The results of the two curves are in good agreement.

E.2 CALIBRATION OF GAMMA-DENSITOMETER

The calibration of the gamma-densitometer using the ultrasonic pulse-echo technique was made in the same way as that for the capacitance transducer. The calibration curve is shown in Figure E.4. The calibration data appears to be close to the linear distribution. This is similar to the behaviour of gamma-rays in steam-water system.

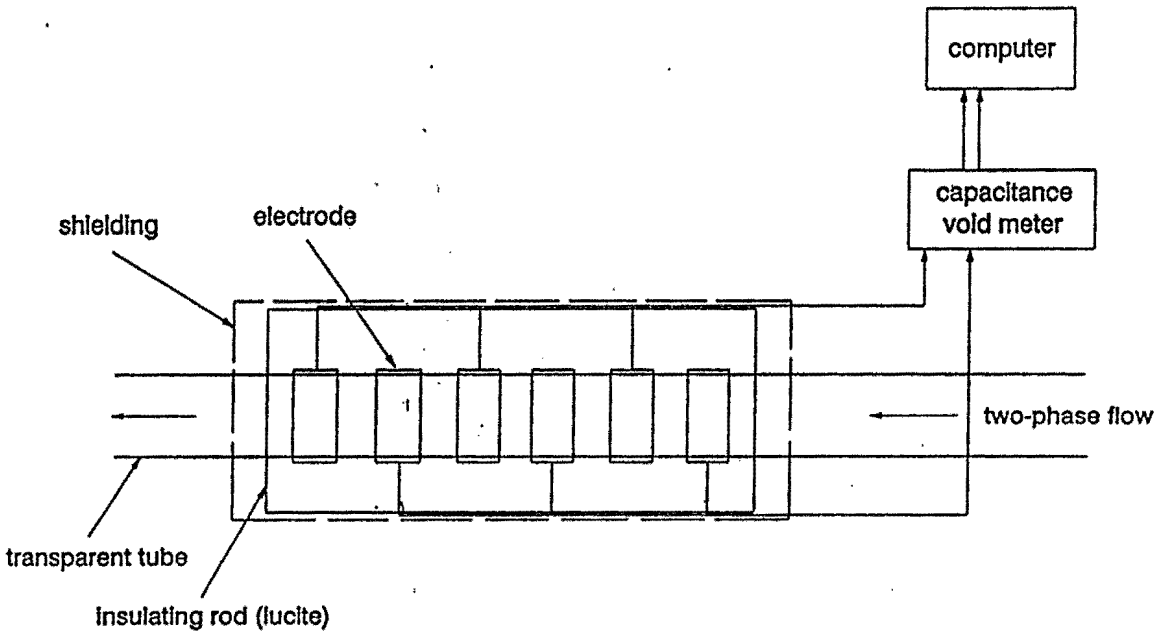

Fig. E.1 Schematic Diagram of Capacitance Transducer

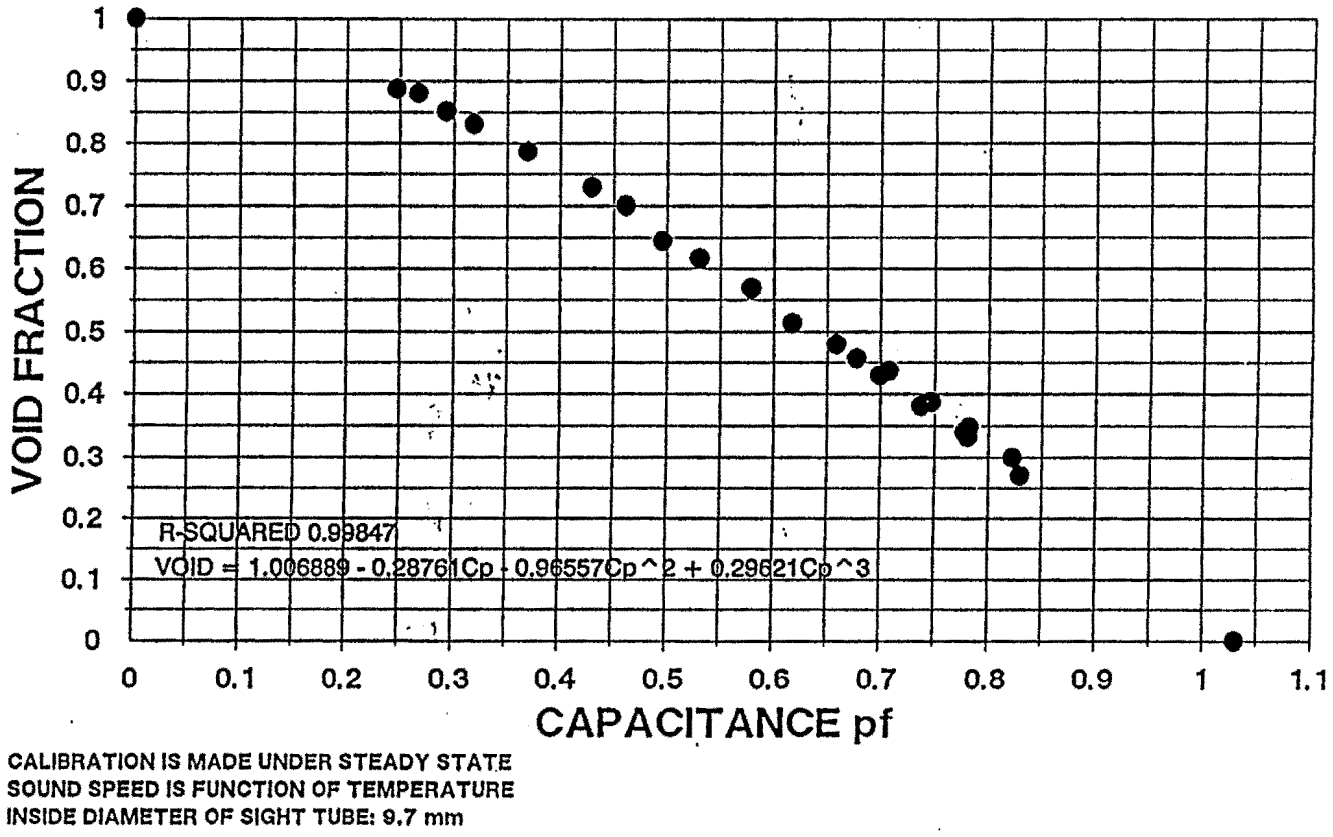

Figure E.2 Calibration of capacitance transducer with R-134a

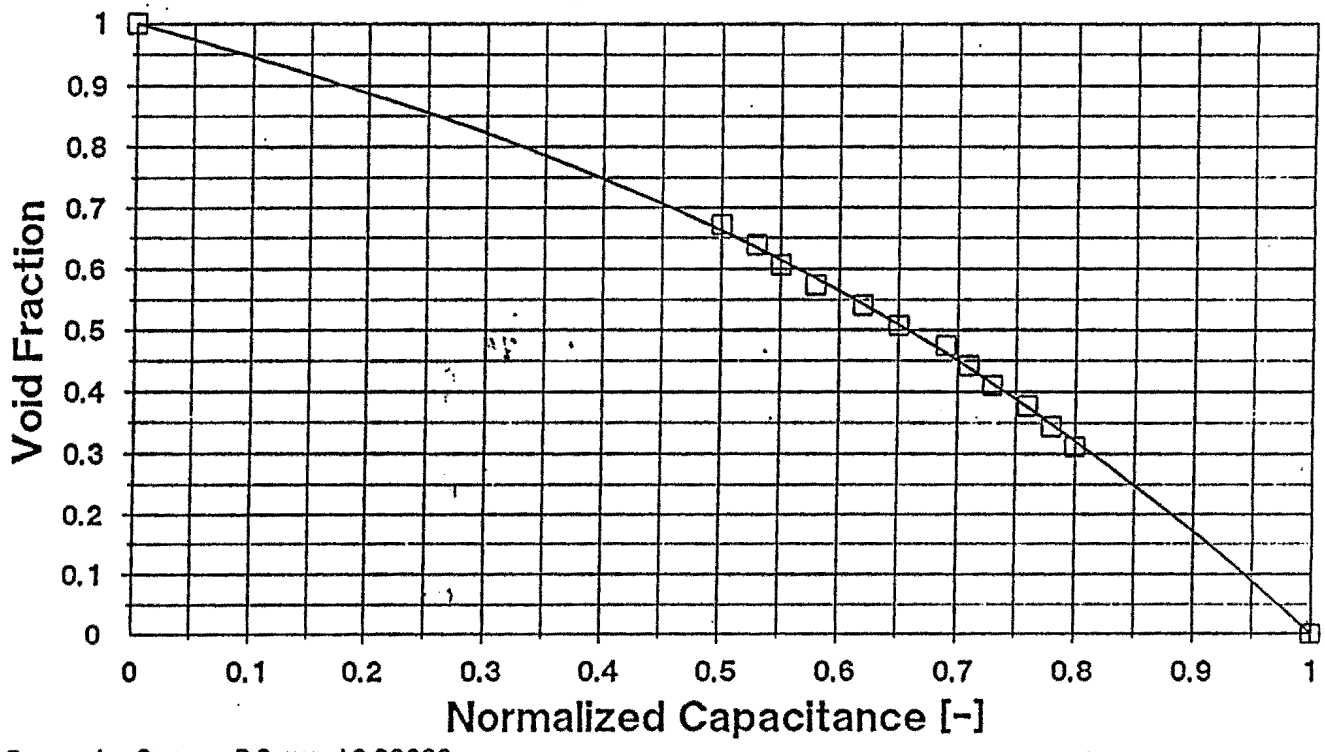

Figure E.3 Calibration of capacitance transducer with water

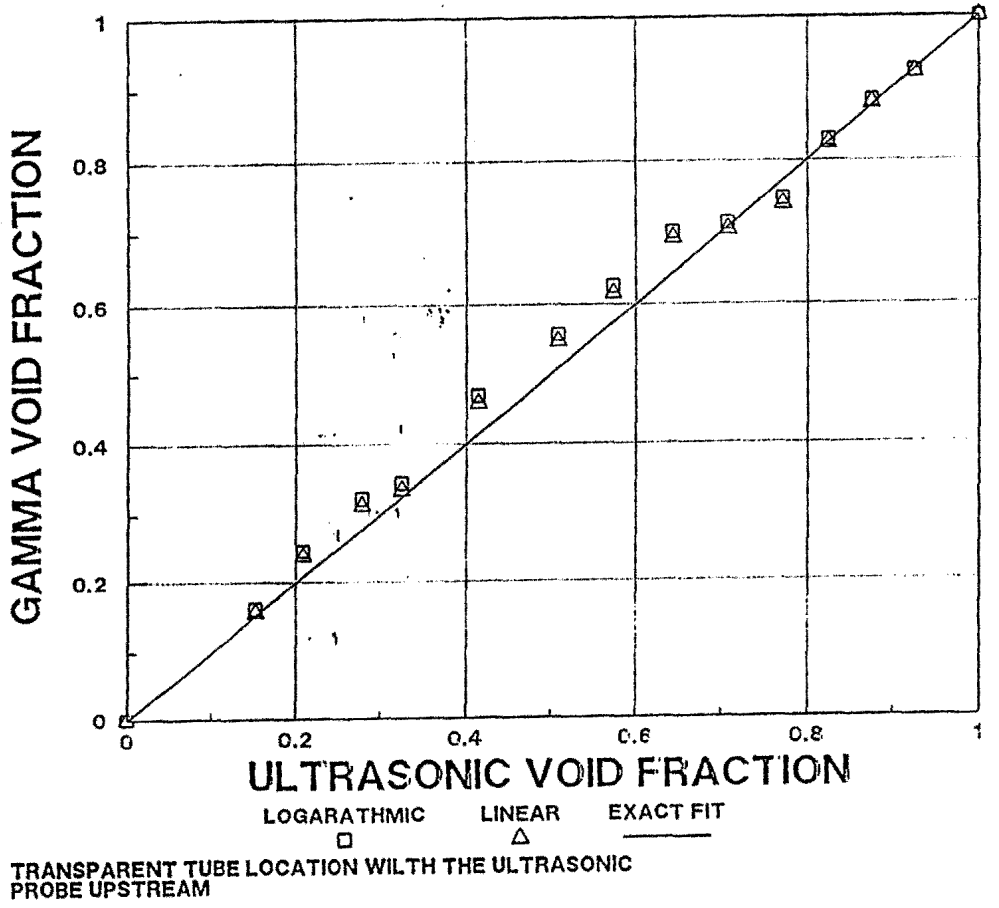

Figure E.4 Calibration of gamma-densitometer with R-134a

APPENDIX F

UNCERTAINTY ANALYSIS

In order to judge the reliability of the experimental results, the uncertainties associated with the calculated parameters are presented here. The structure of the uncertainty analysis was provided by Abdul-Razzak[60]. In general, if one parameter is a function of several variables which is given as follows :

$$R=f(x_1,x_2,\ldots,x_i,\ldots) \tag{F.1}$$

then, its uncertainty can be expressed by:

$$\frac{\Delta R}{R}=[(\frac{\partial R}{\partial x_1}\frac{\Delta x_1}{R})^2+(\frac{\partial R}{\partial x_2}\frac{\Delta x_2}{R})^2+\ldots+(\frac{\partial R}{\partial x_i}\frac{\Delta x_i}{R})^2+\ldots]^{1/2} \tag{F.2}$$

The uncertainties in the basic measurements are estimated to be:

temperature T	± 1 C of reading provided by manufacturer
tube diameter D	± 0.064 mm provided by manufacturer
pressure drop ΔP	± 0.25% of reading provided by manufacturer
volumetric flow rate Q_T	± 0.5% of reading provided by manufacturer
voltage in power supply V	± 0.08%
ampere in power supply I	± 0.02%

Equation (F.2) was used to calculate the uncertainties in all calculated parameters as shown below:

Thermophysical properties:

The thermophysical properties of saturated refrigerant R-134a are functions of temperature. The estimated uncertainties are:

liquid density ρ_f	$\pm$ 0.31%
vapour density ρ_g	$\pm$ 3.0%
specific heat C_p	$\pm$ 0.31%
latent heat h_{fg}	$\pm$ 0.51%

Input power and single-phase mass flow rate:

Q_{power}	$\pm$ 1.0%
M_{single}	$\pm$ 0.59%

Thermodynamic quality:

Using equations (5.3) and (F.2) at a representative test condition, the uncertainty in the thermodynamic quality was calculated to be $\pm$ 1.37%. This representative test condition is given as follows:

Q_{power}	2.73 kW
M_{single}	0.0267 kg/sec
T_{in}	14.2 C
T_{sat}	29.13 C
x	0.463

Void fraction:

The uncertainty of void fraction measured by the gamma-densitometer can be expressed as following equation[2]:

$$\frac{\Delta\alpha}{\alpha}=\frac{\frac{\Delta I}{I}}{\alpha\ln(\frac{I_g}{I_f})}[1+(1-\alpha)^2+\alpha^2]^{1/2} \qquad \text{(F.3)}$$

The sample counting data set is :

I_g	1029 counts/sec
I_f	920 counts/sec
α	0.53
counting time	3 min
$\Delta I/I = N^{-1/2}$	$\pm$ 0.24%

where N is the total counts number of detector counts used to determine the intensity.

Therefore, the uncertainty of void fraction by gamma-densitometer is obtained as:

$$\pm 4.88\%$$

For void fraction measured from the capacitance transducer, the uncertainty is estimated to be within $\pm$ 3%.

Uncertainties in the calculated two-phase mass flow rates:

Using equation (F.2) and the various models described earlier, the uncertainties in the measured two-phase flow rates were calculated. A representative test condition is given here. This test condition corresponds to:

Q_{power}	1.55 kW
M_{single}	0.051 kg/sec
x	0.096
α	0.557

T_{in}	17.9 C
T_{sat}	27.4 C
Q_{TP} (turbine flowmeter output)	7.84 l/min
ΔP_{TP} (across the venturi meter)	0.43 psi (1 kPa=0.145 psi)

Under this test condition, the calculated two-phase mass flow rates and their corresponding uncertainties are given:

Model	**Mass flow rate**	**Calculated uncertainty**
For the venturi flowmeter:		
Chisholm's model	0.054 kg/sec	± 0.75%
Homogeneous density model	0.041 kg/sec	± 0.90%
Separated flow model	0.057 kg/sec	± 0.84%
Equal pressure drop model	0.045 kg/sec	± 1.33%
For the turbine flowmeter:		
Dispersed flow model	0.058 kg/sec	± 1.1%
Homogeneous flow model	0.037 kg/sec	± 1.85%
Separated flow model	0.071 kg/sec	± 1.74%
Rouhani's model	0.065 kg/sec	± 1.55%
For the turbine and venturi flow meters:		
Combined model	0.046 kg/sec	± 0.58%